[redacted]

HQ GRANT
IN-44-CR
183414
143P

K

SSL

SPACE SYSTEMS LABORATORY

(NASA-CR-184023) PRELIMINARY DESIGN OF A HIGH TEMPERATURE SOLAR BRAYTON SPACE POWER SYSTEM (Massachusetts Inst. of Tech.) 143 p

N89-70104

Unclas
00/44 0183414

SPACE SYSTEMS LABORATORY
DEPT. OF AERONAUTICS AND ASTRONAUTICS
MASSACHUSETTS INSTITUTE OF TECHNOLOGY
CAMBRIDGE, MA 02139

PRELIMINARY DESIGN OF A HIGH TEMPERATURE SOLAR BRAYTON SPACE POWER SYSTEM

George R. Whittinghill

February 1983 SSL#7-83

(Under NASA Grant NAGW-21)

ABSTRACT

A high temperature solar Brayton power system was designed for a continuous output of 90 KWe in low earth orbit. The energy is stored in the heat of fusion of silicon. The system was optimized for minimum specific mass. High technology materials are used to lighten structural elements where applicable. Without gimballing to decouple the power section from a space platform, the system optimizes at 28.5 KG/KWe with a cycle efficiency of 25 %. This represents a 3.5 times reduction in mass as compared to equivalent power solar cell/ battery combinations with a threefold increase in system efficiency.

ACKNOWLEDGEMENTS

This work was made possible by a NASA grant, NAGW-21.

My sincere appreciation goes to Professor Manuel Martinez-Sanchez for all his help. Thanks are also due to Professor René Miller and those of the Space Systems Laboratory who assisted in the production of this report.

Table of contents

List of Figures.

List of Figures (cont'd)

List of Tables

Page

Ch 1. Introduction

In the next ten to fifteen years NASA plans to loft a space platform into low earth orbit, a type of modular space station easily configurable to accommodate almost any mission requirement. With such versatility, a scheduled power demand of 90 KWe (continuous) seems reasonable. The various options are nuclear thermionic, nuclear dynamic, solar electric and solar thermal. In the first analysis, the nuclear systems offer tremendous mission flexibility. Almost any power level can be accommodated, in a fairly compact size. The advantage of compactness should not be overlooked, because any object in low earth orbit suffers from orbit decay due to atmospheric drag. The amount of fuel used during a mission lifetime will be directly proportional to the projected area of the satellite. The smaller the satellite, the less the resupply costs become. Unfortunately, any advantage gained here is overshadowed by the characteristic large mass , a sizable fraction of which is the shielding necessary to man rate the system. Various designs have attempted to reduce this shielding mass by employing partial shields, which impose operating constraints on any areas outside the protected zones. Although this could be made to work, there is doubt that such a system would ever be man rated for a manned platform, where considerable extra vehicular activity is expected.

One other option is a solar cell / battery combination, the latter necessary for operation during earth shadow.

Within this power grouping, there are different technologies available for both the solar cells and the storage medium. Unfortunately, such systems suffer from low efficiency (typically 8 to 10 percent) and therefore present large areas for any power level. Drag makeup is then a problem . In addition, solar cells are limited in life to 6 or 7 years from electron and high energy proton dammage, unavoidable consequences of either polar or high altitude orbits. Although the sun pointing requirement is not severe, the attitude control of large arrays is complicated by their high moments of inertia and by their lack of rigidity. However, these systems have logged more flight hours than any other and have the advantage of a very low technological risk. Their ideal application seems to lie with low power systems that operate in benign environments.

Solar thermal systems seem to offer an ideal solution for the projected power levels of a space platform. In the first analysis, they offer at least a 3.5 times decrease in system mass as compared to an equivalent solar electric system, with a threefold increase in system efficiency. This efficiency translates directly to threefold decrease in projected area for the same power output. Within the category of solar thermal systems, the choice of a specific thermodynamic cycle (Brayton, Rankine or Sterling) will affect the performance and specific mass (KG/KWe) of the power system. Of those mentioned, the author chose to investigate in some detail the Brayton cycle, as it responded most favorably to technological improvements with the least amount of

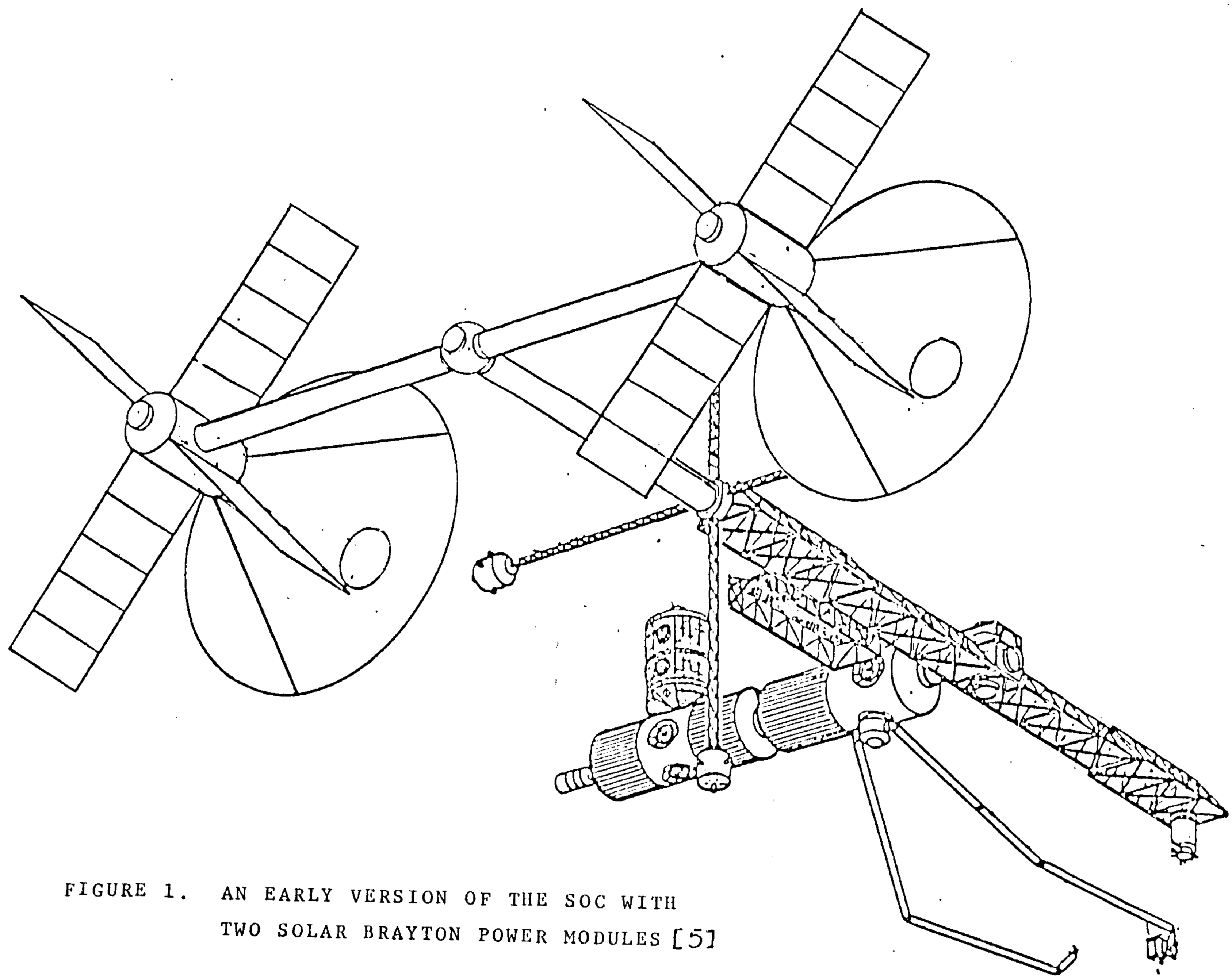

FIGURE 1. AN EARLY VERSION OF THE SOC WITH TWO SOLAR BRAYTON POWER MODULES [5]

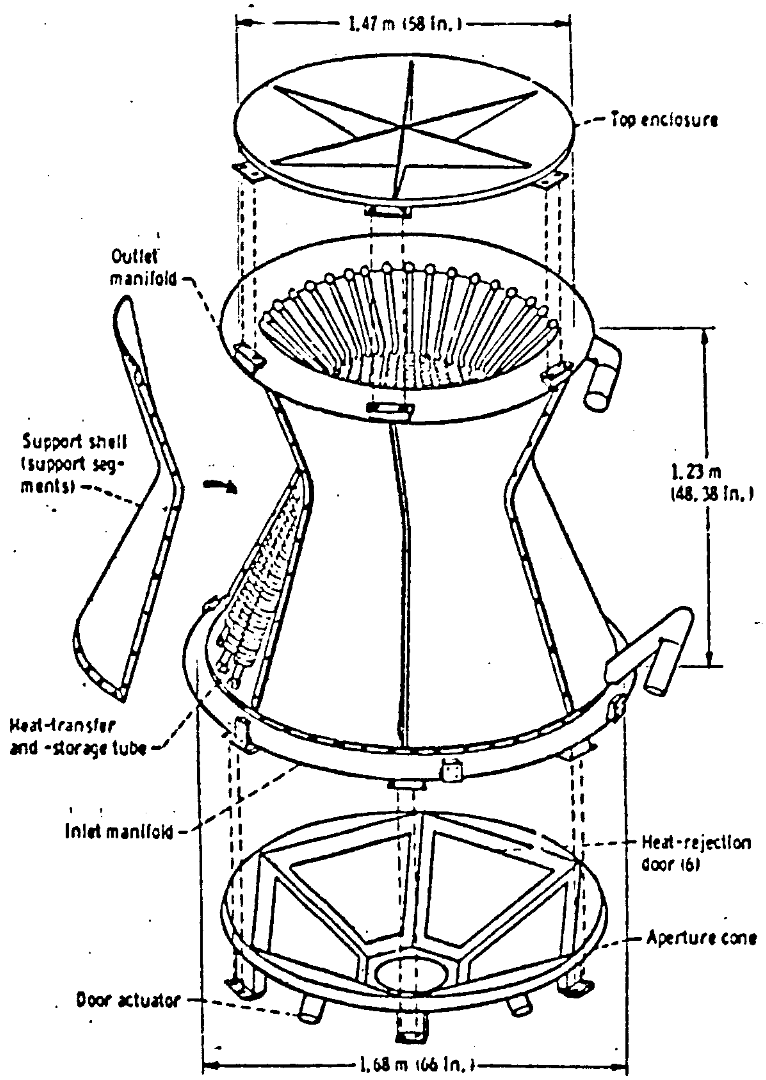

FIGURE 2. EXPLODED VIEW OF A BRAYTON RECEIVER [1]

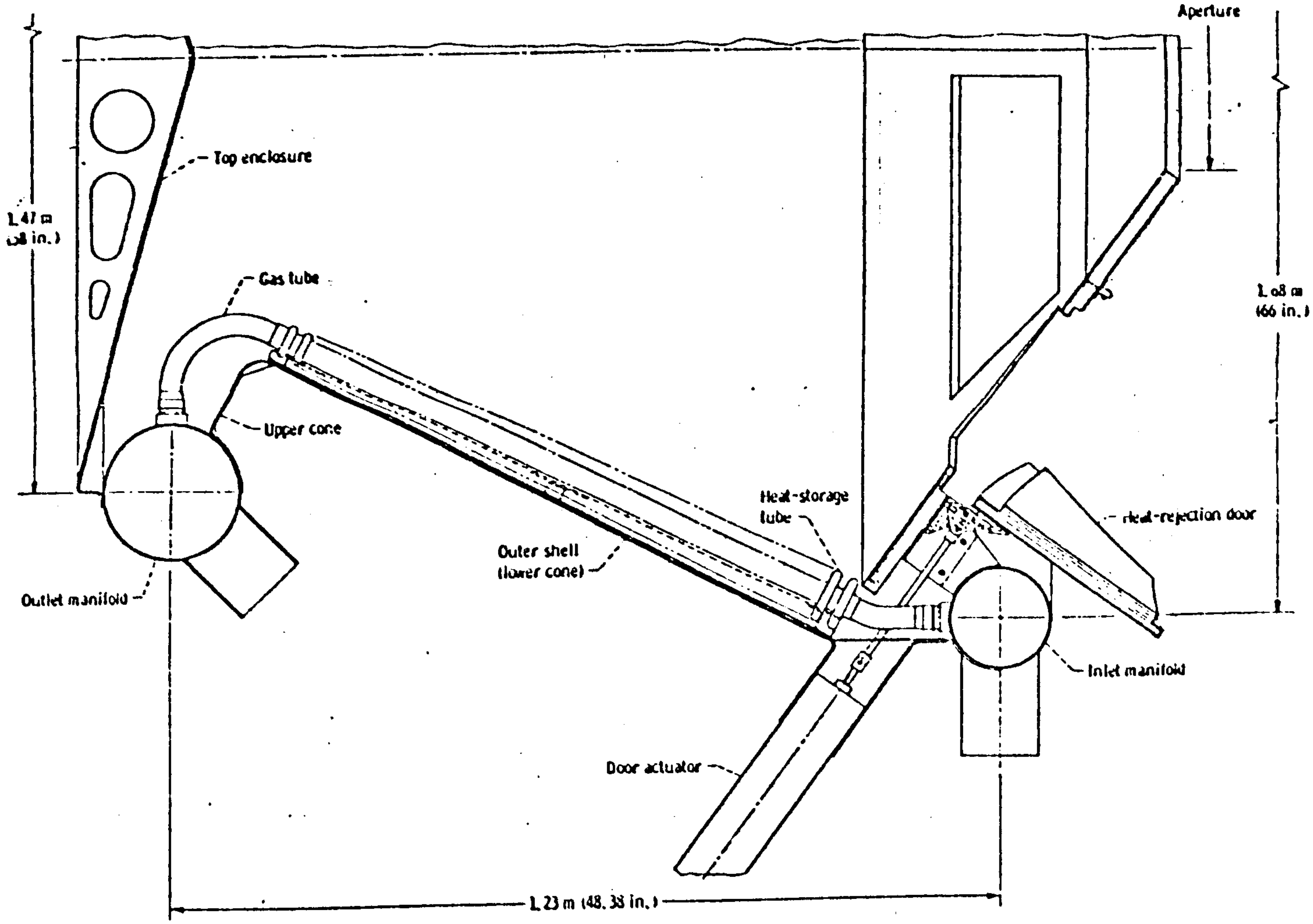

FIGURE 3. RECEIVER SECTION SHOWING HEAT STORAGE TUBE DETAIL[1]

uncertainty.

The design goal of any of these power systems is to meet the requirements with a minimum of cost. Since all of these systems would have to be boosted into low earth orbit, mass becomes the critical variable. Therefore this study optimized a particular Brayton cycle for maximum power and minimum mass. The resultant is not what one could achieve on earth where maximum efficiency probably would be more appropriate.

Figure 1 is an illustration taken from a MDAC study [05] of a space power system. Two redundant power units are connected via a gimbal to the rest of the structure. Each unit is comprised of a collector, a receiver, a rotating group of machinery, heat exchangers and waste heat radiators. The receiver, heat exchangers and the rotating group all are contained in the cylinder at the prime focus of the collector. The rotating group consists of a single stage centrifugal compressor, a single pole pair alternator and a single stage centrifugal turbine, all mounted on a common shaft. The working fluid in the cycle is a mixture of helium and xenon, which are noble gasses, combined to achieve a molecular weight of 40 g / mole. The mixture is inert to eliminate any potential oxidation problems.

An exploded view of the receiver is depicted in figure 2, illustrating the arrangement of tubes through which the working fluid circulates. Figure 3 shows one of these tubes in a little more detail, jacketed by a quantity of lithium flouride contained by another tube. The LiF serves as a heat storage medium during orbital shadow periods. As the satellite enters the earth shadow, all of the LiF is molten. During the transit time, this LiF gradually freezes, releasing the energy contained in the latent heat of fusion (1046 kJ/kg at 1121 K). At shadow exit, all of the LiF is frozen, and slowly starts to melt as sunlight enters the cavity. Figure 5 plots the heats of fusion vs. melting temperatures of other possible storage mediums.

The salient design feature of this system is the large temperature difference available across the cycle. This has been made possible largely by the development of advanced materials. Carbon/carbon composite turbines have been built and tested to 2200 K and 720 m/s rim speeds [12]. Silicon carbide, which melts at 3100 K [06] can easily serve as a high temperature structure. Additionally, it is considerably less dense than the refractory metals it replaces, saving mass. Materials compatibility constraints in the radiators force the minimum cycle operating temperature to 350 K. The effective temperature of the radiator is 470 K, which results in a small area (59 m). It is constructed of molybdenum and circulates a coolant mixture of potassium and sodium.

The next chapter models the thermodynamics of a regenerated Brayton cycle. These mathematical models are coded into a program that optimizes various parameters to minimize the system specific power.

The subsequent chapters take a closer look at the collection system performance, the turbomachinery and the radiator design. The radiator design itself is a complicated optimization that finds a particular configuration that minimizes its contribution to system mass.

The last chapters present the results of this study, along with a sensitivity analysis of the assumed component efficiencies and scaling constants. Finally, some conclusions are drawn and recommendations made based on the research of this topic.

Ch. 2 Regenerative Brayton Cycle Analysis.

The goal here is to quantify primary cycle performance in terms of two basic variables. The first is the ratio of maximum to minimum cycle temperature, θ_t ; the second is the compressor pressure ratio, π_c . These primary variables will be traded against each other to find a system configuration that will maximize the power output for a given mass. The design electrical power is 90 Kw. Other secondary variables such as compressor efficiency η_c , turbine efficiency η_t , regenerator and heat exchanger effectiveness ϵ_1 , ϵ_2 and system pressure drops π_s will then be varied within reasonable bounds for a sensitivity analysis. The initial mass estimates are taken from a MDAC report [05].

The quantity that is minimized is the sum of all of the individual contributions to the system mass: collector, heat storage, regeneration and radiator masses. The turbomachinery itself was considered negligible in the first analysis. Therefore,

$$\frac{Mtot}{Pe} = \frac{Mcoll}{Pe} + \frac{Msto}{Pe} + \frac{Mreg}{Pe} + \frac{Mrad}{Pe}$$

All of these terms are functions of cycle efficiency, so that will be derived first. Consider the schematic and T-S diagrams illustrated in figure 4.

We can start by defining the compressor temperature ratio, τ_c (T1/T0) and the turbine temperature ratio, τ_t (T4/Tm) in terms of the compressor pressure ratio, namely

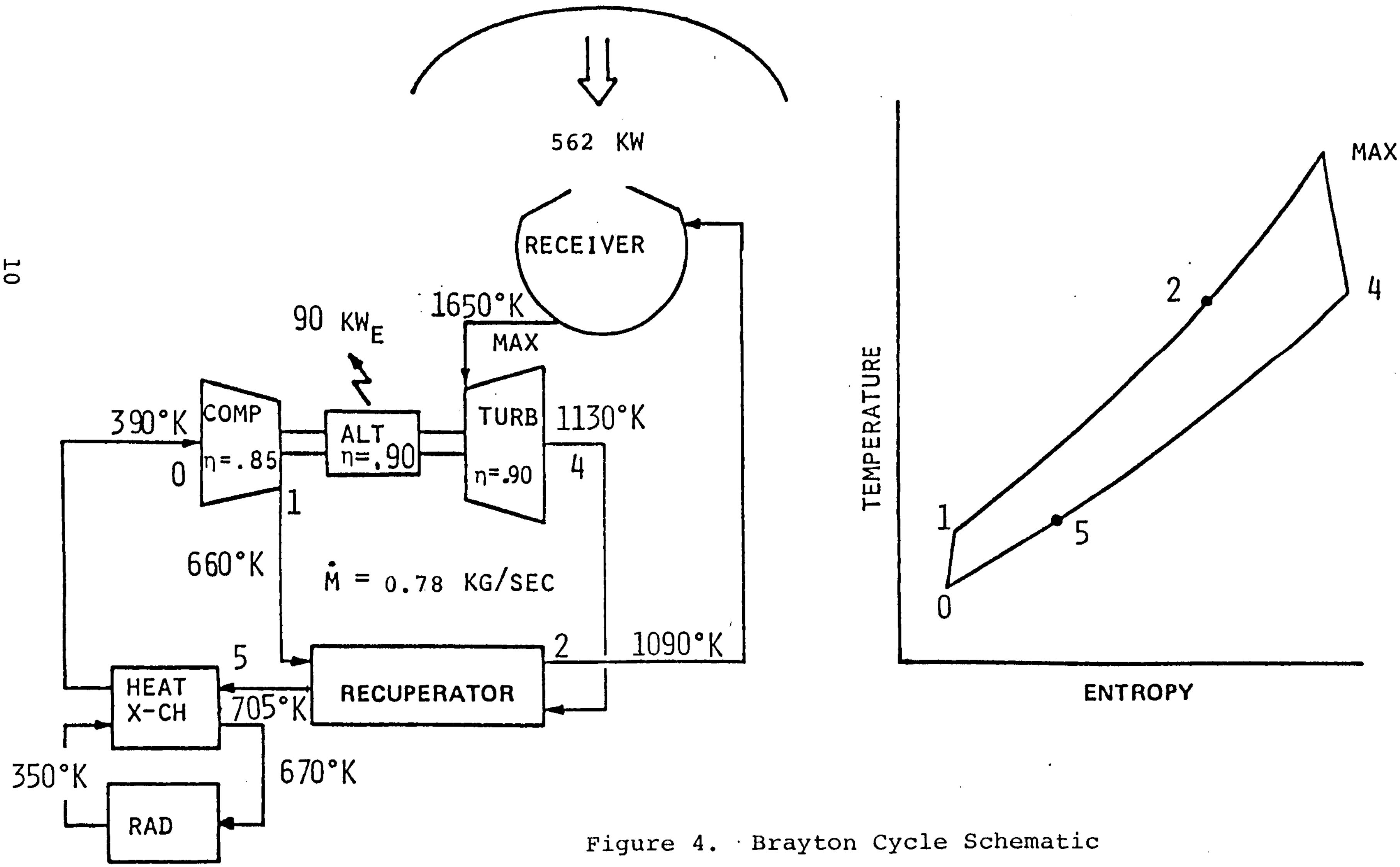

Figure 4. Brayton Cycle Schematic

$$\tau_c = 1 + \frac{\pi_c^{\gamma-1/\gamma} - 1}{\eta_c} \qquad \tau_t = 1 - \eta_t \left[1 - \left(\frac{1}{\pi_c \pi_s} \right)^{\gamma-1/\gamma} \right]$$

where γ is the ratio of specific heats (5/3) of the working fluid. The thermal efficiency is defined as the power extracted over the amount of heat inputted. The extracted power is the fraction of the turbine power that the compressor does not use. The heat input is the power added to the working fluid to take it from T1 to Tm. For low pressure ratio cycles, the turbine exit temperature is considerably higher than the compressor discharge tenperature. The regenerator takes that temperature differential and transfers it to the compressor output stream, thereby reducing the necessary heat input to accomplish the same work. The cycle then becomes more efficient. As the cycle pressure ratio increases, the benefit of regeneration diminishes, and can ultimately become a detriment (T1>T4).

Unfortunately, this transfer of heat is not ideal, and is limited by the heat exchanger effectiveness. It is defined as the actual temperature difference over the available temperature difference. The regenerator and waste heat exchanger effectivenesses become

$$\varepsilon_1 = \frac{T2 - T1}{T4 - T1} \qquad \varepsilon_2 = \frac{T8 - T7}{T5 - T7}$$

The shaft power becomes

$$Ps = \dot{m}\ Cp\ Tm\ (1 - \tau_t) - \dot{m}\ Cp\ To\ (\tau_c - 1)$$

$$\frac{Ps}{\dot{m}\ Cp\ TO} = W = \theta_t (1 - \tau_t) - \tau_c + 1$$

The electrical power is simply the the shaft power times the alternator efficiency. As mentioned before, thermal efficiency is the ratio of the power extracted over the amount of heat added. However, the heat that the cycle sees has been collected by the mirror and transferred to the working fluid through the heat storage medium. Therefore the cycle efficiency becomes

$$\eta_{cy} = \frac{Pe}{Qin} = \eta_{coll}\ \eta_{sto} \frac{\dot{m}\ Cp\ TO\ W}{\dot{m}\ Cp\ (Tm - T2)} \eta_{alt}$$

Then from the definition of regenerator effectiveness,

$$T2 = T1 + (T4 - T1)$$

$$\frac{T2}{TO} = \tau_c + \varepsilon_1 (\theta_t \tau_t - \tau_c)$$

And the cycle efficiency becomes

$$\eta_{cy} = \eta_{coll}\ \eta_{sto} \frac{\theta_t (1 - \tau_t) - \tau_c + 1}{\theta_t - \tau_c - \varepsilon_1 (\theta_t \tau_t - \tau_c)}$$

It is useful at this point to introduce a scaling variable μ, which represents the mass per unit area of that particular component. Proceeding with the collection system one can see that the area required to deliver a certain power is the ratio of electrical power over the product of the cycle efficiency and the solar constant (S) at 1AU.

$$Mcoll = \mu_{coll}\ Acoll = \mu_{coll} \frac{Pe}{S\ \eta_{cy}}$$

However, since there is a heat storage medium, the collector has to be oversized so that during insolation, it is providing enough heat to drive the cycle and liquify the heat storage substance. The heat is stored in the substances' latent heat of fusion. Therefore the collector is oversized by the ratio of the systems' time in shadow over the product of the time in sunlight and storage efficiency.

$$\frac{Mcoll}{Pe} = \frac{\mu_{coll}}{S\ \eta_{cy}} \left(1 + \frac{tsh}{tsun\ \eta_{sto}} \right)$$

One might note that the collector efficiency is a strong function of the surface quality of the mirror. Unfortunately due to its large size (24 m dia), it has to be constructed in segments (akin to those in an umbrella) and assembled by EVA. This process will have an unknown impact on collection system performance. Chapter 3 models the reflector physics and determines the effect of mirror surface quality, mirror rim angle, cavity temperature and aperture size on collection efficiency.

Next, we come to the heat storage medium. The literature suggests that at no time will the space platform be eclipsed for more than 36 minutes in LEO. Any heat storage medium will have to provide enough power during that period to insure steady stae operation. The medium should be sized so that at the start of the eclipse the substance is completely liquid, gradually freezing and releasing heat at its melting point. The substance chosen needs to be compatible with its containment vessel (no corrosion), needs a melting point slightly higher than the maximum cycle temperature and a high heat of fusion.

A plot of the viable candidates is shown in figure 5. Of these, silicon seems best with a melting point at 1685 K and a heat of fusion of 1787 kJ/kg. Then the mass per unit power becomes

$$\frac{Msto}{Pe} = (1 + Fsto)\,\frac{tsh}{\eta_{cy}\ hf}$$

where Fsto is the fraction of the storage mass needed to contain it. This includes the tube structure, the insulation, the aperture and cavity control devices and the receiver walls. This constant was chosen to be 120 percent after [06].

The next item of interest is the regenerator specific mass. If α_{reg} is the regenerator scaling variable (KG/KWt), then from the T-S diagram in figure 4, one can see that the regenerator mass is

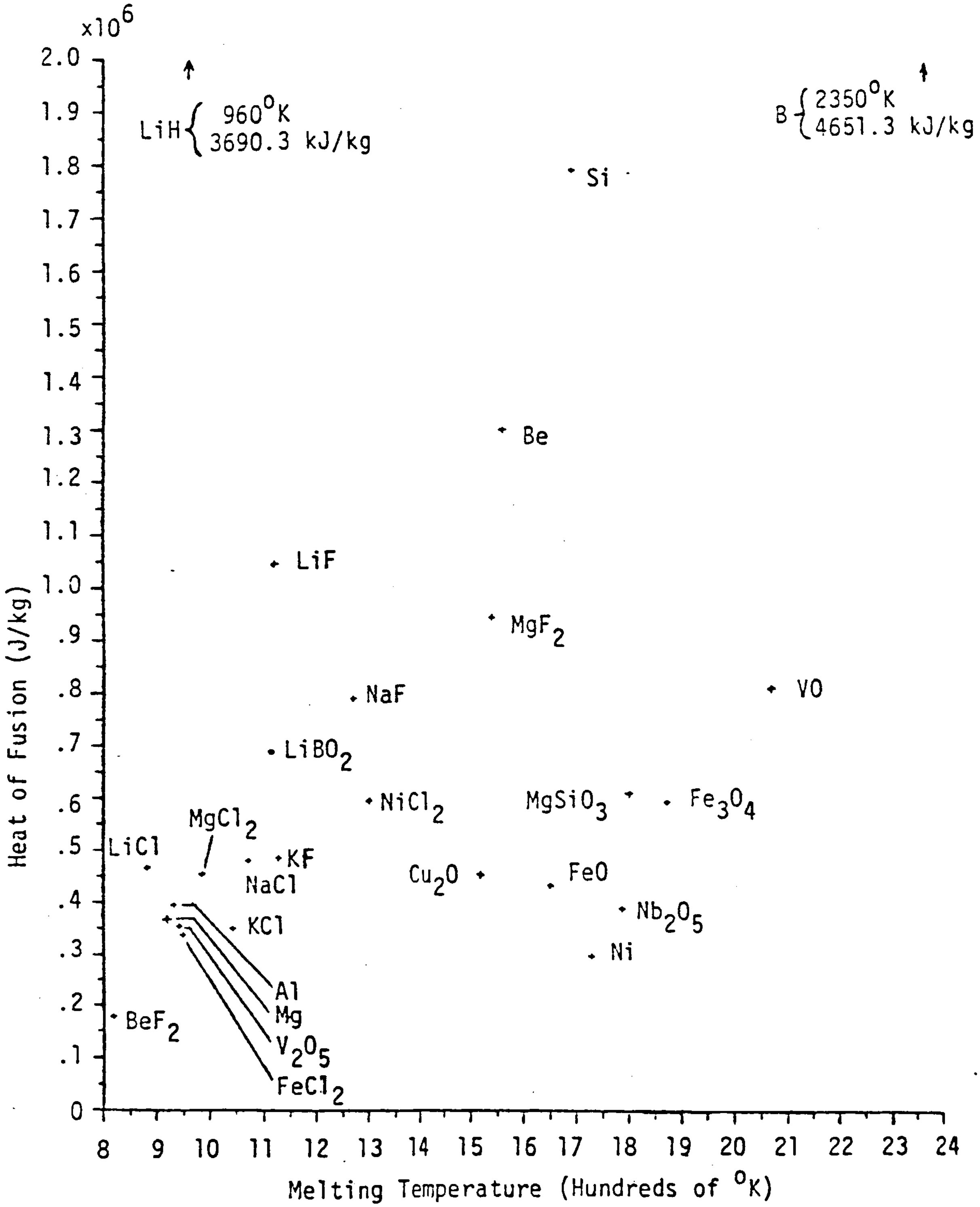

Figure 5. Heats of fusion vs. melting temperature for various substances. [6]

$$Mreg = \lambda_{reg} \, \dot{m} \, Cp \, (T2 - T1) = \lambda_r \, \dot{m} \, Cp \, Tm \, \varepsilon_1 \left(\tau_t - \frac{\tau_c}{\theta_t} \right)$$

Also, from the cycle efficiency calculation, the electrical power can be written as

$$Pe = \eta_{alt} \, \dot{m} \, Cp \, Tm \left(1 - \tau_t - \frac{\tau_c - 1}{\theta_t} \right)$$

Then the mass per unit power for the regenerator becomes

$$\frac{Mreg}{Pe} = \lambda_r \, \varepsilon_1 \left\{ \frac{\tau_t - \dfrac{\tau_c}{\theta_t}}{1 - \tau_t - \dfrac{\tau_c - 1}{\theta_t}} \right\}$$

The last item to consider is the radiator, the purpose of which is to dispose of nonusable heat. Careful attention needs to be paid to the design, as the bottom cycle temperature is a very strong driver of the physical size and mass. For the same useful power output, the higher the cycle temperature is pushed, the smaller the radiator becomes. So the size is set by the dissipation requirement, maximum cycle temperature, cycle efficiency and material choice.

For the purposes of the cycle optimization, a simplified model of a fin and tube design will be considered. Although chapter 5 presents the mathematical models to design the radiator, the program that incorporated these models took too long to execute, and prooved impractical to use as a subroutine in the larger cycle optimization.

For these purposes, only T7 and T8 are of interest. They are related to the main cycle temperatures through the heat exchanger effectivenesses, ε_1 and ε_2.

$$T_7 = \left(1 - \varepsilon_1 - \frac{\varepsilon_1 - 1}{\varepsilon_2}\right) T_4 + \varepsilon_1 \left(1 - \frac{1}{\varepsilon_2}\right) T_1 + \frac{1}{\varepsilon_2} T_6$$

$$T_8 = \left(2 + \varepsilon_1\left(\frac{1}{\varepsilon_2} - 2\right) - \frac{1}{\varepsilon_2}\right) T_4 + \left(2\varepsilon_1 - \frac{\varepsilon_1}{\varepsilon_2}\right) T_1 + \left(\frac{1}{\varepsilon_2} - 1\right) T_6$$

These, in turn can be written in terms of known cycle quantities.

$$\theta_7 = \frac{T_7}{T_m} = \left(1 - \varepsilon_1 + \frac{\varepsilon_1 - 1}{\varepsilon_2}\right) \tau_t + \varepsilon_1 \left(1 - \frac{1}{\varepsilon_2}\right) \frac{\tau_c}{\theta_t} + \frac{1}{\varepsilon_2} \frac{1}{\theta_t}$$

$$\theta_8 = \frac{T_8}{T_M} = \left(2 + \varepsilon_1\left(\frac{1}{\varepsilon_2} - 2\right) - \frac{1}{\varepsilon_2}\right) \tau_t + \left(2\varepsilon_1 - \frac{\varepsilon_1}{\varepsilon_2}\right) \frac{\tau_c}{\theta_t} + \left(\frac{1}{\varepsilon_2} - 1\right) \frac{1}{\theta_t}$$

An order of magnitude sizing would proceed as follows. Consider an incremental radiator section, pictured below.

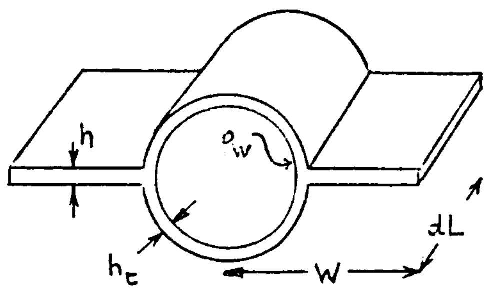

An incremental amount of heat convected out of the working fluid is

$$dQ = \dot{m}\, Cp\, dT$$

Similarly, an incremental amount of heat radiated away (with no background radiation) is

$$dQ = -2 \varepsilon \sigma T^4 dA$$

Equating the two and integrating, one obtains for the area of the radiator divided by the product of the mass flow and the coolant specific heat

$$\frac{Ar}{\dot{m}\, Cp} = \frac{1}{6 \varepsilon \sigma} \left(\frac{1}{Tout^3} - \frac{1}{Tin^3} \right)$$

where Ar is the ideal radiator area divided by the fin efficiency. The radiated power, Qr is

$$Qr = \dot{m}\, Cp \,(Tin - Tout) = Pe \left(\frac{1 - \eta_{th}}{\eta_{th}} \right)$$

Finally, the expression for radiator specific mass becomes

$$\frac{M_{rad}}{P_e} = \mu_{rad} \frac{1}{6 \varepsilon \sigma T_m^4 \eta_{FIN}} \frac{1 - \eta_{th}}{\eta_{th}} \left(\frac{1/\theta_7^3 - 1/\theta_8^3}{\theta_8 - \theta_7} \right)$$

This last expression is a good estimate of the radiator specific mass. The scaling constant was adjusted to match those results obtained in chapter 5 to preserve accuracy in the optimization. The models used in chapter 5 included the effects of an earth background radiation temperature of 270 degrees K.

All of the terms developed in the preceeding pages were coded into the program listed in the back pages of this chapter. The results from the optimization are discussed in chapter 6.

2.2 Working Fluid Molecular Weight

The choice of the working fluid molecular weight is again made with component masses in mind. The most sensitive parameter is the regenerator surface area, where working fluid to working fluid heat transfer is required. The number of turbomachinery stages required for a certain pressure ratio is also a function of the gas molecular weight with an attendant impact on turbomachinery complexity and mass. Similarly the aerodynamic efficiencies of the compressor and turbine will be affected. This last consideration will impact the cycle thermal efficiency and the waste heat load. Within the range of mixtures to choose from, inert gasses are employed to eliminate any potential contaminants from the turbomachinery. The turbine is made out of a carbon/carbon composite and might be sensitive to high temperature reactions.

Helium is a good choice because of its high thermal conductivity which is a driver for small heat exchanger surface areas. It unfortunately also has a high specific heat which, for a given pressure rise (or drop) tends to push a design towards an increasing number of stages. This is the primary trade-off. The solution to this problem is a mixture of He with some other inert gas. Neon, argon, krypton and xenon are all viable possibilities, but only mixtures of He and Xe result in minimal increases (from pure He) in heat

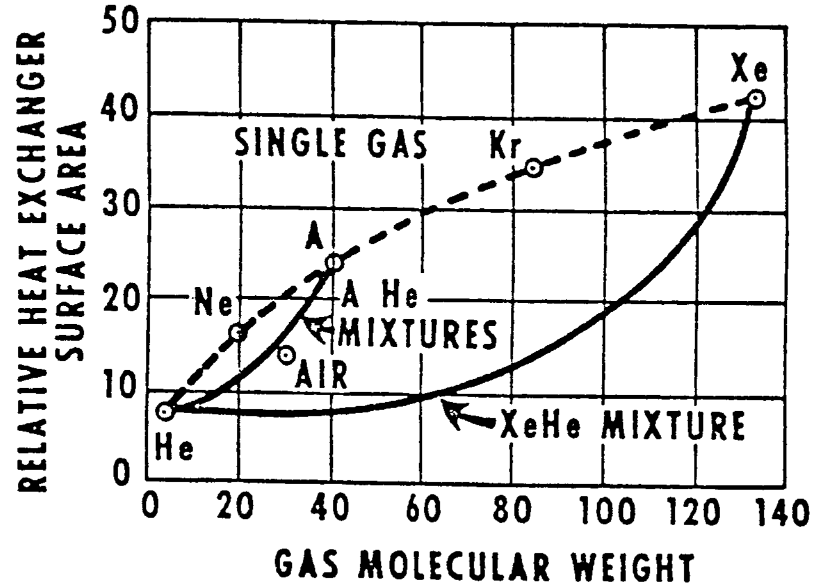

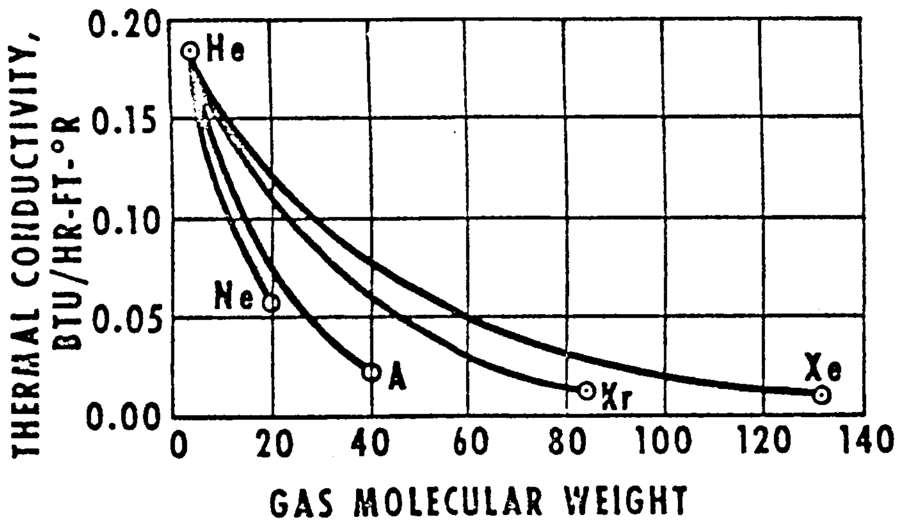

Figure 6. Effects of working fluid molecular weight on relative heat exchanger area and gas thermal conductivity [7]

exchanger area, since the thermal conductivity (for a given molecular weight) remains the highest of all of the mixes (see figure 6). As mentioned earlier, pushing the molecular weight of the mixture will increase the aerodynamic blade efficiencies in a component. This stems from an increased volumetric flow, an increase in blade height, which in turn reduces the endwall losses and thereby increases the stage efficiency.

Chapter 3 Collector Performance

3.1 Collector configuration

The collector of this system measures approximately 12 m in radius. Since the driving factor in making this system competitive is the high power to mass ratio, deployable configurations of the mirror were not considered. The actuating mechanisms would be eliminated, making EVA assembly mandatory. Prefabricated petals, or segments of the mirror would be carefully assembled, resulting in a better quality reflector than might otherwise be possible. Still the author felt it was necessary to study the effects of an imperfect mirror, to see what impact various errors might have on collector performance or system weight. In the first analysis, any misorientation more than half of the sun's projected angle would render the system completly useless. Fortunately, Kaykaty [13,14] has spent some time investigating this problem, and has identified 4 important variables to optimize collector efficiency. These are surface error, mirror rim angle, orientation error and receiver cavity temperature. His calculations were compared with a more accurate simulation given in ref[13] and the results did not differ by more than 1.5%. Unfortuneately, no comparisons were available with actual hardware. That notwithstanding, his methods were duplicated, albeit with some modifications.

When considering a collector system, two configurations come immediately to mind. The simplest is the single reflector, focusing all of the energy at the focal point, which would be the receiver aperture. The other would also consist of a parabolic reflector, but augmented by a secondary reflector, hyperbolic in shape, to bring the focal point behind the primary mirror. (See figure 07). From the structural dynamics viewpoint, the latter is best: all large masses (receiver, radiators and primary reflector) are concentrated in a single area. Low frequency vibrations caused by Shuttles or OTV's docking with the space station would have a minimal effect on optical alignment. Unfortunately, optical quality will be worse since there are two reflectors and second surface longevity would be a problem. This is due primarily to some pretty severe temperature cycling during an orbital period. All of the primary surface's energy is getting reflected by the second surface, which would absorb some of the enegy and reach a high equilibrium temperature before cooling off in the earth shadow. Additionally, it is uncertain whether the blockage due to the radiators and receiver would be any greater than that of the secondary reflector. In light of these factors the simple single reflector system was chosen.

A quick scan of figure 07 will show that approximately half of the energy dissipated by the radiators will sink into the primary reflector. So to check on steady state dish temperatures for both configurations, we can write an energy balance and solve for the temperature

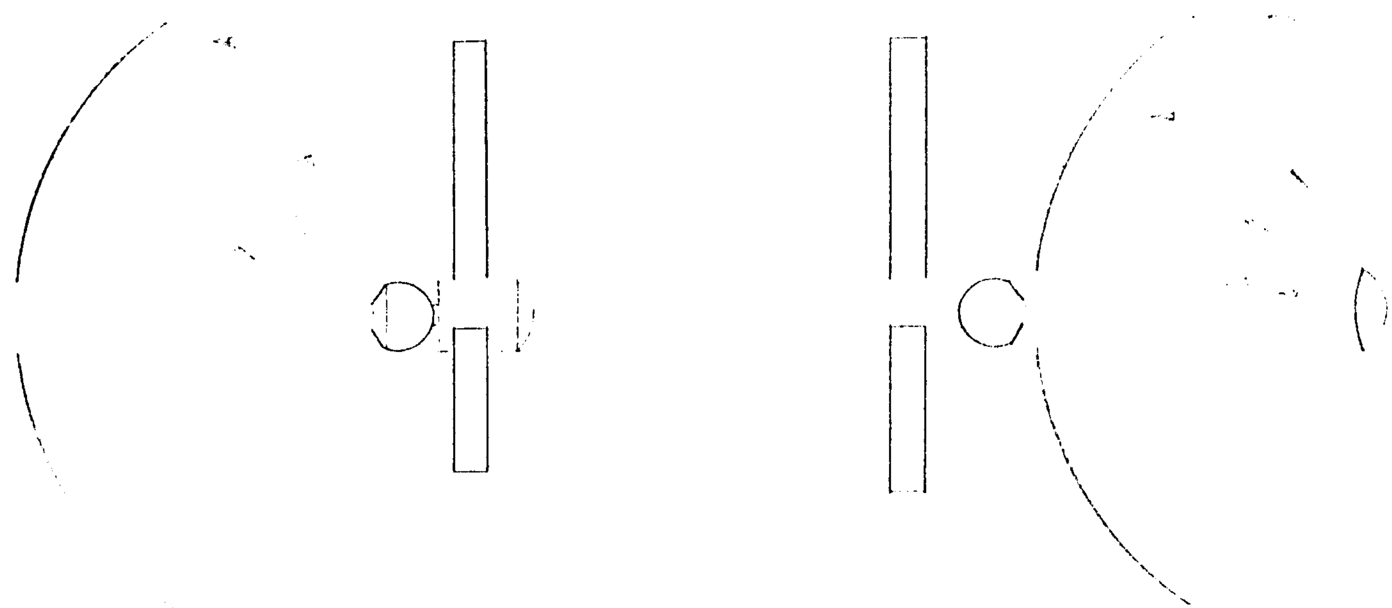

Prime focus

Cassegrain focus

Figure 7 . Two Solar Brayton Power System configurations

$$Pr = Pa + Pd \qquad [C01]$$

where: Pr is the radiated power

Pa is the solar absorbed power

Pd is the radiator dissipated power.

For the single reflector,

$$2 \pi R_m^2 \, sig \, ep \, T^4 = \pi R_m^2 K a + a \frac{90 \text{ KWe}}{2} \frac{1 - Nth}{Nth} \qquad [C02]$$

The nomenclature contains the variable names and meanings. Solving for T

$$T^4 = \frac{K a}{2 \, sig \, em} + \frac{90 \text{ KWe}}{4 \pi R_m^2 \, sig} \frac{a}{em} \frac{1 - Nth}{Nth} \qquad [C03]$$

For silver coated fused silica with an overcoat of vapor deposited Inconel, a = .05 and em = .80. Assuming a cycle efficiency of 25%, (conservative for this system) then the steady state temperature reaches 194 degrees K. The thermal transients during an orbital period are found by solving

$$Qin - Qout = m \, Cp \frac{dT}{dt} \qquad [C04]$$

Since this power system produces energy continually during an orbit, the radiators will dissipate the same power in the shade as in the sun. There is also earth background infrared radiation to consider, but it will be ignored for a maximum transient analysis. So this results in a non linear equation of the form

$$\frac{dT}{dt} = a \frac{90\ KWe}{2} \frac{1 - Nth}{Nth} \frac{1}{m\ Cp} - \frac{2\ pi\ Rm^2\ sig\ em\ T^4}{m\ Cp} \qquad [C05]$$

The presence of the radiator power makes the equation difficult to solve analytically, so a Runge Kutta method was used so solve for T(t). A good figure for collector mass is 2.1 kg/m^2. And Cp(Al) = 896 J/(kg K). Low earth orbit dictates a maximum shadow time of 38 min., and so substituting all the relevant variables gives a value for the minimum temperature of the dish equal to 139 degress K. So thermal transients remain reasonable at 55 degrees K. Repeating this calculation for the secondary mirror (radius = 1 m) of the Cassegrain arrangement, one finds that the steady state temperature is 673 degrees K and that the temperature at shadow exit is 392 degrees K. This gradient is more serious at 281 degrees, grounds enough to justify a single reflector system.

One other phenomenon that will affect collector life was recently observed on STS 4. An experiment was conducted to see if there was any material erosion in LEO, due to free oxygen impacting at orbital velocities, thereby oxidizing the surface . Polished surfaces were exposed in different directions to the flight velocity vector to quantify the effect.

Assuming the material being eroded is aluminium, an erosion rate of up to 40 microns per day was calculated at an orbital altitude of 241 kms. At 420 kms, this rate went down by 2 orders of magnitude. Either way, a mirror whose design life is supposed to be ten years would never last. Solar cells are typically protected with a thin (0.15 mm) coating of quartz. A similar coating might have to be applied at a penalty of about 0.4 kg/m^2.

3.2 The effect of imperfections

The analysis in [13] is outlined as follows. Given the geometry shown in figure 08, it is clear that any errors (misalignment or statistical) will diffuse the energy over a larger area in the focal plane. Additionally, the sun is not a point source, so the image at the focus will have a finite size, depending on the mirror's optical geometry. Any aperture located in the focal plane will have to capture as much energy as possible while limiting the amount of re-radiation coming out of the cavity. The latter is driven primarily by the operating temperature of the receiver to the forth power and directly as the aperture area.

The thermodynamic cycle efficiencies will dictate the amount of power needed in the cavity, which in turn is a function of the mirror radius and achievable collection efficiency. Since scaling relationships between mirror mass and surface quality aren't readily available, the intent of this analysis is to determine a maximum acceptable error

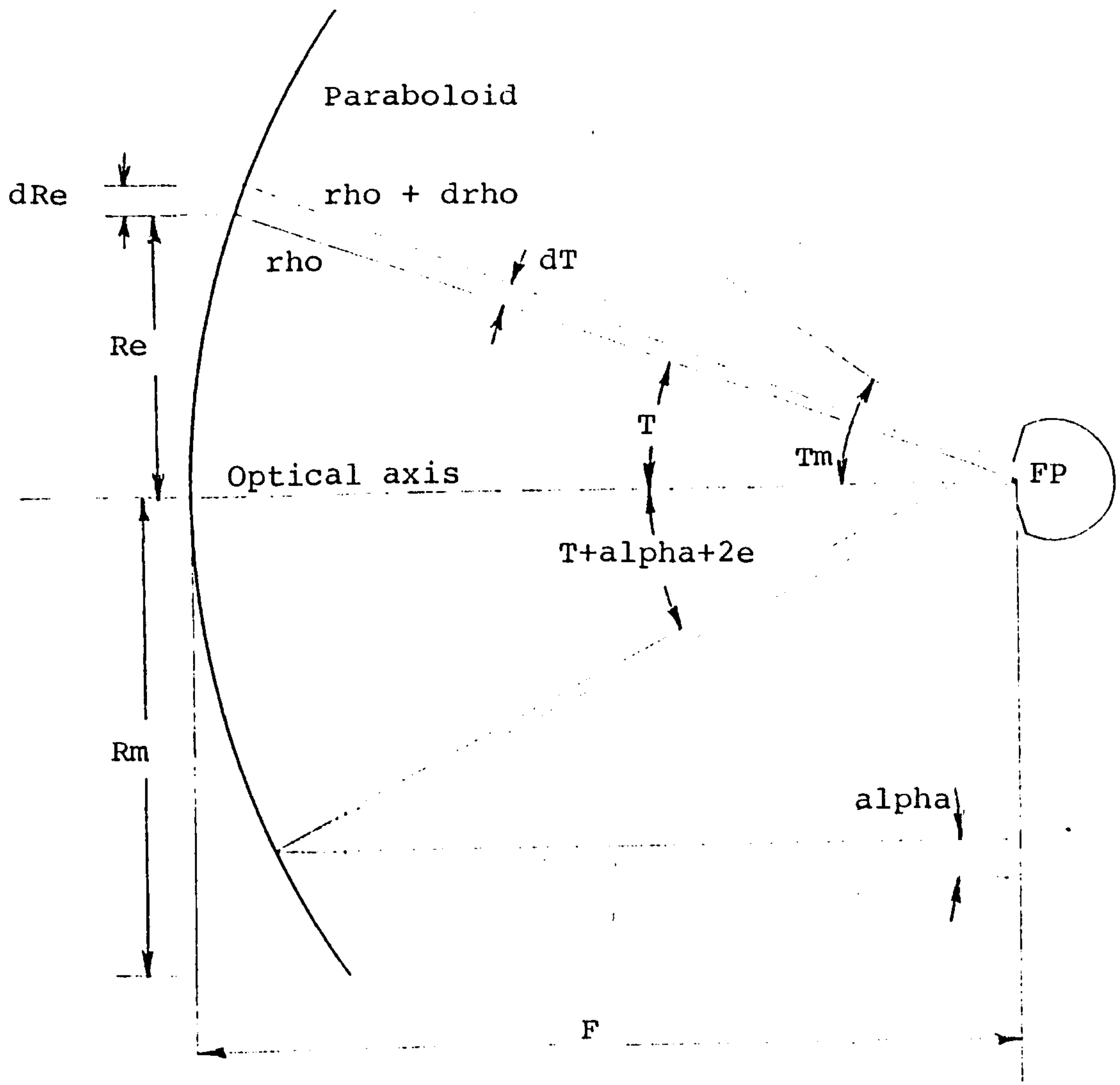

Figure 8. The mirror and associated optics

before collector mass penalties become too great.

As mentioned before, Kaykaty determined that the two key geometrical variables are the mirror radius Rm and the rim angle Tm. These combine to form an expression for the focal length, F

$$F = \frac{Rm\ (1 + \cos(Tm))}{2 \sin(Tm)} \qquad [C06]$$

The equation for a parabola with its origin at the focus is

$$rho = \frac{2\ F}{1 + \cos(T)} \qquad [C07]$$

where rho is the distance from the focus to any point on the surface and T measures the angular position of that point. Restricting the analysis for the present to the perfect mirror, it is clear by referring to figure 08 that if a reflected image of the sun from any point on the surface is viewed normal to the image path, that image will form a circle. At the focal plane, this same image will form an ellipse whose semi-major axis is a function of T. If alpha is defined as the half angle of the sun at 1 AU then the axes are given by

$$b = rho \tan(alpha)$$

$$a = \frac{rho \tan(alpha)}{\cos(T)} \qquad [C08]$$

It makes sense then that the higher the rim angle of the collector, the more diffuse the image will be in the focal plane. As one rotates around the optical axis with a constant T, the image formed at the focal plane will consist of a set of superimposed ellipses all with their origins at the focus. If K is the solar constant, the amount of energy that this swept ring intercepts is simply

$$Ee = K\ 2\ pi\ Re\ dRe \qquad [C09]$$

In polar coordinates

$$Re = rho\ \sin(T)$$

$$dRe = rho\ \cos(T)dT + \sin(T)d(rho) \qquad [C10]$$

$$d(rho) = \frac{rho\ \sin(T)\ dT}{1 + \cos(T)}$$

Upon substitution, eqn[C10] becomes

$$dRe = rho\ \cos(T)\ dT + \frac{rho\ \sin^2(T)\ dT}{1 + \cos(T)}$$

$$= rho\ dT \qquad [C11]$$

Substitution into [C09] gives

$$Ee = 2\ pi\ K\ rho^2\ \sin(T)\ dT \qquad [C14]$$

Integrated from T=0 to Tm this last expression should equal the mirror's projected area times K.

Now since the optimum aperture radius is smaller than the largest of the ellipses axes, not all of the reflected energy is going into the receiver. The presence of any errors will scatter the reflected energy even more over the focal plane, by displacing the centers of the ellipses away from the focal point. The two kinds of errors considered are the statistical surface errors and misorientation error. The surface errors exist as manufacturing imperfections, assumed to follow a normal distribution of 0 mean and some specified standard deviation. As data points, NASA Lewis built a 6.1 m (20 ft) diameter Mg mirror to a 1 sigma value of 1 mrad which massed at 5 kg/m^2 and later, TRW constructed a 0.9 m (3 ft) diameter mirror to 0.3 mrad at 1.3 kg/m^2. For this analysis, the author believes that a 24 m (79 ft) diameter mirror could be built to 1 mrad at 2.1 kg/m^2.

Reference [13] displaced the ellipses only radially away from the focal point, which results in a symmetrical energy distribution around the focal point. This simplifies the analysis, but results in a slightly optimistic level of performance. Consult figure 09. This treatment also makes the analysis of a misoriented system easier as will be discussed. This displacement distance is given by

$$k = \frac{\text{rho} \tan(2\ e)}{\cos(T)}$$

where e is the average error of a narrow band within the statistical distribution of errors.

Now the task at hand is to determine what fraction of a given

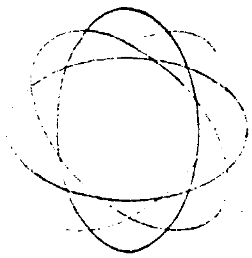

Image superposition in focal plane
for a perfect mirror

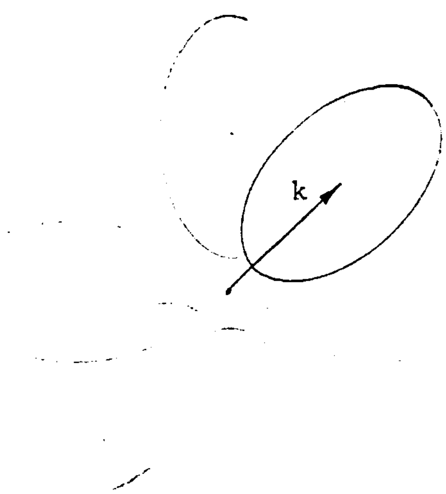

Image superposition in focal plane
for an imperfect mirror

FIGURE 9.

ellipse's area is coincident with the aperture. The simplest way to do this is to perform an integration from 0 to the aperture radius of circular elements that lie within the domain of the ellipses. Several configurations of circular elements and ellipses are possible. Consult figure 10. The progression outlined by cases 1-4 represents different criteria for computing Xi r, the arclength of a circular element common to the circle and the ellipse as one integrates dr from 0 to the aperture radius.

Case 1 holds when the circle lies within the domain of the ellipse. Figuring exactly when this is the case is easier to do when the equation of the ellipse is recast in polar coordinates

$$\left(\frac{x - k}{a} \right)^2 + \left(\frac{y}{b} \right)^2 = 1$$

let $x = r \cos(T)$ $y = r \sin(T)$

$$s = \left(\frac{a}{b} \right)^2 \qquad q = \left(\frac{a}{b} \right)^2 - \left(\frac{k}{b} \right)^2$$

Then solving for r, one obtains

$$r = \frac{k \cos(T) + a \operatorname{sqrt}(q + \cos^2(T) (1 - q))}{s + (1 - s) \cos^2(T)} \qquad [C13]$$

There are really two solutions for r, + and -, the latter having no physical meaning. Taking the derivative of r wrt T will lead a minimum of r and where it is located. Refer to

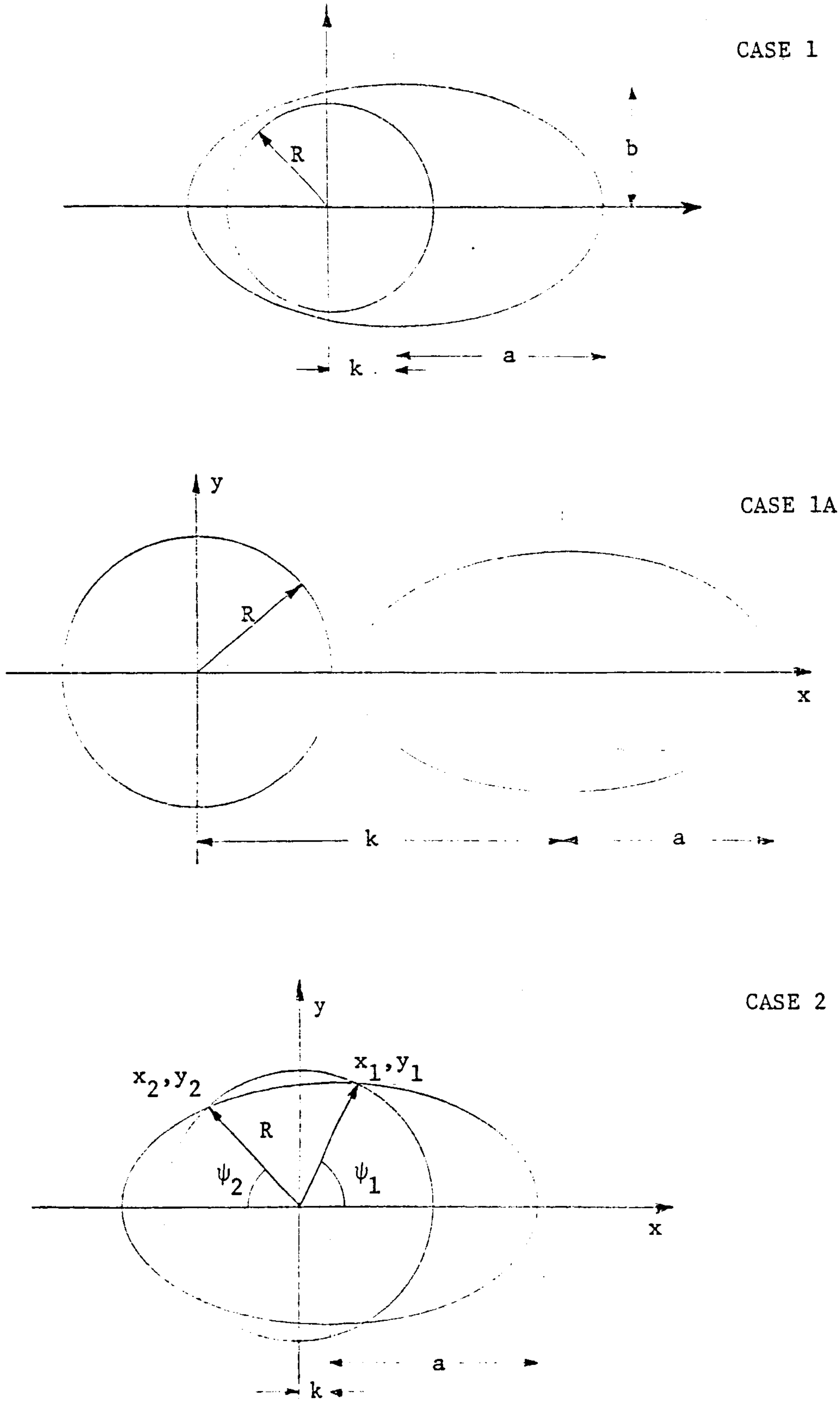

FIGURE 10

CASE 3

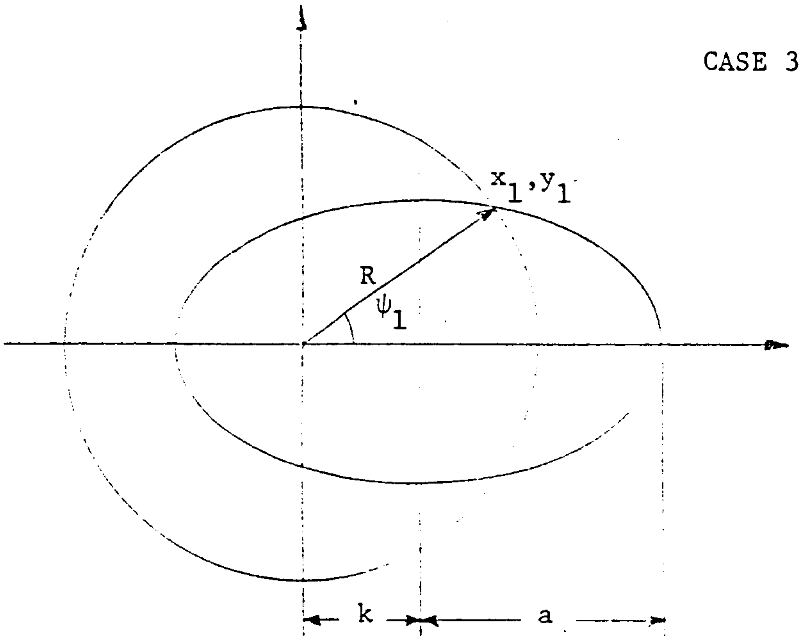

CASE 4

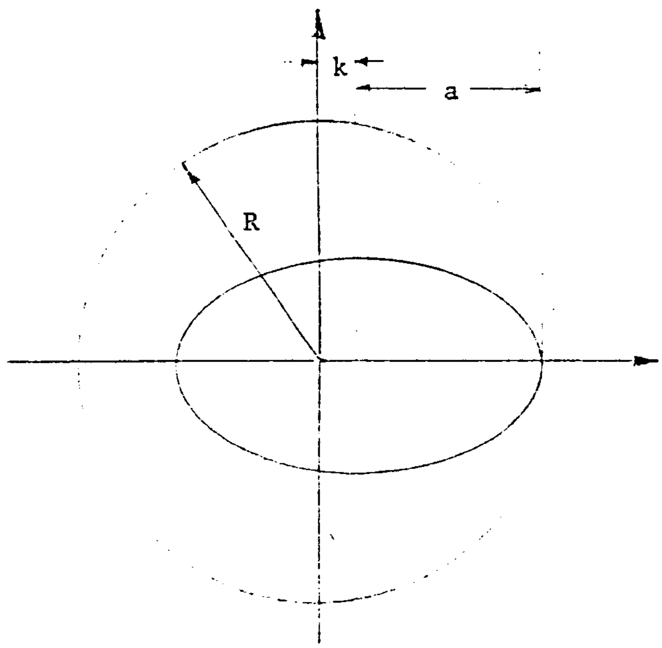

FIGURE 10 (cont.)

figure 10.

$$\frac{dr}{dT} = \frac{-\sin(T)}{[\, s \sin^2(T) + \cos^2(T)\,]^2} * \qquad [C14]$$

$$\left(\frac{a \cos(T)\ (1-q)}{\mathrm{sqrt}(\, q + \cos^2(T)\ (1-q)\,)} + k \right) \left(s + (1-s) \cos^2(T) \right)$$

$$- \; 2 \cos(T)\ (1-s)\ (\, k \cos(T) + a\ \mathrm{sqrt}(\, q + \cos^2(T)\ (1-q)\ )\ )$$

Finding the T's for dr/dT to be zero is not easily accomplished analytically, hence a numerical scheme such as the secant method has to be used. Once the correct solution is found, reinserting T into eqn C13 will yield the maximum radius for a circle to be completely inside the ellipse. Hence the value of the arclength will be

$$S = 2\,\mathrm{pi}\ r$$

Case 1a exists when the ellipse starts out beyond the reach of r. The test for this case is when $r < (k-a)$. And the arclength is simply zero.

Case 2 needs to be treated a bit differently, since Xi/pi is less than 1 and is a function of geometry. This situation holds when $r <$ abs(k-a) and when $r < k+a$. Here it is convenient to solve for the coordinates of the intersection of the circle and ellipse. Given their well known formulas,

$$y^2 = r^2 - x^2 \quad \text{and} \quad y^2 = b^2 - \left(\frac{b}{a}\right)^2 (x - k)^2$$

and setting them equal to each other results in an equation for x .

$$x = \frac{-k b^2 + \mathrm{sqrt}\,(b^4 k^2 - (a^2 - b^2)(a^2 b^2 - b^2 k^2 - a^2 r^2))}{a^2 - b^2} \qquad [C15]$$

Note that the result is different than the one presented in [1]. There are two solutions as expected.

[C16]

$$Xi_1 = \cos^{-1}\left(\frac{x1}{r}\right) \qquad Xi_2 = \cos^{-1}\left(\frac{x2}{r}\right)$$

Therefore the swept arclength that lies within the ellipse is

$$S = 2 r (Xi_1 + Xi_2)$$

Case 3 is similar to case 2 save that only one solution of x is valid. This case is treated when r > abs(k-a) and r < k+a. The negative value of x is simply discarded. Then the arclength becomes

$$S = 2 r \cos^{-1}\left(\frac{x}{r}\right)$$

Case 4 is the simplest. If r > (k+a) then S is zero.

After the arclength has been found for a particular configuration, the following yields the fraction of the ellipse's area that has entered the aperture

$$\frac{1}{\pi a b} \int_{0}^{R_a} S\, dr \qquad [C17]$$

Combining the relevant equations [C11, C17] to come up with the total power in the aperture yields

$$P_{ap} = 2 \pi K \int_{T_0}^{T_m} \left(\frac{1}{\pi a b} \int_{0}^{R_a} S\, dr \right) \rho \sin^2 (T)\, dT \qquad [C18]$$

where TO has been changed from 0 to account for the receiver blockage. The energy efficiency of a particular configuration would be the power going in the aperture divided by the amount of energy being intercepted by the dish.

$$N_e = \frac{2}{\pi R_m^2} \int_{T_0}^{T_m} \left(\frac{1}{a b} \int_{0}^{R_a} S\, dr \right) \rho \sin^2 (T)\, dT \qquad [C19]$$

Misorientation error, which can be thought of as either power system misalignment with the sun or mirror-receiver misalignment, will spread out to an even greater degree the energy in the focal plane. The equation above needs to be modified slightly to account for the effective shift in aperture location. If d quantifies this shift, the interior equation in [C22] changes to

$$\frac{1}{a b} \int_{0}^{R_a + d} \frac{\phi}{\pi} S\, dr$$

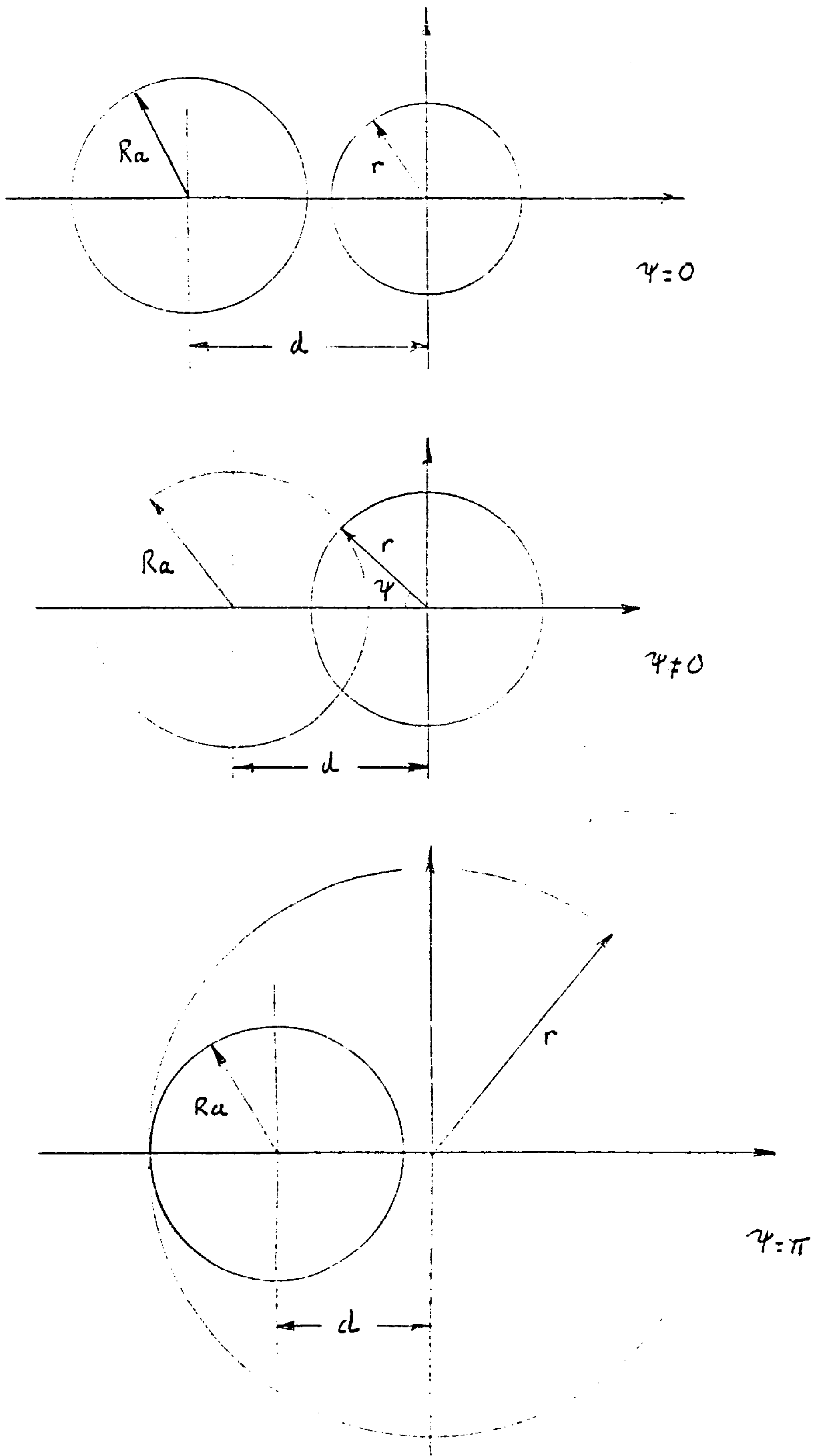

Figure 11. Misaligned aperture geometries in the focal plane.

provided that the energy distribution remains symmetrical about the origin. The shift distance (check figure 11) is quantified by

$$d = F \tan(m) \qquad [C20]$$

For small angles of misorientation, the ellipse displacement k, need not be modified. The ratio phi/pi is found by solving for the intersecting points of the periphery of the aperture and an arbitrary circle of radius r

$$x^2 + y^2 = r^2 \qquad\qquad (x + d)^2 + y^2 = r^2$$

Equating y's and solving for x and phi

$$x = \frac{Ra^2 - r^2}{2\,d} - \frac{d}{2} \qquad [C21]$$

$$phi = \cos^{-1}\left(\frac{x}{r}\right)$$

So once again the energy efficiency with error modeling becomes

$$Ne = \frac{2}{pi\ Rm^2} \int_{To}^{Tm} \left(\frac{1}{a\ b} \int_{0}^{Ra+d} \frac{phi}{pi}\ S\ dr \right) rho\ \sin^2(T)\ dT \qquad [C22]$$

The concentration efficiency is a product of the blockage efficiency, mirror coating efficiency energy efficiency and the effective solar absorptivity of the receiver. However, the receiver can be thought of as a blackbody, so the absorptivity is set to 1. To get the collection efficiency, one needs to include the radiation losses out the aperture. These are

$$Lr = \frac{em\ sig\ Aap\ Tr^{4}}{pi\ Rm^{2}\ K} \qquad [C23]$$

So the overall collection efficiency becomes

$$Nc = Nb\ Nr\ Ne - Lr \qquad [C24]$$

One needs to remember that this efficiency is solely a function of one error e, and one misorientation angle, m. As mentioned before the surface errors behave in a normally distributed manner. So, picking a certain standard deviation, one proceeds to divide up the mirror into specific error bands, each having a certain probability of existing. Then the computation for Ne is run for each error band's average e and for 5 or 6 different aperture to mirror radius ratios. A table can be constructed with all these values, as exemplified in tables 1 - 15. Next all the energy efficiencies common to a certain radius ratio are multiplied by their probability of occurence and then summed. The results of these summations can be plotted for clarity. If the radiation these summations can be plotted for clarity. If the radiation losses are subtracted from these curves, then an optimum collection efficiency should appear at some specific aperture radius. All this computation is for one specific mirror geometry and cavity temperature. The latter is invariant at 1750 degrees K from the cycle analysis. The former is a matter of choice, insofar that the power constraints are satisfied. For a good first guess [16] presents a quick method to find the optimum mirror rim angle, provided that there are no errors, which works out to be 45 degrees.

3.3 Program Results

Figure 12 shows the sensitivity of collection efficiency as a function of misorientation for a given mirror geometry and surface quality. The data is represented in this fashion to show the impact of pointing accuracy on the collection system efficiency. One should notice that the higher the mirror rim angle, the less sensitive the collection efficiency is to variations in pointing accuracy, at the expense of some collection efficiency. A reasonable compromise would be to design the mirror with a rim angle of 55 degrees. Without additional knowledge of mirror quality vs mass, any cycle optimization algorithm will try and drive mirror surface error to 0. Therefore it must be fixed to some reasonable value, say 1 sigma = 1 milliradian. Reference [17] has investigated the effects of higher surface errors and reports that collection efficiency drops to about 64% at 4

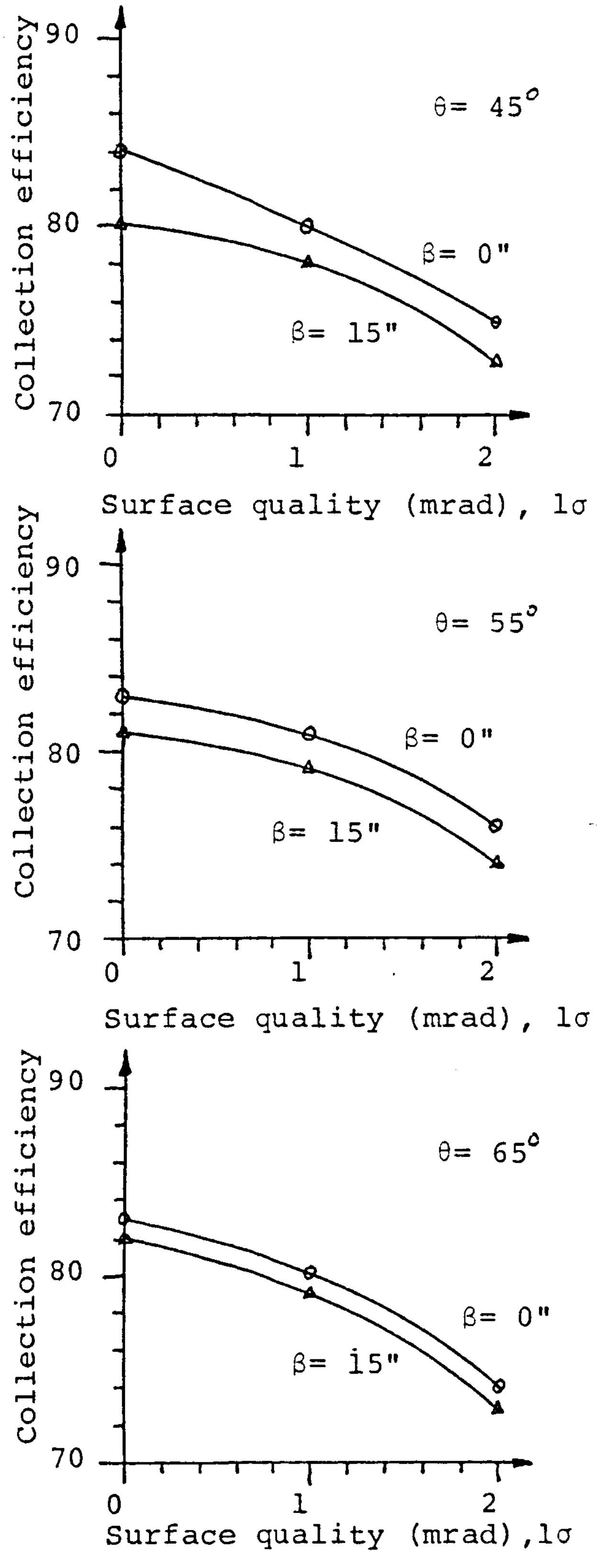
Collection efficiency
90
80
70
θ= 45°
β= 0"
β= 15"
0
1
2
Surface quality (mrad), 1σ
Collection efficiency
90
80
70
θ= 55°
β= 0"
β= 15"
0
1
2
Surface quality (mrad), 1σ
Collection efficiency
90
80
70
θ= 65°
β= 0"
β= 15"
0
1
2
Surface quality (mrad),1σ

Figure 12α.

mrad error and 40% at 8 mrad error if the cavity temperature is held at 1800 degrees K. For a surface quality of 1 mrad, one can acheive a collection efficiency of 81% with some tolerance for misalignment error. The optimum aperture radius to choose is then 14 cm.

Figure 12 b shows some of Kaykaty's work for the same collector. The effect of misaligning the mirror by half of the sun's projected angle at 1 AU (15 min) is clearly shown. The performance is penalized by about 6%. As a matter of interest, the space telescope can achieve sub second pointing accuracy. It is unreasonable to expect a space platform with shifting masses abord to maintain that kind of accuracy. So the author felt that some misalignment error had to be included in the design stage.

Due in part to some differences in the equations, the author's computed values for " in aperture energy efficiency " were somewhat larger (3%), but these differences weren't discernible when collection efficiency was found.

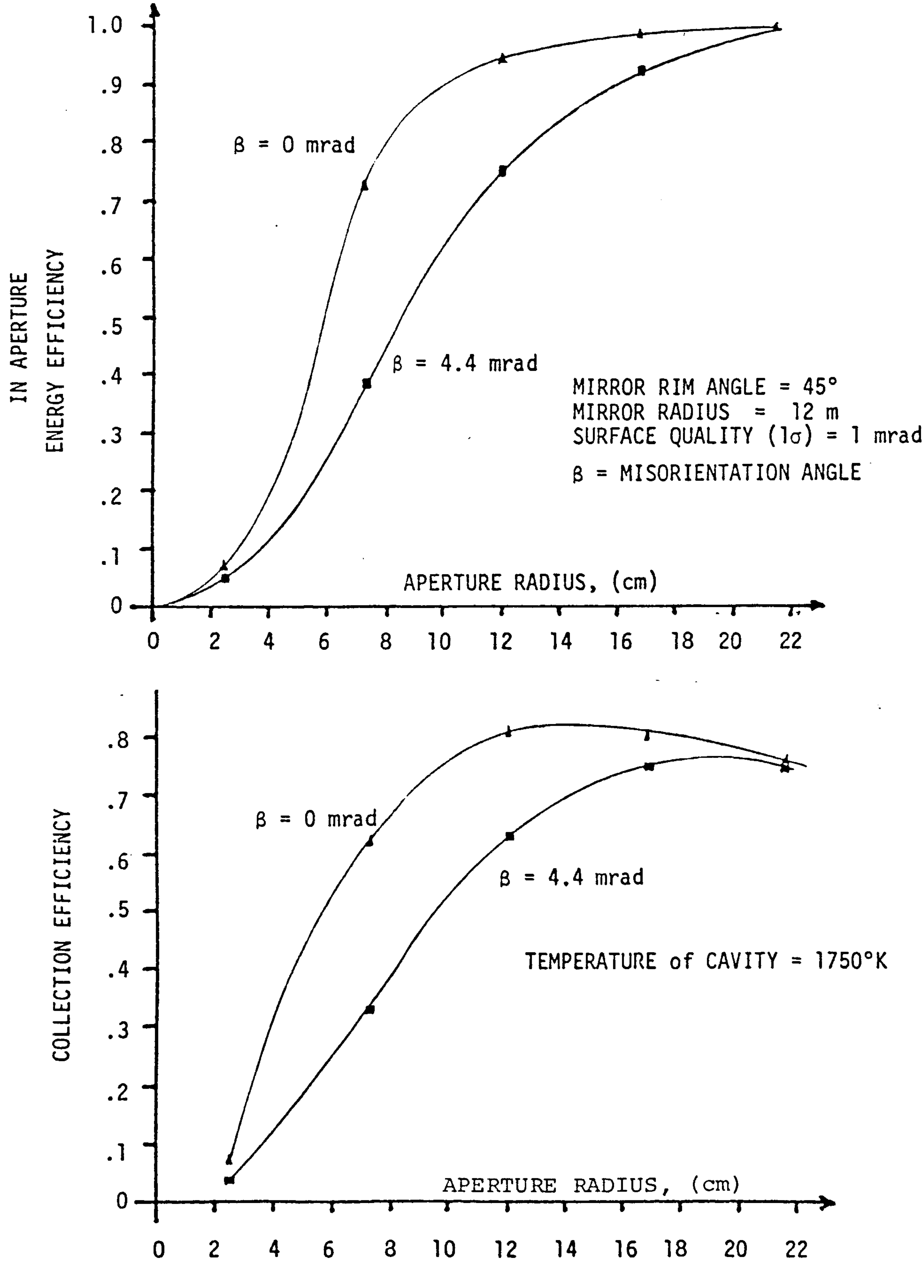

Figure 13. Energy and collection efficiency as a function of receiver aperture radius [13]

TABLE 1

Tabulated values of energy efficiency (η_E) and collection efficiency (η_c) for a 12 m, 30° rim angle and 1 mrad standard deviation mirror.

No misorientation error.

Energy efficiency
as a function of mirror error and aperture to receiver radius

Average error (mrad)	r_a/r_m					Probability of occurence
	.002	.006	.010	.014	.018	
.1	.04	.41	.98	.99	.99	.15850
.3	.04	.41	.95	.99	.99	.15234
.5	.04	.41	.90	.98	.99	.14064
.7	.04	.41	.85	.98	.99	.12480
.9	.04	.41	.80	.98	.99	.10640
1.1	.04	.39	.74	.97	.99	.08718
1.3	.04	.36	.69	.95	.99	.06862
1.5	.04	.32	.64	.92	.99	.05192
1.7	.04	.29	.58	.97	.99	.03792
1.9	.04	.25	.53	.82	.99	.02636
2.1	.03	.21	.48	.77	.97	.01769
2.3	.02	.18	.43	.72	.95	.01141
2.6	.01	.13	.36	.64	.89	.01128
3.1	0	.08	.25	.51	.75	.00444
Σ	.0391	.3802	.8173	.9554	.9863	

Collection efficiency

r_a/r_m	$\eta_B \eta_R \eta_E$	R_L	η_c
.002	.0347	.0015	.0332
.006	.3377	.0138	.3239
.010	.7260	.0383	.6877
.014	.8489	.0750	.7739
.018	.8761	.1240	.7521

Receiver temperature = 1750°K

TABLE 2

Tabulated values of energy efficiency (η_E) and collection efficiency (η_c) for a 12 m, 45° rim angle and 1 mrad standard deviation mirror.

No misorientation error.

Energy efficiency
as a function of mirror error and aperture to receiver radius

Average error (mrad)	r_a/r_m					Probability of occurence
	.002	.006	.010	.014	.018	
.1	.09	.81	.99	.99	1.00	.15850
.3	.09	.79	.99	.99	1.00	.15234
.5	.09	.76	.99	.99	.99	.14064
.7	.09	.70	.98	.99	.99	.1248
.9	.09	.65	.96	.98	.99	.1064
1.1	.09	.60	.94	.98	.99	.08718
1.3	.09	.56	.91	.98	.99	.06862
1.5	.09	.51	.87	.98	.99	.05192
1.7	.08	.46	.84	.98	.99	.03772
1.9	.07	.41	.79	.97	.99	.02636
2.1	.06	.36	.74	.96	.99	.01769
2.3	.04	.32	.69	.94	.99	.01141
2.6	.02	.25	.61	.89	.99	.01128
3.1	0	.15	.48	.80	.96	.00444
Σ	.0867	.6710	.9435	.9822	.9922	

Collection efficiency

r_a/r_m	$\eta_B \eta_R \eta_E$	R_L	η_c
.002	.0770	.0015	.0755
.006	.5960	.0138	.5822
.010	.8381	.0383	.7998
.014	.8725	.0750	.7975
.018	.8813	.1240	.7573

Receiver temperature = 1750°K

TABLE 3

Tabulated values of energy efficiency (η_E) and collection efficiency (η_c) for a 12 m, 55° rim angle and 1 mrad standard deviation mirror.

No misorientation error.

Energy efficiency
as a function of mirror error and aperture to receiver radius

Average error (mrad)	r_a/r_m					Probability of occurence
	.002	.006	.010	.014	.018	
.1	.12	.88	.98	1.00	1.00	.15850
.3	.12	.87	.98	1.00	1.00	.15234
.5	.12	.84	.98	.99	1.00	.14064
.7	.12	.81	.98	.99	1.00	.12480
.9	.12	.77	.98	.99	1.00	.10640
1.1	.12	.69	.95	.99	.99	.08718
1.3	.12	.63	.93	.98	.99	.06862
1.5	.12	.59	.91	.98	.99	.05192
1.7	.11	.54	.87	.98	.99	.03792
1.9	.09	.49	.84	.97	.99	.02636
2.1	.07	.44	.80	.96	.99	.01769
2.3	.05	.39	.77	.94	.99	.01141
2.6	.02	.32	.70	.91	.98	.01128
3.1	.01	.20	.56	.84	.96	.00444
Σ	.1154	.7572	.9512	.9876	.9959	

Collection efficiency

r_a/r_m	$\eta_B \eta_R \eta_E$	R_L	η_c
.002	.1025	.0015	.1010
.006	.6726	.0138	.6588
.010	.8450	.0383	.8067
.014	.8773	.0750	.8023
.018	.8846	.1240	.7606

Receiver temperature = 1750 K

TABLE 4

Tabulated values of energy efficiency (η_E) and collection efficiency (η_c) for a 12 m, 65° rim angle and 1 mrad standard deviation mirror.

No misorientation error.

Energy efficiency
as a function of mirror error and aperture to receiver radius

Average error (mrad)	r_a/r_m					Probability of occurence
	.002	.006	.010	.014	.018	
.1	.15	.86	.98	.99	1.00	.15850
.3	.15	.85	.98	.99	.99	.15234
.5	.15	.82	.97	.99	.99	.14064
.7	.15	.81	.97	.99	.99	.12480
.9	.15	.78	.95	.99	.99	.10640
1.1	.15	.73	.95	.99	.99	.08718
1.3	.15	.68	.94	.98	.99	.06862
1.5	.14	.62	.89	.98	.99	.05192
1.7	.13	.58	.85	.95	.99	.03792
1.9	.11	.53	.82	.95	.99	.02636
2.1	.09	.48	.79	.93	.99	.01769
2.3	.06	.43	.75	.91	.97	.01141
2.6	.03	.33	.70	.87	.96	.01128
3.1	.01	.24	.58	.80	.93	.00444
Σ	.1435	.7617	.9434	.9814	.9901	

Collection efficiency

r_a/r_m	$\eta_B \eta_R \eta_E$	R_L	η_c
.002	.1275	.0015	.1260
.006	.6766	.0138	.6628
.010	.8380	.0383	.7997
.014	.8718	.0750	.7968
.018	.8795	.1250	.7545

Receiver temperature = 1750 K

TABLE 5

Tabulated values of energy efficiency (η_E) and collection efficiency (η_C) for a 12 m, 45° rim angle and 2 mrad standard deviation mirror.

No misorientation error.

Energy efficiency
as a function of mirror error and aperture to receiver radius

Average error (mrad)	r_a/r_m					Probability of occurence
	.002	.006	.010	.014	.018	
0.2	.09	.80	.98	.99	1.-	.15850
0.6	.09	.74	.98	.99	.99	.15234
1.0	.09	.63	.96	.99	.99	.14064
1.4	.09	.53	.90	.99	.99	.12480
1.8	.08	.43	.82	.98	.99	.10640
2.2	.05	.34	.72	.95	.99	.08718
2.6	.02	.25	.61	.89	.99	.06862
3.0	0	.17	.50	.82	.97	.05192
3.4	0	.10	.40	.74	.95	.03772
3.8	0	.04	.31	.65	.89	.02636
4.2	0	0	.21	.54	.84	.01769
4.6	0	0	.13	.44	.56	.01141
5.2	0	0	.04	.30	.44	.01128
6.2	0	0	0	.07	.38	.00444
Σ	.0661	.5005	.7987	.9246	.9692	

Collection efficiency

r_a/r_m	$\eta_B\eta_R\eta_E$	R_L	η_C
.002	.0054	.0015	.0039
.006	.4446	.0138	.4308
.010	.7095	.0383	.6712
.014	.8205	.0750	.7455
.018	.8610	.1240	.7370

Receiver temperature = 1750 K

TABLE 6

Tabulated values of energy efficiency (η_E) and collection efficiency (η_c) for a 12 m, 55° rim angle and 2 mrad standard deviation mirror.

No misorientation error.

Energy efficiency
as a function of mirror error and aperture to receiver radius

Average error (mrad)	r_a/r_m					Probability of occurence
	.002	.006	.010	.014	.018	
.02	.12	.87	.99	.00	1.0	.15850
.06	.12	.83	.99	.99	.00	.15234
1.0	.12	.72	.93	.99	.99	.14064
1.4	.12	.61	.91	.99	.99	.12480
1.8	.11	.51	.86	.98	.99	.10640
2.2	.07	.41	.78	.95	.99	.08718
2.6	.02	.32	.70	.91	.98	.06862
3.0	0	.22	.57	.85	.97	.05192
3.4	0	.14	.49	.80	.93	.03792
3.8	0	.08	.39	.73	.91	.02636
4.2	0	.03	.31	.64	.86	.01769
4.6	0	.01	.22	.56	.81	.01141
5.2	0	0	.11	.42	.72	.01128
6.2	0	0	.02	.22	.34	.00444
Σ	.0883	.5731	.8273	.9370	.9745	

Collection efficiency

r_a/r_m	$\eta_B\eta_R\eta_E$	R_L	η_c
.002	.0784	.0015	.0769
.006	.5091	.0138	.4953
.010	.7349	.0383	.6966
.014	.8323	.0750	.7573
.018	.8657	.1240	.7417

Receiver temperature = 1750 K

TABLE 7

Tabulated values of energy efficiency (η_E) and collection efficiency (η_c) for a 12 m, 65° rim angle and 2 mrad standard deviation mirror.

No misorientation error.

Energy efficiency
as a function of mirror error and aperture to receiver radius

Average error (mrad)	r_a/r_m					Probability of occurence
	.002	.006	.010	.014	.018	
.2	.15	.85	.98	.99	1.00	.15850
.6	.15	.81	.98	.98	.99	.15234
1.0	.15	.76	.94	.98	.99	.14064
1.4	.14	.65	.90	.97	.99	.12480
1.8	.12	.55	.84	.95	.99	.10640
2.2	.07	.45	.77	.92	.98	.08718
2.6	.03	.33	.70	.87	.96	.06862
3.0	0	.25	.59	.81	.93	.05192
3.4	0	.18	.50	.76	.88	.03792
3.8	0	.11	.44	.68	.85	.02636
4.2	0	.06	.36	.63	.81	.01769
4.6	0	.04	.28	.57	.75	.01141
5.2	0	0	.18	.45	.66	.01128
6.2	0	0	.07	.30	.52	.00444
Σ	.1061	.5907	.8267	.9188	.9653	

Collection efficiency

r_a/r_m	$\eta_B\eta_R\eta_E$	R_L	η_c
.002	.0942	.0015	.0927
.006	.5247	.0138	.5109
.010	.7344	.0383	.6961
.014	.8162	.0750	.7412
.018	.8575	.1240	.7335

Receiver temperature = 1750 K

TABLE 8

mirror radius (m)	12
focal length (m)	14.5
rim angle (degrees)	45
speed	.6
coating efficiency	.9
blockage efficiency	.987
cavity temp (°K)	1750
percent convergence	.007
mirror surface error (mrad)	0
intercepted energy (W)	628,800

r_a (m)	η_E	η_C
.05	.40	.35
.06	.57	.50
.07	.78	.68
.08	.91	.79
.09	.98	.85
.10	.98	.85
.11	.99	.85
.12	.99	.84
.13	.99	.83
.14	.99	.83
.15	.99	.82

TABLE 9

Tabulated values of energy efficiency (η_E) and collection efficiency (η_c) for a 12 m, 45° rim angle and 1 mrad standard deviation mirror.

15 minutes misorientation error.

Energy efficiency
as a function of mirror error and aperture to receiver radius.

Average error (mrad)	r_a/r_m					Probability of occurence
	.002	.006	.010	.014	.018	
.1	.08	.43	.86	.99	1.00	.15850
.3	.07	.42	.85	.98	1.00	.15234
.5	.07	.42	.85	.98	1.00	.14069
.7	.06	.42	.83	.98	1.00	.12480
.9	.06	.41	.80	.98	.99	.10640
1.1	.05	.38	.78	.97	.99	.08718
1.3	.05	.38	.76	.95	.99	.06862
1.5	.05	.36	.72	.94	.99	.05192
1.7	.04	.34	.69	.92	.99	.03792
1.9	.04	.31	.66	.90	.99	.02636
2.1	.04	.29	.62	.87	.98	.01769
2.3	.04	.26	.58	.84	.98	.01141
2.6	.03	.22	.52	.80	.97	.01128
3.1	.02	.16	.42	.71	.95	.0444
Σ =	.061	.395	.801	.964	.994	

Collection efficiency (T_r = 1750°K)

r_a/r_m	$\eta_B\eta_R\eta_E$	R_L	η_c
.002	.054	.0015	.053
.006	.351	.0138	.337
.010	.712	.0383	.673
.014	.856	.0750	.781
.018	.883	.1240	.759

TABLE 10

Tabulated values of energy efficiency (η_E) and collection efficiency for a 12 m, 55° rim angle and 1 mrad standard deviation mirror.

15 minutes misorientation error.

Energy efficiency
as a function of mirror error and aperture to receiver radius

Average error (mrad)	r_a/r_m					Probability of occurence
	.002	.006	.010	.014	.018	
.1	.10	.56	.96	.99	1.00	.15850
.3	.10	.56	.95	.99	1.00	.15234
.5	.09	.55	.94	.99	1.00	.14069
.7	.09	.54	.93	.99	.99	.12480
.9	.07	.53	.91	.99	.99	.10640
1.1	.07	.52	.87	.98	.99	.08718
1.3	.06	.49	.86	.98	.99	.06862
1.5	.05	.46	.82	.96	.99	.05192
1.7	.05	.43	.79	.95	.99	.03792
1.9	.05	.40	.75	.94	.99	.02636
2.1	.05	.37	.71	.93	.98	.01769
2.3	.04	.34	.68	.90	.97	.01141
2.6	.04	.29	.62	.86	.97	.01128
3.1	.03	.20	.52	.79	.94	.0444
Σ =	.079	.520	.898	.977	.993	

Collection efficiency (T_r = 1750°K)

r_a/r_m	$\eta_B\eta_R\eta_E$	R_L	η_C
.002	.070	.002	.069
.006	.464	.014	.448
.010	.798	.038	.759
.014	.868	.075	.793
.018	.882	.124	.758

TABLE 11

Tabulated values of energy efficiency (η_E) and collection efficiency for a 12 m, 65° rim angle and 1 mrad standard deviation mirror.

15 minutes misorientation error.

Average error (mrad)	r_a/r_m					Probability of occurence
	.002	.006	.010	.014	.018	
.1	.12	.66	.96	.99	1.00	.15850
.3	.12	.66	.95	.99	1.00	.15234
.5	.11	.65	.94	.99	.99	.14069
.7	.11	.64	.93	.98	.99	.12480
.9	.10	.61	.92	.98	.99	.10640
1.1	.10	.60	.89	.97	.99	.08718
1.3	.09	.57	.87	.97	.99	.06862
1.5	.08	.53	.84	.95	.99	.05192
1.7	.07	.49	.81	.95	.99	.03792
1.9	.06	.45	.78	.93	.98	.02636
2.1	.05	.41	.74	.91	.98	.01769
2.3	.05	.37	.70	.89	.98	.01141
2.6	.04	.31	.64	.85	.96	.01128
3.1	.03	.22	.54	.79	.91	.0444
$\Sigma =$	.103	.605	.905	.974	.991	

Collection efficiency (T_r = 1750°K)

r_a/r_m	$\eta_B \eta_R \eta_E$	R_L	η_c
.002	.092	.002	.090
.006	.537	.014	.524
.010	.804	.038	.766
.014	.865	.075	.790
.018	.880	.124	.756

TABLE 12

Tabulated values of energy efficiency (η_E) and collection efficiency for a 12 m, 45° rim angle and 2 mrad standard deviation mirror.

15 minutes misorientation error.

Average error (mrad)	r_a/r_m					Probability of occurence
	.002	.006	.010	.014	.018	
.2	.07	.42	.87	.99	1.00	.15850
.6	.07	.42	.84	.99	.99	.15234
1.0	.05	.39	.79	.97	.99	.14069
1.4	.05	.37	.74	.97	.99	.12480
1.8	.04	.33	.67	.91	.99	.10640
2.2	.04	.27	.59	.85	.98	.08718
2.6	.03	.22	.52	.80	.95	.06862
3.0	.03	.17	.44	.73	.91	.05192
3.4	.02	.13	.36	.65	.87	.03792
3.8	.01	.10	.29	.58	.81	.02636
4.2	0	.07	.23	.49	.75	.01769
4.6	0	.04	.17	.41	.68	.01141
5.2	0	.01	.11	.30	.56	.01128
6.2	0	0	.04	.16	.36	.0444
Σ	.047	.324	.679	.882	.958	

Collection efficiency (T_r = 1750°K)

r_a/r_m	$\eta_B \eta_R \eta_E$	R_L	η_c
.002	.042	.002	.040
.006	.288	.014	.274
.010	.603	.038	.565
.014	.784	.075	.709
.018	.851	.124	.727

TABLE 13

Tabulated values of energy efficiency (η_E) and collection efficiency for a 12 m, 55° rim angle and 2 mrad standard deviation mirror.

15 minutes misorientation error.

Average error (mrad)	r_a/r_m					Probability of occurence
	.002	.006	.010	.014	.018	
.2	.10	.56	.96	.99	1.00	.15850
.6	.09	.55	.92	.98	.99	.15234
1.0	.07	.52	.89	.98	.99	.14069
1.4	.06	.48	.84	.96	.99	.12480
1.8	.05	.42	.77	.94	.99	.10640
2.2	.04	.35	.70	.91	.98	.08718
2.6	.04	.29	.62	.86	.97	.06862
3.0	.03	.21	.54	.80	.95	.05192
3.4	.02	.15	.46	.73	.91	.03792
3.8	.01	.11	.37	.67	.87	.02636
4.2	.01	.08	.30	.59	.82	.01769
4.6	0	.06	.23	.51	.76	.01141
5.2	0	.02	.15	.39	.66	.01128
6.2	0	0	.06	.23	.48	.0444
Σ	.061	.423	.773	.911	.969	

Collection efficiency (T_r = 1750°K)

r_a/r_m	$\eta_B \eta_R \eta_E$	R_L	η_c
.002	.054	.002	.052
.006	.376	.014	.362
.010	.687	.038	.649
.014	.809	.075	.734
.018	.861	.124	.737

TABLE 14

Tabulated values of energy efficiency (η_E) and collection efficiency for a 12 m, 65° rim angle and 2 mrad standard deviation mirror.

15 minutes misorientation error.

Average error (mrad)	r_a/r_m .002	.006	.010	.014	.018	Probability of occurence
.2	.12	.67	.96	.99	1.00	.15850
.6	.11	.64	.94	.98	.99	.15234
1.0	.10	.60	.90	.97	.99	.14069
1.4	.08	.55	.84	.96	.99	.12480
1.8	.07	.47	.80	.94	.99	.10640
2.2	.05	.39	.72	.90	.97	.08718
2.6	.04	.31	.64	.85	.96	.06862
3.0	.03	.24	.56	.80	.92	.05192
3.4	.02	.18	.48	.75	.87	.03792
3.8	.01	.13	.40	.68	.84	.02636
4.2	.01	.09	.33	.61	.79	.01769
4.6	0	.07	.26	.53	.73	.01141
5.2	0	.04	.19	.43	.65	.01128
6.2	0	.01	.10	.28	.50	.0444
Σ	.077	.488	.788	.910	.963	

Collection efficiency (T_r = 1750°K)

r_a/r_m	$\eta_B \eta_R \eta_E$	R_L	η_c
.002	.068	.002	.066
.006	.434	.014	.420
.010	.700	.038	.662
.014	.808	.075	.733
.018	.855	.124	.731

TABLE 15

mirror radius (m)	12
focal length (m)	14.5
rim angle (degrees)	45
speed	.6
coating efficiency	.9
blockage efficiency	.987
cavity temp (°K)	1750
percent convergence	.7
mirror surface quality (mrad)	0
misorientation error (min)	15
intercepted energy (W)	628821

r_a/r_m	η_E	η_C
.024	.08	.07
.072	.43	.37
.120	.86	.73
.168	.99	.80
.216	1.00	.76

Chapter 4. Turbomachinery design

4.1 General considerations

To simplify the dynamics of the power station, the author has chosen a sun pointing system. This eliminates any problems of transmitting power through a gimbal. The design will revolve around a single rotating group consisting of a single stage centrifugal compressor and turbine and a single pole pair alternator all on a common shaft, much like the Garrett BRU's developped for NASA a decade ago (see figure 13). The problem of attitude control in the face of speed variations of the turbomachinery needs to be addressed.

Figure 14 is a good design chart for dimensioning the turbomachinery. The choices of specific speed, Ns, and specific diameter, Ds, (defined by equations 4 and 5) are endless, even within a desired efficiency range. To define the proper region of operation, one needs to consider the aerodynamic, stress and bearing limitations.

The bearing limitation encountered in most turbopumps does not apply here, since this configuration uses air-bearings with no mechanical contact between the shaft and foil bearing surface. Of more concern would be the labrinth type seals on either end of the alternator. The working pressure differential across them is not severe, but the high temperatures on the turbine side might cause some concern.

A maximum of 610 m/s was imposed on the rotating components rim speed to avoid potential failures due to creep or root stress. Existing gas turbines operate with rim speeds

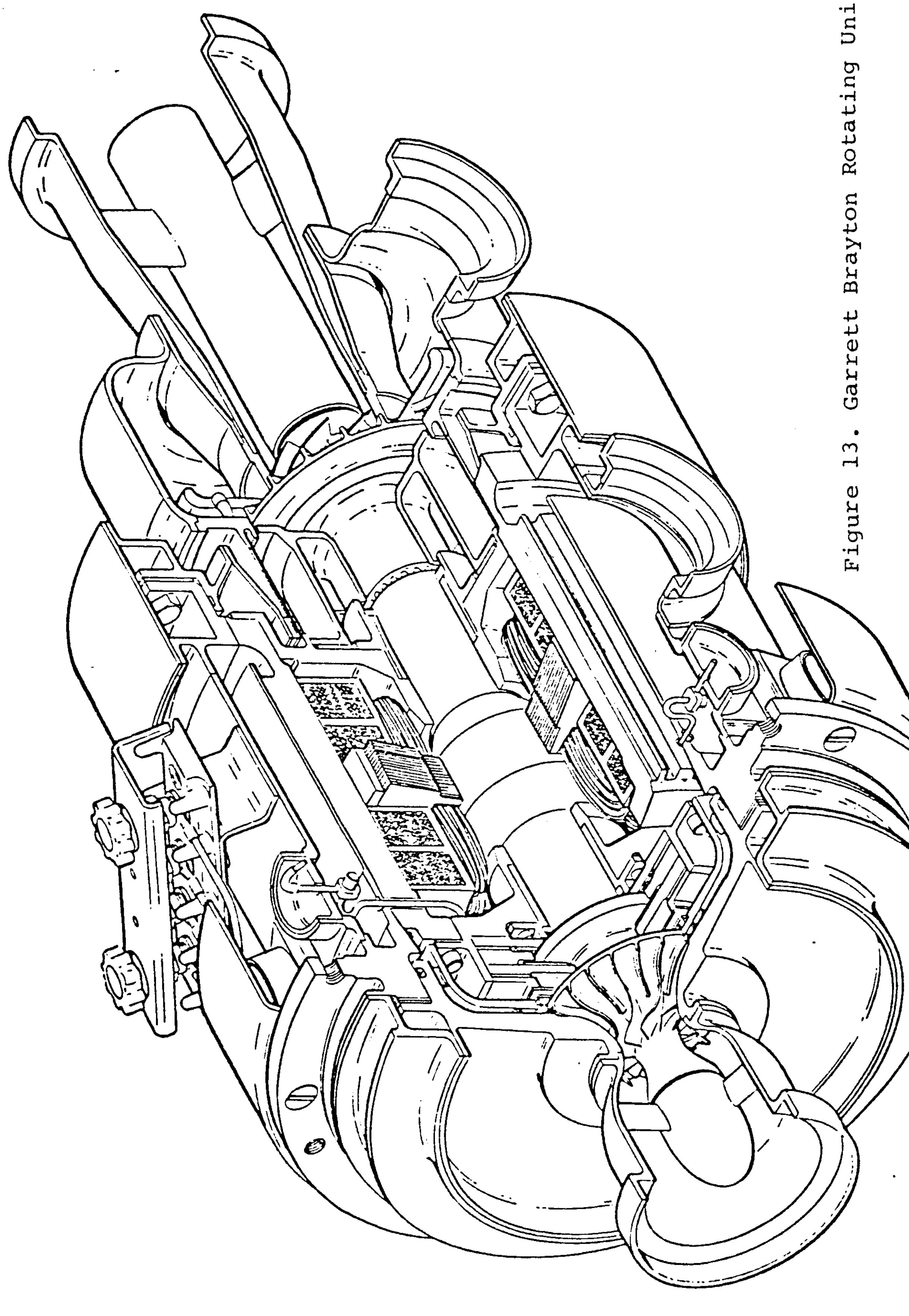

Figure 13. Garrett Brayton Rotating Unit

around 550 m/s, using high strength alloys. The material that should be used in this application is a carbon/carbon composite, whose strength increases with temperature. The physical properties of this layup and the construction details are classified, but calculations using unidirectional graphite/epoxy composites are valid, yet conservative. A typical density for a graphite/epoxy composite is 1525 kg/m. The yield stress is 1661 megaPascals. Considering only hoop stresses, one finds that

$$\sigma = \rho V^2$$

This results in a maximum rim speed of 1040 m/s before failure. Even with all of the conservative assumptions, there is a factor of safety of 1.7 for a rim speed of 610 m/s.

Fluid mechanics also imposes a minimum acceptable rim speed for the given enthalpy rise of 150 m/s, labelled "limit line for dynamic pumps" in figure 14. Between these constraints, there is a choice between the desired head rise and the obtainable efficiency, both subject to the specific heat (molecular weight) of the working fluid. The objective is to choose a mixture with a molecular weight that is as low as possible to improve the heat transfer effectiveness of the recuperator. The rationale for this is discussed in chapter 2.

4.2 Turbine design.

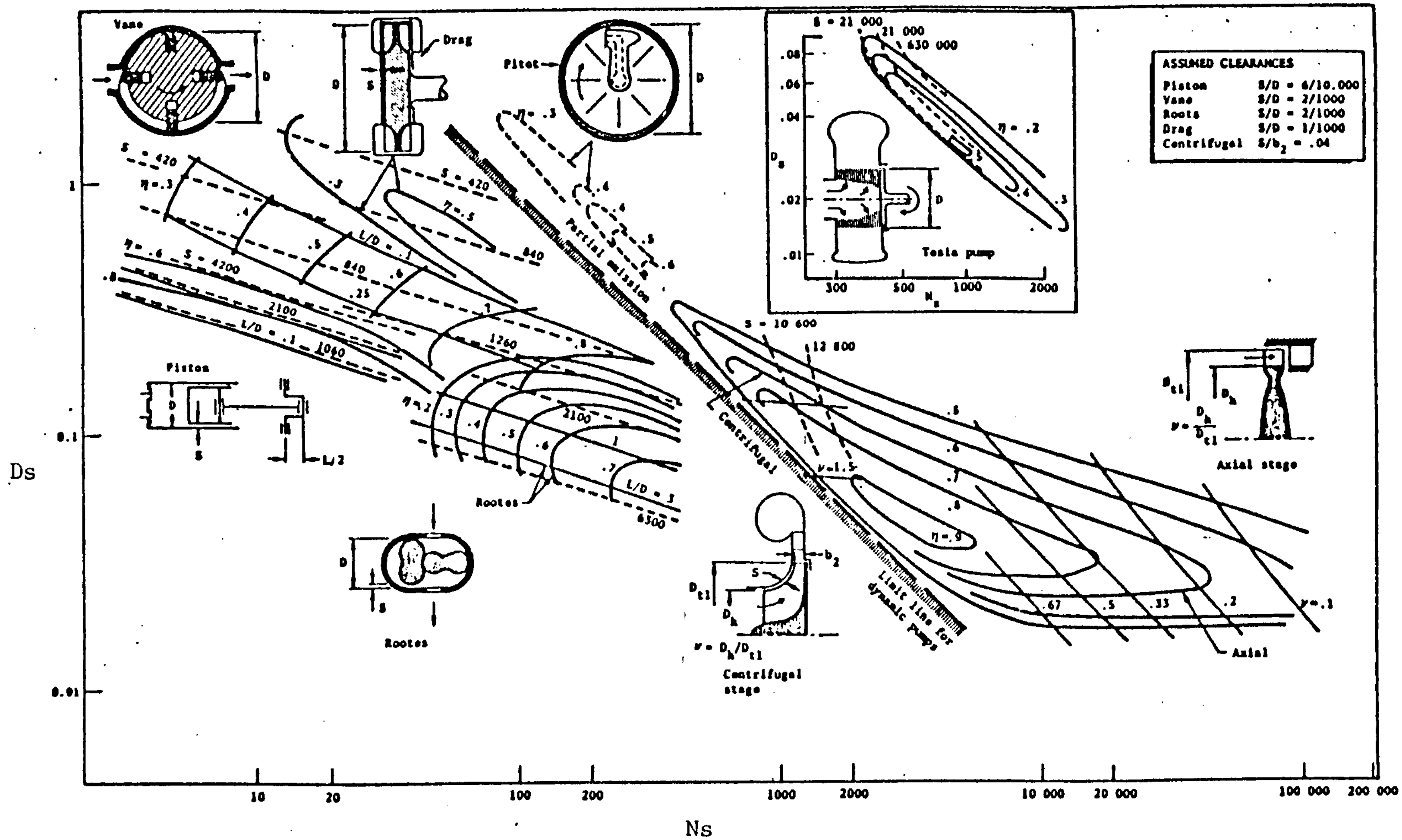

FIGURE 14 Ns - Ds DIAGRAM FOR VARIOUS PUMPS

In most gas turbine applications, the turbine is the most highly stressed component of the rotating group, being subject to the highest temperatures and operating at the highest rim speed. As previously discussed, we are going to limit the latter to 610 m/s. With this in mind, one can proceed to find the geometrical properties of the impeller. One must start by computing the head loss required, defined by

$$gH = Cp \; Tmax \; (1 - \tau_t) \qquad [1]$$

where $Cp = (\gamma/\gamma-1)\, R/\mathcal{M}$. Right away, the choice of the molecular weight affects the design. Lowering the molecular weight increases the head loss and drives the stage efficiency towards lower values. The flow coefficient, ψ, is defined as

$$\psi = \frac{gH}{(\Omega R)^2} \qquad [2]$$

where R is the rim speed. For reasons of flow stability, one would like to keep the value of ψ less than unity. At unity, the flow passages along the impeller blades are perfectly radial while at values less than unity they become 'backwards leaning'. Additionally, if one operates in english units, the following expression relates specific speed to diameter by

$$NsDs = \frac{108.3}{\sqrt{\psi}} \qquad [3]$$

This relationship is plotted in figure 14 for ψ = 1. This is the lower rim speed limit line. This means simply that ψ >1 is not acceptable. So one normally would pick an operating point in the region of highest efficiency to the right of the appropriate limit line. As mentioned earlier, however, one would like to choose a low molecular weight working fluid. If the rim speed is held constant, lowering the gas mixture molecular weight will increase the head rise [eq. 1] and the flow coefficient [eq 2], and reduce the product Ns Ds [eq. 3]. Selecting too low a molecular weight would constrain the operating point to regions of poor efficiency (see figure 14). Table 16 presents the specific heats, head losses, flow coefficients and maximum achievable stage efficiencies as a function of gas mixture molecular weight. From this data, a molecular weight of 40 was selected. The attendant head loss is 271,000 J/kg and the flow coefficient is 0.728. Substituting the flow coefficient in equation 3 and picking a design point within the 90% efficiency contour gives

Ns = 2,400 Ds = .053 (english units)

To calculate the geometry of the impeller disk, one needs to express the nondimensional specific speed and diameter in terms of physical properties, namely

TABLE 16

Turbine performance vs. working fluid molecular weight.

	M He - Xe molecular weight			
	20	40	60	80
C_p	1039.5	519.75	346.5	259.875
gH	542,000	271,000	180,670	135,500
ψ	1.457	0.728	0.486	0.364
η_{max}	?	.90	.95	.95

$$Ns^* = \frac{\Omega Q^{1/2}}{(gH)^{3/4}} \quad \text{and} \quad Ds^* = \frac{D\ (gH)^{1/4}}{Q^{1/2}} \qquad [4]$$

where Q and are the volumetric flow rate and the rotational frequency. These non-dimensional groups are related to the english quantities by

$$Ns = 2{,}728\ Ns^* \qquad Ds = .01985\ Ds^* \qquad [5]$$

So in nondimensional units these values become

$$Ns^* = .879 \qquad Ds^* = 2.67$$

Before proceeding, we need to select either Ω or D. For convenient electrical design, the author chooses to have a single pole pair alternator spinning at 800 rev/sec which gives 800 Hz at rated power. Therefore, the compressor, alternator and turbine will all spin at 48,000 rpm or 5026.6 rad/sec. This immediately fixes the radius of the impeller to 12.14 cm. The volumetric flow rate can be simply found from [4]

$$Q = \frac{(Ns^*)^2\ (gH)^{3/2}}{\Omega^2} \qquad [6]$$

and is equal to 4.314 m /sec. Another way of writing [6] would be

$$Q = 2\ \ R\ b\ Vr \qquad [7]$$

where R is the impeller radius, b is the flow passage width at the rim and Vr is the (subsonic) radial gas velocity also at the rim. Tentatively selecting a mach number of .5 for the radial gas flow in the rotating frame, one can find Vr indirectly through energy conservation. Given

$$Cp\ Tm = Cp\ T + \frac{Vr^2}{2} \quad \text{and} \quad \frac{Vr}{\sqrt{\gamma R T}} = .5 \qquad [8]$$

where Tm is the maximum turbine inlet temperature, one can solve for Vr yielding

$$Vr = \left[\frac{2 \gamma R\ Tm\ Cp}{8\ Cp + \gamma R} \right]^{1/2} \qquad [9]$$

Proper substitution of the appropriate values gives a radial gas velocity of 363 m/sec. Then from equations 4 and 7 one obtains the ratio of flow passage width to impeller radius from

$$\frac{b}{R} = \frac{2}{\pi} \frac{1}{Vr} \frac{(gH)^{1/2}}{(D^*)^2} \qquad [10]$$

This final value is 0.128. The final geometry is sketched in figure 15, along with that of the compressor.

4.3 Compressor design

The compressor is sized in exactly the same fashion as the turbine. The head rise, in this case is

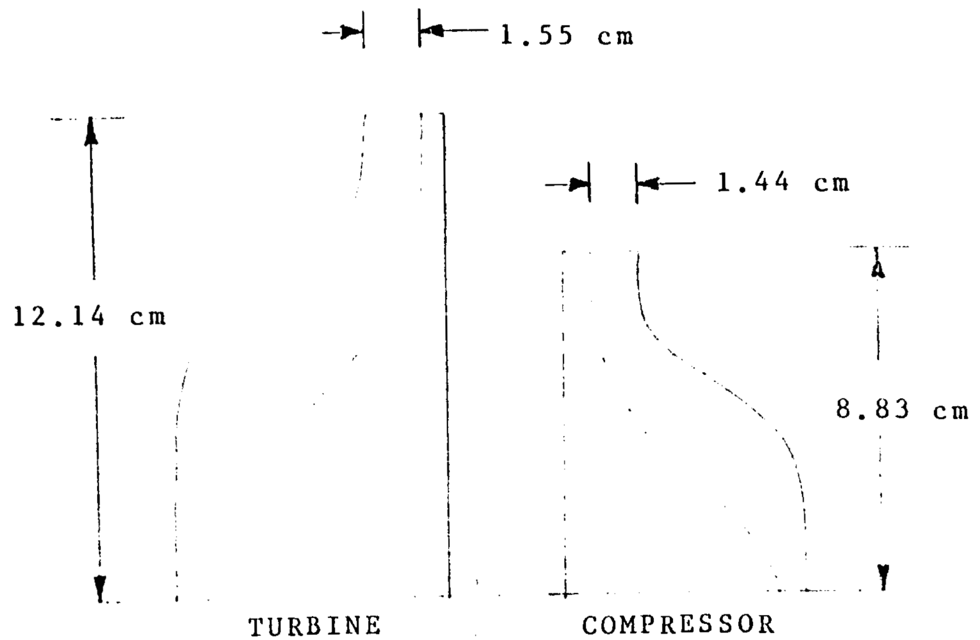

FIGURE 15 DIMENSIONS OF TURBINE AND COMPRESSOR IMPELLERS.

$$gH = C_p \, T_o \, (\tau_c - 1) \qquad [11]$$

The specific heat has already been determined and τ_c = 1.714 from the cycle analysis. Then the head rise is 143,192 J/kg. For convenience, if we choose the same non-dimensional specific speed and diameter for the compressor as the turbine, the rim speed can be found from

$$Ns^* \; Ds^* = \frac{\Omega D}{(gH)^{1/2}} \qquad [12]$$

and yields a value for Ω r = 444 m/sec. The volumetric flow rate can then be found from equation 6, remembering that has the same value for all of the rotating components. Q then becomes 1.657 m /sec. If one can assume that the impeller disks remain similar geometrically, then the ratio b/R stays the same at .128. The radial gas velocity then results from equation 10 and is equal to 264 m/sec. The temperature of the gas at the impeller rim can be found from equation 8 and is 319 K. The speed of sound at that point is 332 m/s. This implies that the radial gas flow in the rotating frame is at M = 0.79, which is a bit high for this application. Recasting the equation for b/R [10] in terms of Mach number

$$\frac{b}{R} = \frac{2}{\pi} \left[\frac{2 \, Cp + M^2 \gamma \, R}{2 \, M^2 \gamma \, R \, Cp \, T} \right] \frac{(gH)^{1/2}}{(D^*)^2} \qquad [13]$$

Picking a radial gas Mach number of 0.6 (207.3 m/s) gives a value for b/R equal to 0.163. The Mach number in the diffuser then becomes

$$M_D = \sqrt{\frac{\Omega r + Vr}{V^*}} \qquad [14]$$

The speed of sound at the rim is 345.5 m/s and the diffuser Mach number in the rest frame is 1.42. This allows us to ultimately calculate the cycle peak pressure. We know that

$$\rho = \frac{\dot{m}}{Q}$$

where m is the mass flow through the cycle. With a gas molecular weight of 40, the mass flow works out to 0.7051 kg/sec, and the density becomes 0.4256 kg/m . The compressible flow function for density is

$$\rho_{tot} = \rho \left(1 + \frac{\gamma - 1}{2} M_D^2\right)^{1/\gamma - 1}$$

so that the flow stagnates ideally to a density of 0.92 kg/m Since the temperature at that point is 662 K, this gives a cycle peak pressure of

$$P = \rho R_J T = 126{,}544 \text{ N/m}$$

This corresponds to 1.25 atmospheres, a very acceptable value.

Ch. 5 Waste Heat Radiators

5.1 Perspective

Traditionally, the waste heat radiators of a Brayton cycle were the most massive components of the system. Thermodynamics dictate a non isothermal radiator design, which needs increasing area to radiate power as the temperature drops. Previous designs used organic coolants which could not operate much above 500 K. The effective temperature (that which would dissipate the required power if the radiator was isothermal) was then quite low. These two reasons were primarily responsible for the large masses of these designs. The key to this design is the high operating temperature. Intuitively, the lower the bottom cycle temperature, the more work is available from the system. Unfortunately, there is the background earth infra-red radiation to contend with, with an energy spectrum that corresponds to a blackbody radiating at 270 K. This effect cannot be ignored, since the energy that is being rejected by the cycle is right in that range. Therefore special coatings, etc. are useless. This then imposes a constaint or a maximum value on the cycle temperature ratio.

There are also material constraints, not only in the physical properties (melting, freezing points) of the coolant and in the choice of fin material, but of compatibility of the fin and tube material to the coolant. At radiator inlet temperatures of 675 K corrosion problems may be quite severe.

The combination of aluminium and mercury was ruled out for that reason. Additionally, the material chosen for the piping cannot soften at radiator inlet temperatures for both micrometeorite protection and internal pressure considerations. Judging from some strength vs. hours at temperature curves, the tube fin material has to have a melting point at least twice the maximum working temperature. In light of all these factors, molibdenum was chosen for the radiator material and potassium selected for the coolant. Potassium is a liquid metal which freezes at 337 K, so the minimum cycle temperature was raised to 350 K. Further thought must be given to the start up problem since potassium is frozen at room temperature. A 76.7 to 23.3 percent (by weight) mix of potassium and sodium will lower the freezing point of the mixture to 260 K, thereby resolving that problem. Figure R1 is a phase diagram of mixtures of NaK. For purposes of analysis though, only pure potassium was used.

Another matter worth considering is the reliability of the radiators. A leak in a liquid coolant fin and tube design would prove disastrous. A more reliable system would use a quantity of heat pipes, each independant of the other. Single point failure would then be eliminated, and repair could be carried out without powering down the whole system. A good simulation of the physics of such a system and some algorithm to optimize a given configuration was beyond the scope of this treatise. However, the analysis and optimization of the more conventional fin and tube radiator was a more reasonable task. It is generally accepted that the mass to power ratio of a heat pipe radiator is less than its flow-type counterpart, so any estimates made with the latter should be conservative. Finally, since the radiator in this design is the least massive of the major components of the power cycle, any errors introduced by conservatism will be minimal.

5.2 Design Considerations

To account for some protection against micrometeorites, it is necessary to add material to the manifolding and the tubes for some reliability. The quantity added is a function of the desired time to perforation. The design life of this system is 10 years, so there is no need to protect the system against the 10,000 year impact. Ref[11] presents some fitted empirical data for micrometeorite impacts at near earth conditions. The reference gives certain formulas that relate perforation rate to skin thickness. These are plotted in figure 16b for 2024 aluminium. Reading off the pessimistic curve, a 10 year life dictates a skin thickness of .2 cm. Furthermore, the author states that the equivalent times for steel should be increased by a factor of 10. Molibdenum is even denser than steel, so it is unlikely that perforation will ever occur during the design life of the radiator.

In the past, the classic shape of a power system's radiator consisted of many stacked radiating panels, all connected to inlet and outlet headers (see figure 17). The design made for convenient deployment, being packaged much like the solar cells on Skylab's telescope mount. Since the

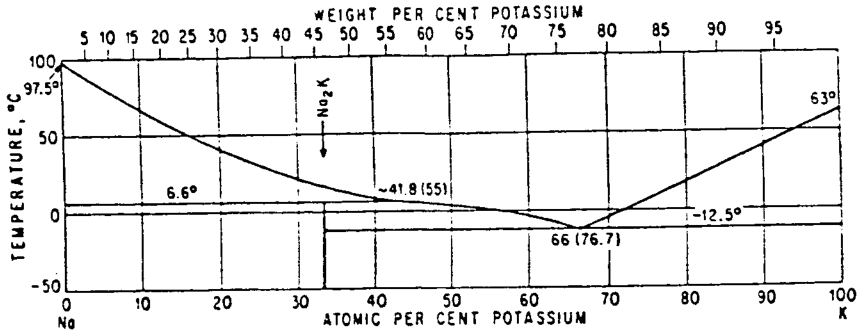

Figure 16a. Freezing point of NaK vs. composition [2]

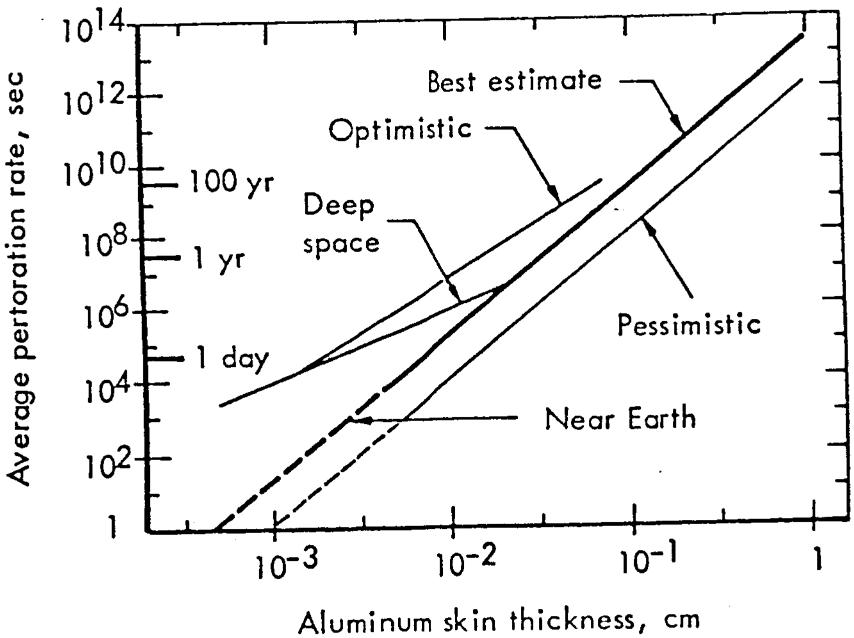

Figure 16b. Meteorite puncture rate vs. Al. skin thickness. [11]

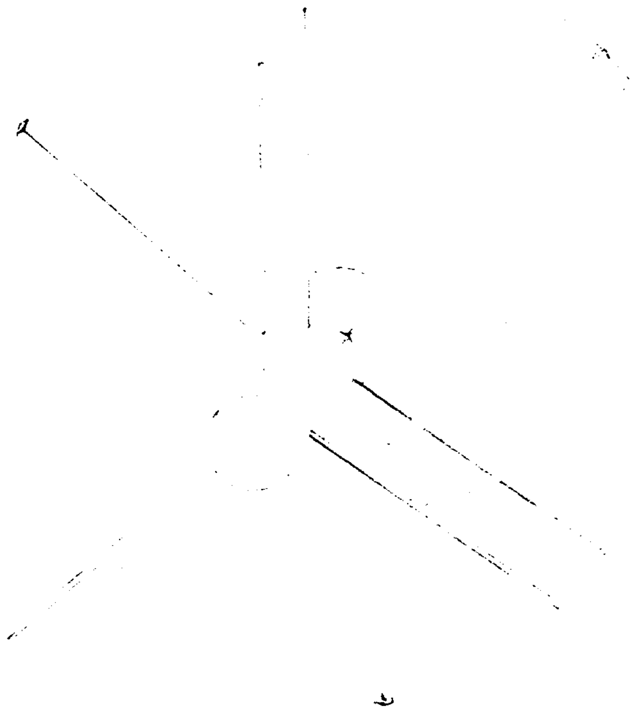

Figure 17. 3/4 view of Brayton Space Power System showing radiator manifolding detail.

design seems like a good one, this author chose to optimize the configuration for most power radiated and minimum mass. The simplest optimization to visualize is the search for the optimum number of stacked panels that results in the least mass. If there were only one panel it would have to carry the entire heat load, would be very long and have a large wetted perimeter. Most of the mass would be tied up in the single tube carrying the coolant.If this single panel were bent into a U there would be zero manifolding mass. On the other hand, if there were hundreds of these stacked assemblies, the heat load per panel would be quite small with a correspondingly small wetted perimeter. But the manifolding mass becomes prohibitive. So an optimum number of stacked assemblies does exist. Within this optimim search there are also sub optimizations on the width and thickness of the fins, coolant Reynolds number and the length of the panels. The wetted perimeter is only a function of the number of stacked assemblies and the Reynolds number inside the pipe.

Since realistic deployment schemes and Shuttle packaging were factors in the layout of the radiators, 3 wings of stacked assemblies symmetrically arranged around the reciever cavity housing were envisioned. This analysis did not consider that some of the dissipated energy from one wing would be seen by another. For that reason 2 wings might have been better, but the packaging bulk on either side of the receiver housing may not have fit inside the cargo bay.

While carrying out the process of optimization, the physical properties of the mass flow times the heat capacity of the cycle working fluid was matched by the coolant.

5.3 Radiator Modeling

The equations that model the heat flow in this particular case tie in the total heat lost along the tube length to the heat flow into the pipe wall and finally to the heat radiated from the fins. Mathematically this becomes

$$\mathrm{mdot}\ Cp\ \frac{dTl}{dx} = -hf\ (\ Tl - Tw\ )\ pw = -\ 2\ h\ \mathrm{lamb}\left(\frac{dT}{dy}\right)_{y=0} \qquad \text{eqn.[01]}$$

where mdot Cp is the mass flow times the specific heat of the coolant

Tl is the liquid temperature at the core of the pipe

Tw is the temperature of the pipe wall

hf is the film coefficient

pw is the wetted perimeter

h is the fin thickness

lamb is the heat conductivity of the fin material

$\left(\frac{dT}{dy}\right)_{y=0}$ is the temperature gradient at the fin root

If one can assume that the ratio of the wall to the liquid temperature remains constant along the tube length or

$$Tw = b\ Tl \qquad \text{eqn.[02]}$$

then eqn.[01] can be rewritten as

$$\mathrm{mdot}\ C_p \frac{dT1}{dx} = -hf\ T1\ (1 - b)\ pw$$

Check figure R3 for clarity. Integrating from 0 (the entrance to the pipe) to some distance x down the pipe, the liquid temperature at that point becomes

$$T1 = T1(0)\ \exp\left[-(1 - b) \frac{hf\ pw}{\mathrm{mdot}\ C_p} x \right]$$

where T1(0) is the inlet temperature, abbreviated Tin. We can also rewrite this equation as

$$\frac{T1}{Tin} = \exp - \left[(1 - b) \frac{hf\ pw}{\mathrm{mdot}\ C_p} L \right) \frac{x}{L} \qquad \text{eqn.[03]}$$

If the integration is carried out along the total length of the pipe, we can obtain an expression for the exit to inlet liquid temperature which can be defined as the quantity mu.

$$\frac{Tout}{Tin} = \exp -\left[(1 - b) \frac{hf\ pw}{\mathrm{mdot}\ C_p} L \right] = mu$$

So then eqn.[03] can be written simply as

$$\frac{T1}{Tin} = mu^{x/L}$$

Assigning z to the dimensionless quantity x/L, the expression for the wall temperature becomes

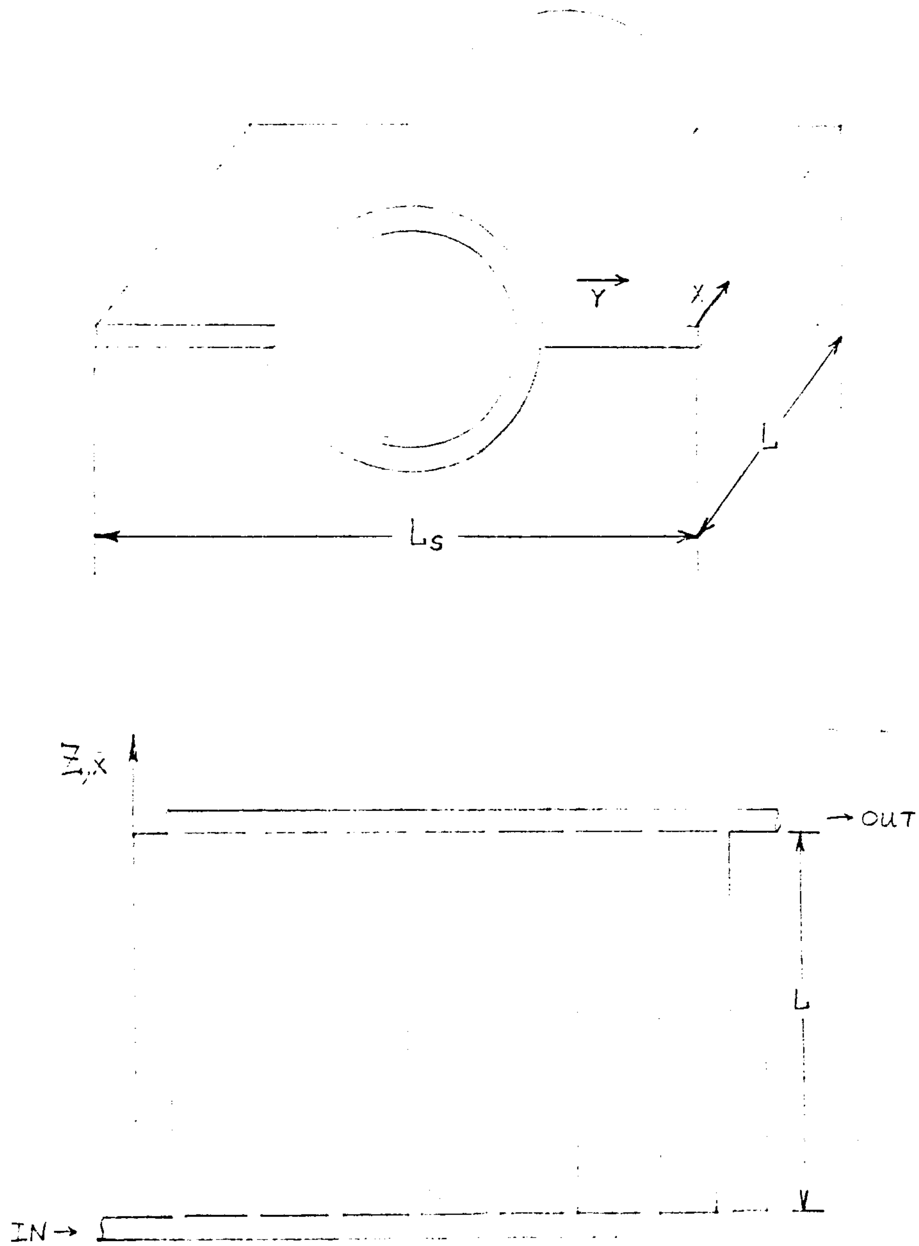

Figure 18. Radiator panel section and panel detail comprising of 8 stacked panel assemblies.

$$T_w = b\, T_{in}\, mu^{z} \qquad \text{eqn.[05]}$$

On the other side of the wall, a different energy balance holds for the heat flow from the fin. Here the assumption is made that the fin conducts heat in only one dimension, away from the pipe. In reality, the problem is two dimensional, but errors introduced as a result of this assumption are reported [NN] to be virtually insignificant.

$$\frac{d}{dy}\left(h\ lamb\ \frac{dT}{dy} \right) = em\ sig\ \left(T^{4} - Ts^{4} \right) \qquad \text{eqn.[06]}$$

where em is the fin emissivity at the appropriate wavelength

sig is the Stephan Boltzmann constant

Ts is the background sink temperature, here 270 K

One boundary condition comes from eqn.[05] and the other from the fact that there can be no temperature gradient at the fin tip

$$T(0) = Tw \quad \text{and} \quad \left(\frac{dT}{dy} \right)_{y=w} = 0$$

Then the power radiated per panel becomes

$$\frac{Q}{Ns} = -\, 2\ lamb\ h \int_{0}^{L} \left(\frac{dT}{dx} \right)_{y=0} dZ \qquad \text{eqn.[07]}$$

Furukawa [09] combined eqns. 05,06,and 07 by the method of calculus of variations to come up with an expression that relates all the key variables to the dissipated power. His equation served as a starting point for the optimized design of the fin and tube radiator. The equation is as follows:

$$\frac{Q}{Ns} = \frac{23\, lamb\, h\, l}{10\, w} \int_0^1 \frac{\dfrac{ep\, sig\, w^2}{lamb\, h} \left(Tb^4 - Ts^4 \right)}{1 + \dfrac{8\, ep\, sig\, w^2}{5\, lamb\, h}\, Tb^3}\, dz$$

where Tb is the base or wall temperature, renamed. See eqn.[05].

The program that optimizes the Brayton power system calls a radiator design subroutine with a desired dissipated power, an inlet temperature, an outlet temperature and the mass flow rate times the specific heat of the coolant. The subprogram then optimizes the radiator configuration for the minimum mass (or volume). This results in a four variable optimization for a particular design point. The variables are (l, w, h, and Ns) and the cost is volume or mass. Several constraints need to be considered: that the liquid flow within the radiator tubes remain turbulent in all sections to assure good heat transfer, and that the dissipated power is always achieved. The Reynolds number was arbitrarily picked at 4000, a number that results in barely turbulent flow. Even though higher Reynolds numbers would result in a lighter design, the pressure drop in all the passages would become too costly in terms of pumping power. Therefore, a maximum of one kilowatt was assigned for the task. The expression for the pressure drop (in Pascals) from Blasius' turbulent friction factor [10] is

$$\Delta P = 0.158\, L\, \rho^{3/4}\, \mu^{1/4}\, d^{-5/4}\, V^{7/4}$$

where rho is the coolant density

mu is the coolant viscosity

d is the pipe diameter

V is the coolant velocity in the pipe

One other variable that was affected by the choice of geometrical parameters is the film coefficient. In mks units it combines the dimensionless Nusselt number, the conductivity of the coolant and the pipe diameter to arrive at

$$hf = 0.023\, Re^{0.8}\, Pr^{0.33}\, \frac{k}{d}$$

The aforementioned cost is the total volume or mass of the radiator, comprised of the radiating panels and the manifolding. The volume of the panels is simply

$$PV = 2\, Ns\, l\, w\, h + Ns\, ht\, l\, (pw + pi\, ht) \qquad \text{eqn.[09]}$$

The expression for the manifolding is a bit more involved since it is tapered to save mass. First the cross sectional area in a panel is computed

$$AW = \frac{pw^2}{4\, pi}$$

In order to maintain a constant mass flow rate through the manifolding, the manifold area at the i^{th} section will simply be

$$MA(i) = AW\ i$$

The length of a section (refer to fig R3) is

$$LS = 2\ w + \frac{pw}{pi} + 2\ ht$$

Then the total volume of the manifold becomes twice the sum of all the individual sections, since there are inlet and outlet headers

$$TMV = 2 \sum_{i=1}^{Ns} ht\ (4\ pi\ MA(i)^{1/2} + pi\ ht)\ LS \qquad \text{eqn.[10]}$$

The total radiator volume is then

$$TRV = PV + TMV \qquad \text{eqn.[11]}$$

5.4 Optimization detail

It is fairly clear that many combinations of Ns, L, w and h will satisfy the required dissipated power. The key is to find the particular one that results in the minimum mass. Equation 8 can be thought of as the constraint equation, that is the quantity Q/Ns is always fixed within an optimization of L, w and h. The number of stacked assemblies (Ns) has to be an integer, so to remove a degree of freedom from the computations, the optima of L, w and h can be plotted as a function of Ns. The resulting peak in the curve will be the global optimum for the design. In an abbreviated form, eqn.[08] can be recast as

$$\frac{Q}{Ns} = const = XI\ (\ Ns,\ L,\ w,\ h\ ) \qquad \text{eqn.[12]}$$

The equation that is being optimized (maximized) is

$$\frac{Q/Ns}{TRV} = PHI\ (\ Ns,\ L,\ w,\ h\ ) \qquad \text{eqn.[13]}$$

The simplest way to do this is by one variable at a time, and then repeat the proceedure until some convergence criterion is met. The author recognizes that this method is inefficient, yet it is simple to implement. For example, one could start by optimizing width to length while holding the thickness h constant. Taking the differential of eqn.[12] gives

$$d\ (\ \frac{Q}{Ns}\ ) = XI_w dw + XI_l dL = 0$$

where the subscripts mean the partial of XI with respect to w (or L). Solving for dL gives

$$dL = \frac{-XI_w}{XI_l}\ dw \qquad \text{eqn.[14]}$$

Similarly for eqn.[13]

$$dPHI = PHI_w dw + PHI_l dL = 0$$

Or using eqn.[14]

$$dPHI = \left(PHI_w - \frac{XI_w}{XI_l} PHI_l \right) dw = 0$$

where
$$PHI_w = \frac{XI_w\,(TRV) - XI\,(TRV)_w}{TRV^2}$$

and
$$PHI_l = \frac{XI_l\,(TRV) - XI\,(TRV)_l}{TRV^2}$$

substituting and simplifying, one finds that the condition that needs to be met is

$$\frac{(\,TRV\,)_w}{XI_w} = \frac{(\,TRV\,)_l}{XI_l}$$

Notice that this ratio is just the "Lagrange multiplier" in this constrained optimization. A similar expression for a thickness optimum can be found, but methods to compute the actual answers became very time intensive. The quickest and easiest solution turned out to be that of successive one dimensional minimizations. Therefore the elegant methods were discarded. For illustration, the partial derivatives are included in appendix [A] for possible future use. The author resorted to computing the quantity represented by eqn.[13] and marching one direction at a time to the maximum, satisfying the constraint equation at every step, until the maxima converged.

5.5 Optimization Results

After all the relevant equations were coded, the subprogram did indeed find an optimum configuration. From the thermodynamic cycle analysis, the desired dissipated power was to be 118,100 watts coming into the radiators at 673 K and exiting at 350 K. The product of coolant mass flow and specific heat was to be 408 J/sec/K. As discussed before, there are 3 wings of stacked panels. Their overall dimensions worked out to 1.7 by 11.6 meters each, consisting of 200 stacked panels in each wing. The actual mass of the assemblies was computed to 148.5 kg. The author added an arbitrary 20 per cent to that figure to account for deployment mechanisms and stiffening braces, as well as another 1.55 KG/Kwe (1.1 KG/KWt) for the waste heat exchanger. Therefore the total mass of the radiator system came out to 320 kg. The optimum fin thickness worked out to 0.016 cm., with a corresponding internal tube diameter of 0.354 cm. The power to circulate the coolant through all of the tubes was only 24 watts. The pressure drop calculation is optimistic since the pressure drops in the manifolding were not computed, nor that through the waste heat exchangers. Figure 19 shows the sensitivity of the geometrical dimensions to the number of stacked assemblies. Also note that the specific mass of these off-optimum designs do not differ from the chosen design by more than 0.07 kg/kWe, which is not too significant. Therefore one could conclude that since the radiators in this design are the lightest components of the power system, minor adjustments in configuation could be made without incurring any great penalties.

Table 17

Properties of liquid potassium
and liqiud sodium - potassium
(NaK) at 533 K

	$\nu \times 10^7$ m^2/sec	ρ kg/m^3	Cp J/kg °K	$\mu \times 10^4$ kg/m sec	K W/m°K
K	3.097	782	792	2.42	42.74
NaK 56/44	3.7	851	1076	3.15	27.17

from ref [15]

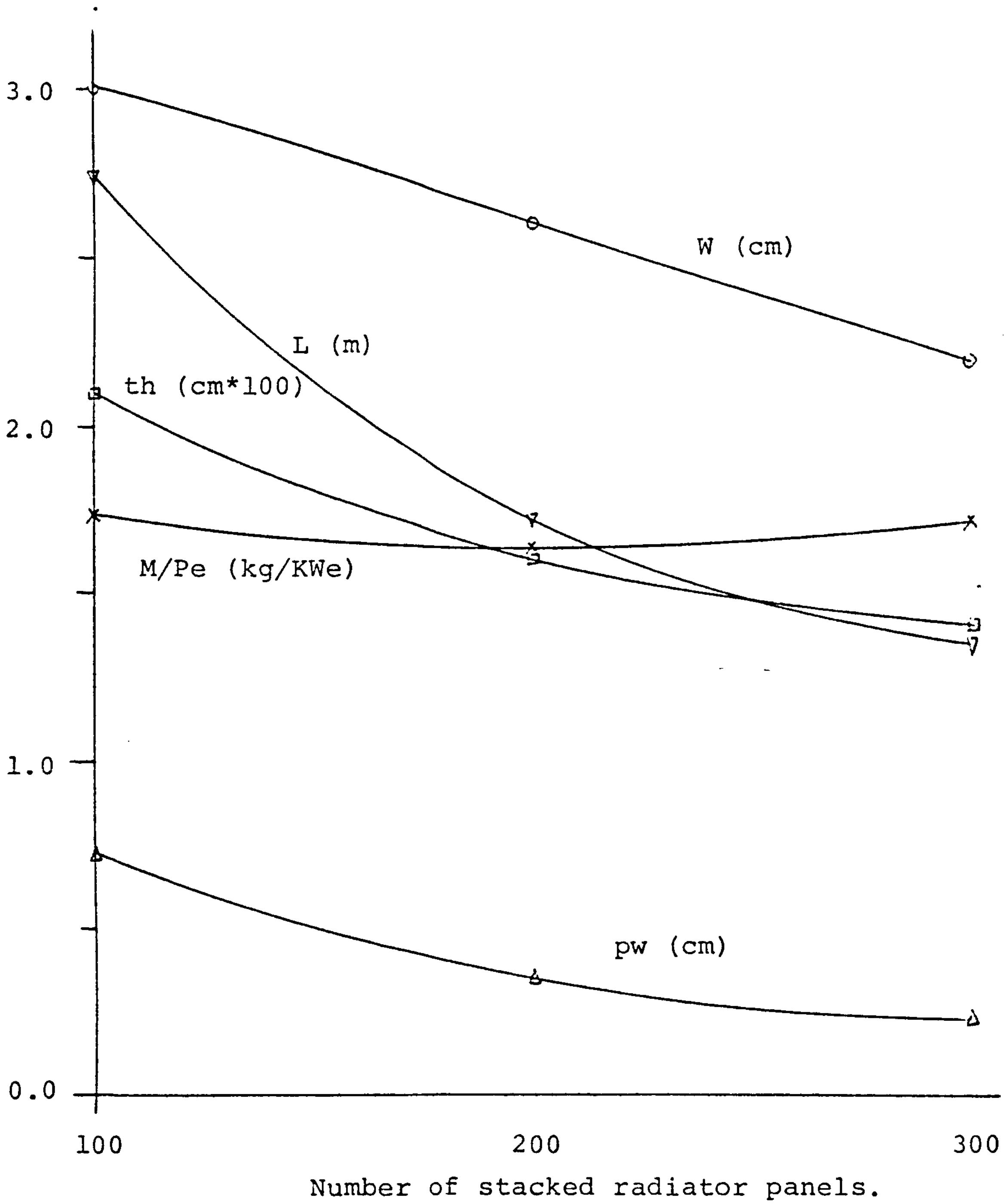

Figure 19. Radiator geometric sensitivity to the number of stacked radiator panels.

Chapter 6. Results

Table 18 is a sample output from the program listed in the back of chapter 2. The component efficiencies and the scaling variables are the author's best estimate of current technology. The numbers are a result of an optimized search through compressor pressure ratio and cycle temperature ratio space for a minimum specific mass (KG/KWe). The two constraints on the system are 1) the top cycle temperature (1685 K), prescribed by the melting point of silicon and 2) the bottom radiator temperature (350 K), chosen for ease of radiator design (see ch. 2). As such, there is not much room for cycle temperature ratio variations and is therefore not the sensitive parameter. Compressor pressure ratio, however, suffers from no constraints and is free to float. It centers around 3.3 with an efficiency of 85%. This is well within the capability of a single stage centrifugal compressor pumping a fluid with a molecular weight of 40. The total specific mass of this system then calculates out to 28.5 KG/KWe. The contributions are 8.9 KG/KWe for the collector, 10.5 KG/KWe for the receiver (mass of silicon included), 5.5 KG/KWe for the regenerator and 3.5 KG/KWe for the radiator system. Since the compressor and turbine are made of carbon/carbon composites and are therefore very light, no attempt was made to scale the rotating group, as their contribution is well within the uncertainty of some of the other major components scaling variables.

Table 18. Sample output from cycle optimization.

```
Maximum cycle temperature  1650
Compressor efficiency   .85
Turbine efficiency  .9
Alternator efficiency .9
Reflector efficiency  .81
System pressure losses  .10
Heat of fusion of storage medium  427 cal/gr
Heat storage efficiency  .8
Heat storage containment structure fraction  1.2
Regenerator effectiveness .9
Heat exchanger effectiveness  .9
Mu reflector  2.1   Kg/m²
Mu radiator  4.700   Kg/KWc
Regenerator alpha  3.22  Kg/KWc

Press ratio     Theta t          Total m/p
Refl m/p        Storage m/p      Regen m/p       Rad m/p
TAU C           TAU T            CYCLE EFF.       Kg/KWc
Trad in (°K)    Trad out (°K)    THERM EFF

 3.273131        4.276249         28.51339 Kg/KWc
 8.920528 Kg/KWc 10.5404 Kg/KWc   5.517756 Kg/KWc  3.5347
 1.713985        .6841981         .2522273
 350.0465        672.2975         .4324884

POWER(WATTS) TO DISSIPATE = 118098.1
MDOT*CP(WATTS/DEG K) OF SYSTEM  407.1986
```

Traditionally, the radiators have been the most massive single components of Brayton systems. As this research began, a lot of effort was expended in modeling the radiators, to come up with an accurate estimate of mass. Therefore, there is confidence in the radiator specific mass. Here, the radiator has become the least massive component of the system. This is primarily due to the elevated operating temperatures. The system itself is a fin and tube type radiator built out of molybdenum with a mixture of sodium and potassium serving as the coolant.

Considerable effort also was expended to model the performance of the collection system, but relatively little data was available to scale the masses appropriately. Performance was quantified in terms of surface accuracy of the mirror surface (mrad) and sun pointing error. The former obviously is a function of mass, and for a zero mean, 1 mrad standard deviation surface a scaling constant of 2.1 kg/m was selected. This figure lies within the range of actual hardware, so there is also a high degree of confidence associated with the collector mass.

The receiver is the most massive component of this system, containing all of the silicon needed for heat storage during shadow periods. That alone is responsible for 4.8 KG/KWe of the receiver mass. The rest is tied up in structure, insulation and cavity temperature control. The material used for the structure is silicon carbide, some 6.5 times lighter than the refractory materials that have been used in the past for a prototype [04]. Lurio [06] has spent considerable effort modeling the receiver, and has developed a good mass model for this component. So there is also a good degree of confidence for the receiver specific mass.

No effort was spent on properly modeling the regenerator and waste heat exchanger, as there is a large data base for existing ones. Additionally, in the early stages of this research, the cycle optimized to a high pressure ratio system, with very little regeneration needed. A more realistic assessment of the radiator design (raising the bottom radiator temperature) reversed the trend, and the cycle converged to a modest pressure ratio system with a significant amount of regeneration. The scaling variable selected for the specific mass calculation for the regenerator was 3.22 KG/KWt, derived from ref[05]. In retrospect, this figure is unnecessarily large. Reference [05] designed the unit out of refractory metals, and circulated a high molecular weight (80) working fluid through it. Later Garrett [07] designs have brought this figure down to 0.85 KG/KWt for a system circulating inert gas mixtures of 40 g/mole. Therefore, the regenerator specific mass is some 3.8 times heavier than need be.

6.2 Parametric studies

To properly identify this system's sensitivity to the choices of scaling variables and assumed efficiencies, a sensitivity analysis was conducted on all the relevant parameters. Collector efficiency and radiator specific mass estimates were exempt from this analysis for reasons previously discussed.

Figures 20 through 25 summarize the results of the sensitivity analysis. The first quantity varied (fig. 20) is the collector scaling constant. The range spans 1.5 kg/m to 5.0 kg/m , and the nominal value was picked at 2.1 kg/m . Since the collector is already a sizable portion of the power system, this perturbation pushes the specific mass of the system from 25.9 to 40.9 KG/KWe. Overall cycle efficiency displays a slight dependance on this scaling constant going from 25.2 to 25.3, due to re- optimization at a higher pressure ratio. Right away, one can identify the need for an accurate number for this scaling constant.

Since the regenerator specific mass estimate was uncertain, its scaling constant was varied from 1 to 4 and the nominal value was chosen at 3.22 KG/KWt. The overall cycle efficiency showed little sensitivity, varying from 24.9 to 25.2 percent. The specific mass ranged from 24.8 to 29.8 KG/KWe, a significant variation, illustrating the need for a better estimate for this scaling constant.

Figure 21 relates system specific mass and overall efficiency to compressor and turbine efficiency variations. Of the two, excursions in turbine efficiency had the most impact on system performance, although not by much. Compressor efficiency was varied from 80 to 90 percent, which pushed the cycle efficiency from 23.4 to 26.7 per cent. Specific mass correspondingly went down from 30.5 to 26.9

KG/KWe. Traditionally, the turbine can achieve more efficiency in a stage than can a compressor, so the compressor efficiency was varied from 85 to 95 percent. Cycle efficiency went from 23.3 to 26.9 percent, while specific mass decreased from 31.6 to 26 KG/KWe.

Figure 22 relates in similar fashion alternator efficiency and storage efficiency to specific power and cycle efficiency. Of the two the storage efficiency, which is a measure of the quantity of insulation in the receiver, is the more sensitive parameter. It was varied from 80 to 95 percent, and pushed the cycle efficiency from 25.2 to 29.9 percent. The specific mass went from 28.5 to 24.3 KG/KWe, a significant drop. This result is a bit contrived, since there was no mass penalty for the extra insulation. The alternator efficiency also was varied from 80 to 95 percent, and similarly drove the cycle efficiency from 23.8 to 26.6 percent. The specific mass dropped from 30 to 27.2 KG/KWe.

Figure 23 illustrates the impacts of the regenerator and waste heat exchanger effectiveness on cycle efficiency and specific power. Since these units are similar in function, their effectivenesses were varied over the same range, namely from 85 to 95 percent. I discovered that the waste heat exchanger had a larger impact on system performance than the regenerator, undoubtedly due to the necessary added mass of the radiators. The waste heat exchanger variations pushed the cycle efficiencies from 24.2 to 26.2 percent and drove the specific mass levels from 30.2 to 27.1 KG/KWe. The regenerator variations perturbed the cycle efficiencies from 24.1 to 26.5 percent and moved the specific mass levels from 29.2 to 27.9 KG/KWe.

Figure 24 shows how technology level might affect overall cycle efficiency and specific mass. Worst case is defined as taking all the above efficiencies and scaling constants that would result in the heaviest system and optimizing the resultant. Best case is the converse. The nominal technology level is what can be achieved today, and results in an overall cycle efficiency of 25.2 percent with a specific mass of 28.5 KG/KWe. The best that one can achieve is in this author's opinion, 14.4 KG/KWe and the worst would center around 60 KG/KWe.

Figure 25 shows the mass breakdowns of the components vs. the same technology level. Notice that the receiver remains a fairly constant, large fraction of the power system. Also, as the technology level increases, the regenerator becomes a less significant portion of the system mass, to the point where it might be better to neglect it entirely.

To present these results in a better light, consider that over the range of values of the perturbations, the decreasing order of impact is as follows: reflector scaling constant (15 KG/KWe), turbine efficiency (5.6 KG/KWe), regenerator scaling constant (5 KG/KWe), storage efficiency (4.2 KG/KWe), compressor efficiency (3.6 KG/KWe), waste heat exchanger effectiveness (3.1 KG/KWe), alternator efficiency (2.5 KG/KWe) and finally, regenerator effectiveness (1.3 KG/KWe). This listing should not be taken as an absolute measure of relative importance, since the limits of the variations were somewhat arbitrarily chosen. Had different limits been chosen, the order of impact might have been different.

Figure 20.

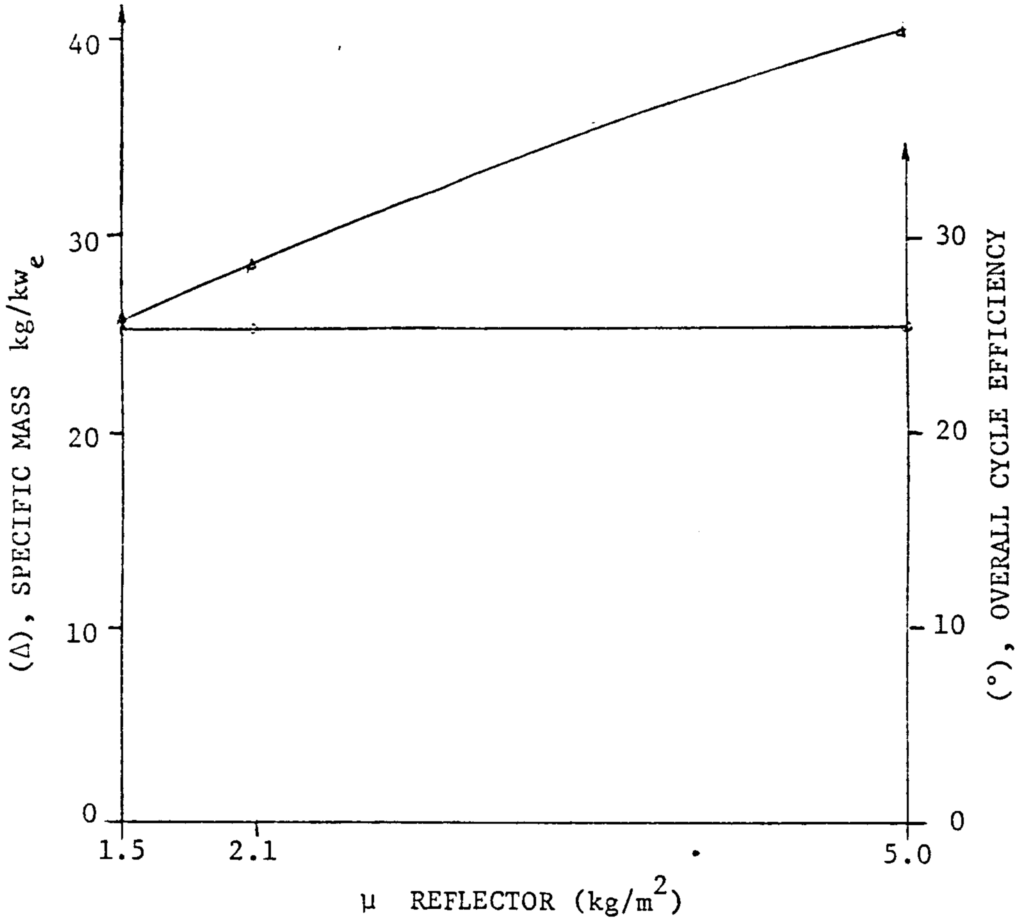
40
30
20
10
0
(Δ), SPECIFIC MASS kg/kwe
30
20
10
0
(°), OVERALL CYCLE EFFICIENCY
1.5
2.1
5.0
μ REFLECTOR (kg/m2)

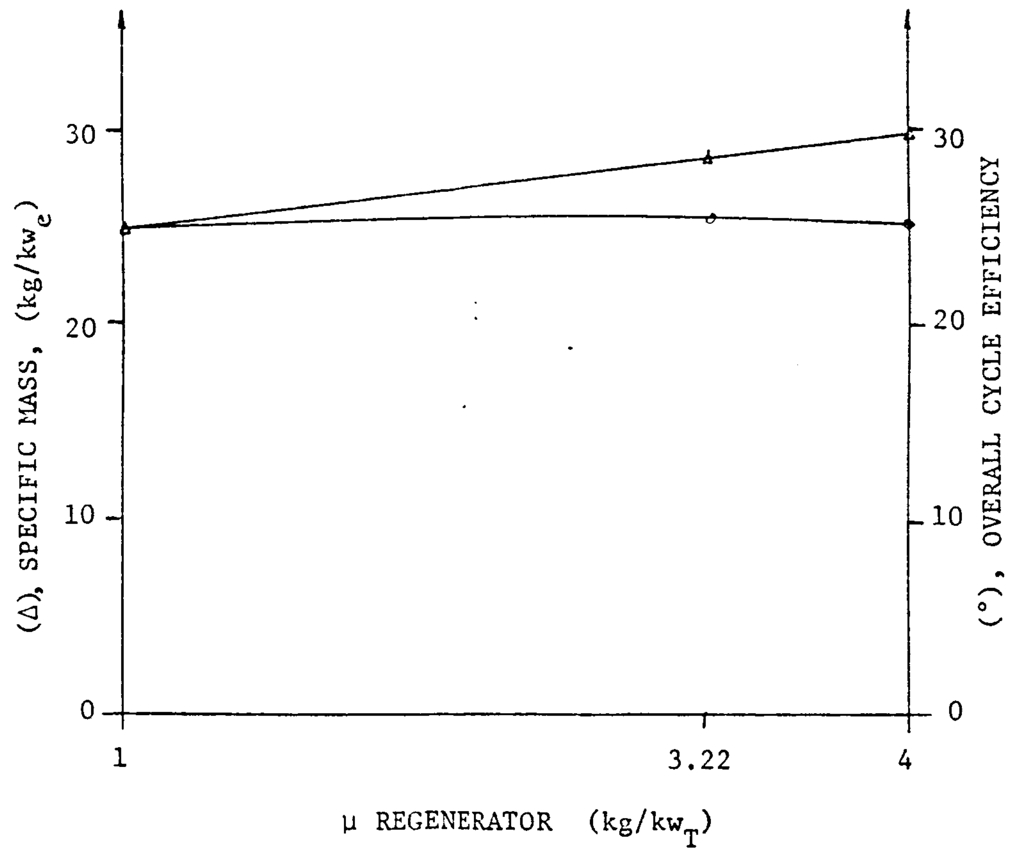
30
20
10
0
(Δ), SPECIFIC MASS, (kg/kwe)
30
20
10
0
(°), OVERALL CYCLE EFFICIENCY
1
3.22
4
μ REGENERATOR (kg/kwT)

Figure 21.

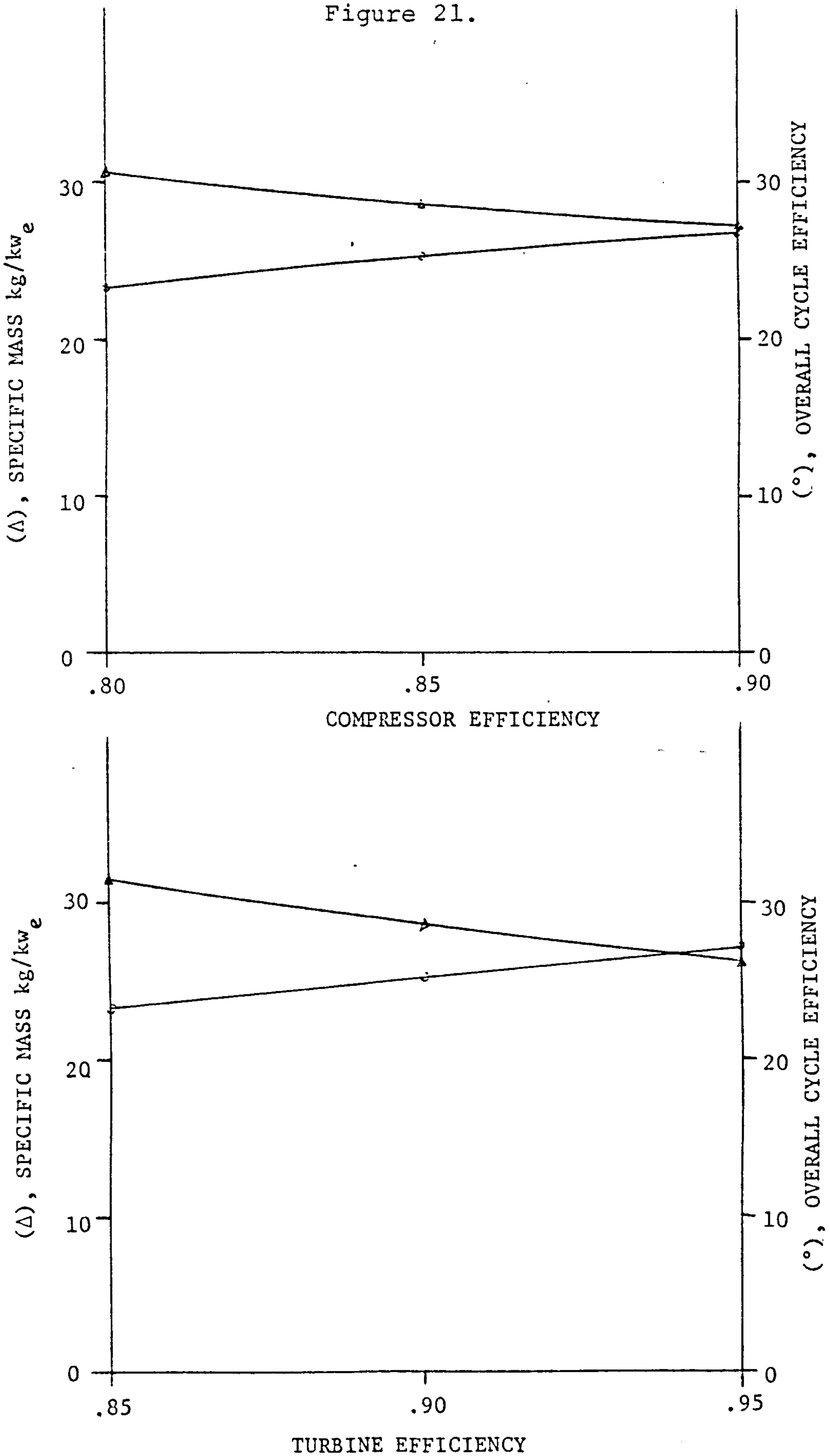

(Λ), SPECIFIC MASS kg/kw$_e$
(°), OVERALL CYCLE EFFICIENCY
0
10
20
30
.80
.85
.90
COMPRESSOR EFFICIENCY
(Δ), SPECIFIC MASS kg/kw$_e$
(°), OVERALL CYCLE EFFICIENCY
0
10
20
30
.85
.90
.95
TURBINE EFFICIENCY

Figure 22.

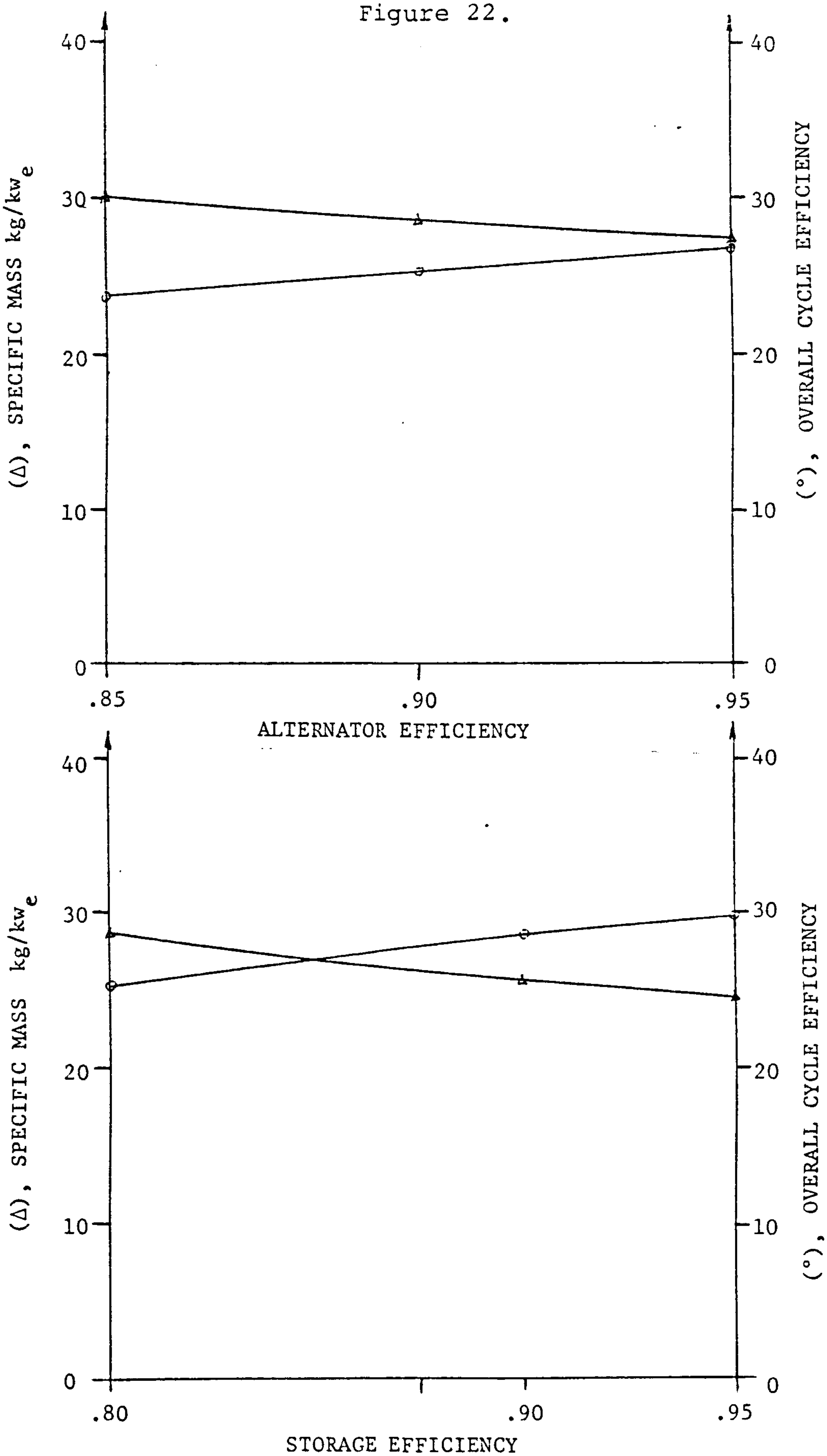
40
30
20
10
0
(Δ), SPECIFIC MASS kg/kw_e
40
30
20
10
0
(°), OVERALL CYCLE EFFICIENCY
.85
.90
.95
ALTERNATOR EFFICIENCY
40
30
20
10
0
(Δ), SPECIFIC MASS kg/kw_e
40
30
20
10
0
(°), OVERALL CYCLE EFFICIENCY
.80
.90
.95
STORAGE EFFICIENCY

Figure 23.

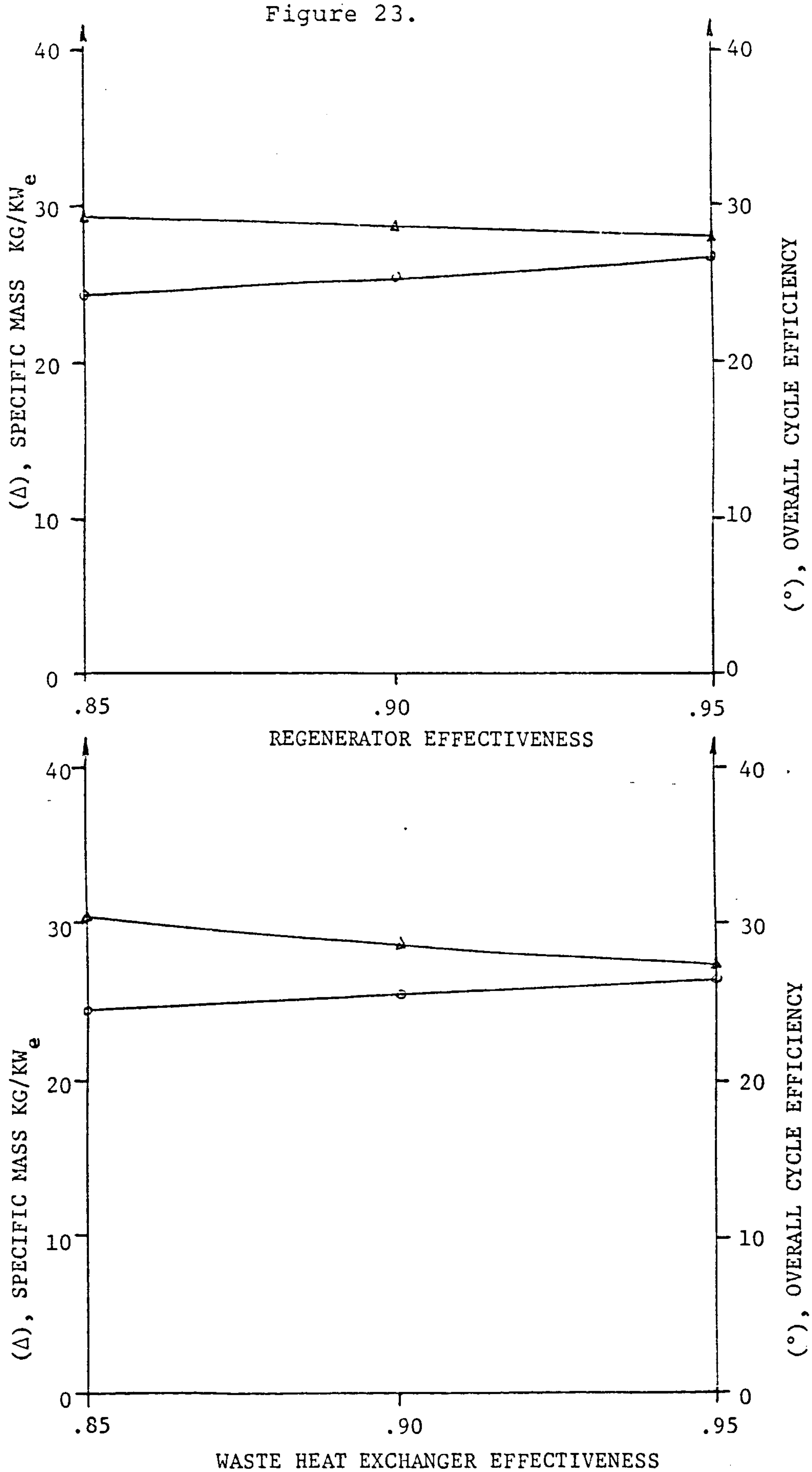

40
30
20
10
0
(Δ), SPECIFIC MASS KG/KW$_e$
40
30
20
10
0
(°), OVERALL CYCLE EFFICIENCY
.85
.90
.95
REGENERATOR EFFECTIVENESS
40
30
20
10
0
(Δ), SPECIFIC MASS KG/KW$_e$
40
30
20
10
0
(°), OVERALL CYCLE EFFICIENCY
.85
.90
.95
WASTE HEAT EXCHANGER EFFECTIVENESS

Figure 24.

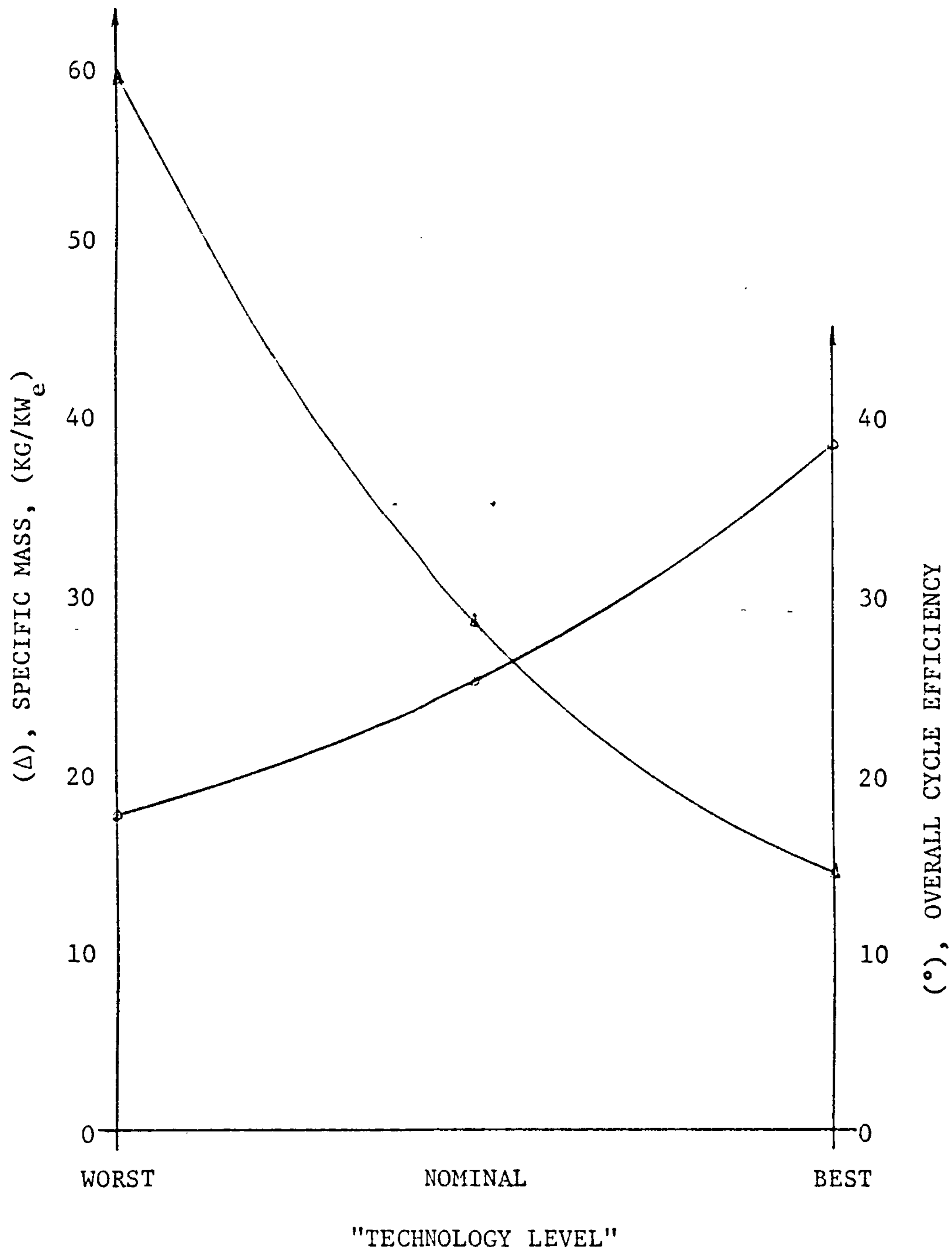
60
50
40
30
20
10
0
(Δ), SPECIFIC MASS, (KG/KW$_e$)
40
30
20
10
0
(°), OVERALL CYCLE EFFICIENCY
WORST
NOMINAL
BEST
"TECHNOLOGY LEVEL"

Figure 25.

COMPONENT SPECIFIC MASS BREAKDOWNS
VS "TECHNOLOGY LEVEL"
(SEE TEXT)

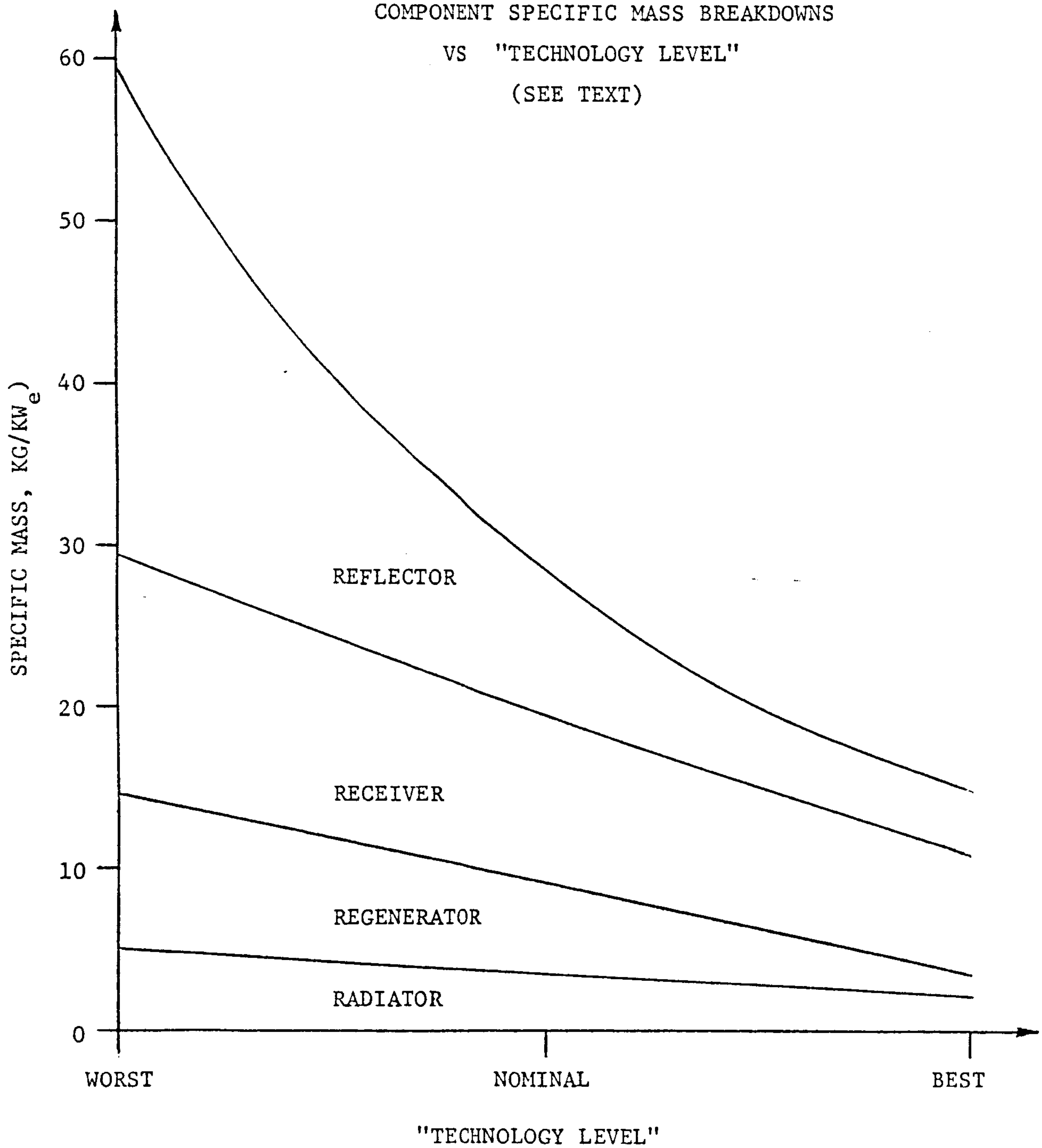

Chapter 7. Conclusions and recommendations

This thesis certainly has validated the concept of a high temperature solar Brayton cycle with latent heat of fusion energy storage. The power system was optimized for minimum specific mass, and converged to 28.5 KG/KWe. The corresponding cycle efficiency was 25.2 percent. The author did not consider gimballing or redundant sets of turbomachinery, which would add at least 10 KG/KWe to the system mass. Those decisions would have to be made after a more detailed study of the space station's attitude (earth or sun pointing) and reliability requirements.

However, there are still some fine points to consider. The concept of thermal storage tubes was tested by Lewis Research Center [1], albeit with different materials. Their goal was to achieve a gas working temperature of 1090 K throughout an orbital period. The gas temperature varied from 26 K above to 18 K below the nominal temperature, during simulated ,orbital periods. The tubes were constructed from columbium - 1% zirconium and were filled with LiF, which releases 1046 kJ/kg at 1121 K. These tubes were tested for 1251 sun - shade cycles with no real problems other than some local distortions in the outer tube convolutions. This was probably a combined effect of gravity and a 30% change in volume during the change of phase. This probably would not have occured in 0 gravity. In short that program was successful. In my particular application, the tubes are built of silicon carbide, and the energy storage is accomplished with silicon, which releases 1787 kJ/kg at 1685 K. Additionally, silicon undergoes only an 8 percent volume change during the change of phase. The silicon carbide ceramic is necessary because of the elevated temperature. In the first analysis the long term compatability of silicon carbide with hot silicon should not present any problems, but there is no hard data to verify this assumption.

Another area that needs to be verified is the durability of carbon/carbon turbines at temperature and speed. Although the environment is benign with almost no thermal cycling, these turbines are still experimental. As stated earlier, they have been tested to 2200 K and to 720 m/s. These results [12] are encouraging, but definitive design data is not yet available.

The alternator, even with an assumed efficiency of 90%, is going to produce 10Kw of heat for an electrical output of 90 KWe. Therefore, alternator cooling cannot be ignored. Injecting cooled gasses (He) in the alternator housing is a solution, but windage losses could become significant. The mass of this other cooling system would then have to be accounted for. Since all of the machinery rotates on a common shaft, another solution could be envisioned. Heat pipes could be routed from the windings through the hollow shaft, through the compressor face, and ultimately sink their heat load into the incoming compressor stream. Careful design would have to insure that the vapor pressure at the evaporator could overcome the local centrifugal force, but this same force would assist in the return of the condensed vapor through the wick. If this could prove possible, then the alternator could spin in vacuum, reducing the windage losses to zero. The peak cycle pressure is only 1.25 atmospheres, so the sealing requirements aren't severe. Naturally, the system would have to be re-optimized for a compressor inlet temperature that would be some 25 K warmer.

Another pivotal topic is the seals that isolate the compressor and turbine from the alternator. These seals should have no problem dealing with the pressures in the rotating machinery. But their design would have to minimize leaks over a ten year life at very high temperatures. No attempt was made to look into this subject, but it needs to be addressed if this concept is ever taken to a more complete design.

Unfortunately, the capability of achieving at least a half of a degree pointing accuracy for the collector needs to be looked at more seriously. This concern ties in with the rest of the design of the space platform. Docking perturbations, shifting masses and the quality of the attitude control all affect the pointing accuracy requirement. There also will be some continuous expenditure of energy in one form or another to meet this criterion. The complete impact of this concern needs further research.

The subject of mirror surface quality degradation quickly was analysed in chapter 3. The conclusion there was that a thin coating of quartz might have to be applied to the mirror surface to protect it from free oxygen in low earth orbits. If this system is used to power a low thrust orbital transfer vehicle that operates between LEO and GEO, it will have to traverse the Van Allen radiation belts. It is questionable to assume that the mirror will be unaffected by high energy protons. Either a laboratory experiment or a flight test might have to be conducted to fully quantify this effect.

As discussed earlier, the radiators are constructed out of molybdenum and circulate a coolant composed of sodium and potassium. The solubility of molybdenum in hot NaK [3] also needs to be checked and evaluated over a mission lifetime. If it should prove unacceptable, some other material will have to be chosen (stainless steel) for the tube and fin material, and the radiators redesigned. Stainless is a worse conductor of heat, so the radiator mass would have to increase.

In general, the high temperature solar Brayton space power system is a simple, reliable concept that does not suffer from insurmountable technological difficulties. All of the potential problems addressed above can be solved with a minimum of effort along with a better understanding of the power system's integration with the larger system. The author feels that this system has a definite niche in the power options being considered for the 1990's.

Appendix A

This appendix lists the various partial derivatives of equation 8 in section 6.3 that are used in any optimization algorithm. One can start by recasting equation 8 with a change of variables. Let

$$g = \frac{em\ sig\ w^2}{h\ lamb}$$

Then equation 8 becomes

$$\frac{Q}{Ns} = \frac{23\ lamb\ h\ 1}{10\ w} \int_0^1 \frac{g\ (Tb^4 - Ts^4)}{1 + \frac{8}{5}\ g\ Tb^3}\ dz$$

Can start by computing d(Q/Ns)/dw: For clarity, the operation is shown in pieces.

$$\frac{d(Q/Ns)}{dw} = \frac{23\ lamb\ h\ 1}{10\ w}\ \frac{d}{dw} \int_0^1 \frac{g\ (Tb^4 - Ts^4)}{1 + \frac{8}{5}\ g\ Tb^3}\ dz$$

$$+ \int_0^1 \frac{g\ (Tb^4 - Ts^4)}{1 + \frac{8}{5}\ g\ Tb^3}\ dz\ \ \frac{d}{dw}\left(\frac{23\ lamb\ h\ 1}{10\ w}\right)$$

The derivative of the integral becomes

$$\int_0^1 \frac{2\ g\ (Tb^4 - Ts^4)}{w\ (1 + \frac{8}{5}\ g\ Tb^3)} - \frac{16\ g^2\ Tb^3\ (Tb^4 - Ts^4)}{5\ w\ (1 + \frac{8}{5}\ g\ Tb^3)^2}\ dz$$

Or simplifying,

$$\int_0^l \frac{g\,(Tb^4 - Ts^4)}{1 + \frac{8}{5}\,g\,Tb^3} \left\{ \frac{2}{w} - \frac{16\,g\,Tb^3}{5\,w\,(1 + \frac{8}{5}\,g\,Tb^3)} \right\} dz$$

Additionally, the derivative of the first part of [A2] is

$$- \frac{23\ lamb\ h\ l}{10\ w^2}$$

Rewriting [A2] in terms of [A3] and [A4]

$$\frac{23\ lamb\ h\ l}{10\ w} \int_0^l \frac{g\,(Tb^4 - Ts^4)}{1 + \frac{8}{5}\,g\,Tb^3} \left\{ \frac{2}{w} - \frac{16\,g\,Tb^3}{5\,w\,(1 + \frac{8}{5}\,g\,Tb^3)} \right\}$$

$$- \frac{23\ lamb\ h\ l}{10\ w^2} \int_0^l \frac{g\,(Tb^4 - Ts^4)}{1 + \frac{8}{5}\,g\,Tb^3}\, dz$$

This last equation can be simplified one step further. So the equation for d(Q/Ns)/dw becomes

$$\frac{23\ lamb\ h\ l}{10\ w} \int_0^l \frac{g\,(Tb^4 - Ts^4)}{1 + \frac{8}{5}\,g\,Tb^3} \left\{ \frac{1}{w} - \frac{16\,g\,Tb^3}{5\,w\,(1 + \frac{8}{5}\,g\,Tb^3)} \right\} dz$$

Next on the list to figure is d(Q/Ns)/dl. This derivative is a bit more involved since [A1] is being integrated over a normalized length. As before,

$$\frac{d(Q/Ns)}{dl} = \frac{23\ \text{lamb}\ h\ l}{10\ w}\ \frac{d}{dl} \int_0^1 \frac{g\ (Tb^4 - Ts^4)}{1 + \frac{8}{5}\ g\ Tb^3}\ dz$$

$$+ \int_0^1 \frac{g\ (Tb^4 - Ts^4)}{1 + \frac{8}{5}\ g\ Tb^3}\ dz\ \ \frac{d}{dl}\left(\frac{23\ \text{lamb}\ h\ l}{10\ w} \right) \qquad \text{[A6]}$$

If one functionally rewrites the derivative of the integral above as

$$\frac{d}{dl} \int_0^1 f(z,l)\ dz \qquad \text{[A7]}$$

where $z = \frac{Z}{L}$ and $dz = \frac{1}{L}\ dZ$

Then [A7] becomes

$$\frac{d}{dL} \int_0^L f\left(\frac{Z}{L}, L\right) \frac{1}{L}\ dZ$$

or

$$\int_0^L \frac{d}{dL} \left\{ \frac{1}{L} f\left(\frac{Z}{L}, L\right) \right\} dZ \quad + \quad \frac{1}{L} f(1,L) \qquad \text{[A8]}$$

Expanding the term inside the integral one obtains

$$-\frac{1}{L^2} f(z) \; - \; \frac{1}{L} \left(\frac{\partial f(z)}{\partial Z} \right)_L \frac{Z}{L^2} \; + \; \frac{1}{L} \left(\frac{\partial f(z)}{\partial L} \right)_{Z/L}$$

The subscript next to the partials indicates which variable is treated as a constant. Carrying out the integration one obtains

$$-\frac{1}{L}\int_0^1 f(z)\,dz \quad -\frac{1}{L}\int_0^1 \left(\frac{f(z)}{z}\right) z\,dz \quad + \frac{1}{L}\int_0^L \left(\frac{\partial f(z)}{\partial L}\right)_{Z/L} dZ$$

Substituting this expression into [A8] will transform [A7] into the proper form of

$$\int_0^1 \left(\frac{\partial f(z)}{\partial L}\right)_{Z/L} dz \qquad [A9]$$

Substituting in all the proper variables for [A9], one gets

$$\int_0^1 \frac{mu^z\ Cp\ mdot\ \log(mu)}{hf\ L^2\ pw\ \log(10)} \left\{ \frac{24/5\ g\ Tb^2\ (Tb^4 - Ts^4)}{1 + \frac{8}{5} g\ Tb^3} - 4\ g\ Tb^3 \right\} dz$$

[A10]

Note that this last expression only takes care of the first line of [A6]. The last derivative of [A1] that needs to be found is $d(\dot{Q}/Ns)/dh$. Eliminating the lengthy alebra, one arrives at

$$\frac{23\ lamb\ h\ l}{10} \int_0^1 \frac{g\ (Tb^4 - Ts^4)}{1 + \frac{8}{5} g\ Tb^3} \cdot \frac{8\ g\ Tb^3}{5\ h\ (1 + \frac{8}{5} g\ Tb^3)}\ dz \qquad [A11]$$

To complete the analysis, the same sequence of derivatives is needed for eqn.[11] in section 6.3, which is the expression for the total radiator volume. These are quite simply

$$\frac{d}{dw}(TRV) = 2\ Ns\ L\ h + 4 \sum_{i=1}^{Ns} ht\ (\ pw\ (i)^{1/2} + ht\ pi\ )$$

$$\frac{d}{dL}(TRV) = 2\ Ns\ w\ h + Ns\ ht\ (\ pw + ht\ pi\ )$$

$$\frac{d}{dh}(TRV) = 2\ Ns\ L\ w$$

Appendix B.

```
5 LPRINT
10 TMAX= 1650
12 INPUT"LOWER TEMPERATURE LIMIT";TLOW
14 LPRINT
20 LPRINT"Maximum cycle temperature ";TMAX
30 NC= .8499999
40 LPRINT"Compressor efficiency ";NC
50 NT= .9#
60 LPRINT"Turbine efficiency ";NT
70 NR= .81
72 NA = .9
74 LPRINT"Alternator efficiency";NA
80 LPRINT"Reflector efficiency ";NR
90 PIL=.9
100 LPRINT"System pressure losses ";1-PIL
110 HF= 427
120 LPRINT"Heat of fusion of storage medium ";HF
130 NS= .8
140 LPRINT"Heat storage efficiency ";NS
150 FST= 1.2
160 LPRINT"Heat storage containment structure fraction ";FST
170 E1=.9
180 LPRINT"Regenerator effectiveness";E1
190 E2= .9#
200 LPRINT"Heat exchanger effectiveness ";E2
210 INPUT"Mu reflector ";MUR
220 LPRINT"Mu reflector ";MUR
230 INPUT"Mu radiator ";MRD
240 LPRINT"Mu radiator ";MRD
250 INPUT"Regenerator alpha ";AR
260 LPRINT"Regenerator alpha ";AR
270 LPRINT
```

```
280 LPRINT"Press ratio","Theta t","Total m/p"
290 LPRINT"Refl m/p","Storage m/p","Regen m/p","Rad m/p"
300 LPRINT"TAU C","TAU T","CYCLE EFF."
310 LPRINT"Trad in","Trad out"
320 LPRINT
330 REM INITIALIZE
340 RSTEP= .1
350 PIC=3!
360 THT= 4!
370 LPIC= PIC
380 LTHT= THT
390 OPIC= PIC
400 OTHT= THT
410 GOSUB 880
420 LMTP= 100
430 MMTP= 100
440 REM
450 REM COMPUTE THE DERIVATIVES
460 PIC= PIC+.01
470 GOSUB 880
480 DPIC=(MTP-LMTP)/.01
490 PIC= LPIC
500 THT= THT+.01
510 GOSUB 880
520 THT=LTHT
530 DTHT= (MTP-LMTP)/.01
540 REM
550 REM COMPUTE SEARCH DIRECTION
560 THETA= ATN(DPIC/DTHT)
570 IF THETA <0 THEN IF DTHT<0 THEN THETA= THETA+ 3.1415927#
580 IF THETA >0 THEN IF DTHT<0 THEN THETA= THETA- 3.1415927#
590 THETA=THETA+3.14159
600 REM SAVE VALUES OF LAST POINT
610 LPIC=PIC
620 LTHT= THT
630 REM
```

```
640 REM START SEARCH ALONG VECTOR
650 RANGE=0
660 RANGE= RANGE+ RSTEP
670 PIC= LPIC+ RANGE*SIN(THETA)
680 THT=  LTHT +RANGE*COS(THETA)
690 GOSUB 880
700 IF MTP>LMTP THEN GOTO 770
710 LMTP= MTP
720 LPIC= PIC
730 LTHT= THT
740 GOTO 660
750 REM
760 REM CHECK CONVERGENCE AND COMPUTE NEW RANGE STEP SIZE
770 IF ABS((LMTP-MMTP)/LMTP)<.0008 THEN GOTO 1080
780 PRINT"PI C=";LPIC,"THETA T";LTHT
790 MMTP= LMTP
800 RMAG=SQR((LPIC-OPIC)^2+(LTHT-OTHT)^2)
810 RSTEP= RMAG/10
820 OPIC=LPIC
830 OTHT=LTHT
840 PIC= LPIC
850 THT=LTHT
860 MTP= LMTP
870 GOTO 450
880 TC= 1+((PIC^.4)-1)/NC
890 TT=1!-NT*(1!-(1!/(PIC*PIL))^.4)
900 NU= NR*NS*(THT*(1!-TT)-TC+1!)*NA
910 NL= THT-TC-E1*(THT*TT-TC)
920 N= NU/NL
930 MRP= (MUR/(1.4*N))*(1!+(36!/(90!*NS)))
940 MSP= (1+FST)*(2160/(N*HF*4.186))
950 MR1=AR*E1*(TT-TC/THT)
960 MR2= 1!-TT-(TC-1!)/THT
970 MGP= MR1/MR2
```

```
980 THA= 1!-E1+(E1-1!)/E2
990 THB= E1*(1!-(1!/E2))
1000 TH7= THA*TT+THB*(TC/THT)+(1!/(THT*E2))
1010 THC= 2!+E1*((1!/E2)-2!)-(1!/E2)
1020 THD= E1*(2!-(1!/E2))
1030 TH8= THC*TT+THD*(TC/THT)+((1!/E2)-1!)/THT
1040 MRAD1= ((1!-N)/N)*(((1!/TH7^3!)-(1!/TH8^3!))/(TH8-TH7))
1050 MDP= MRAD1*MRD/(TMAX^4!*.8*6!*5.67E-08*.9)
1052 IF TMAX*TH7>TLOW THEN GOTO 1060
1054 MDP = MDP*(1+(TLOW-TMAX*TH7))
1060 MTP= MRP+MSP+MGP+MDP
1070 RETURN
1080 PIC= LPIC
1090 THT= LTHT
1100 GOSUB 880
1110 LPRINT PIC,THT,MTP
1120 LPRINT MRP,MSP,MGP,MDP
1130 LPRINT TC,TT,N
1140 LPRINT TH7*TMAX,TH8*TMAX, Nth
1150 LPRINT
1160 LPRINT"POWER(WATTS) TO DISSIPATE =";90000!*(1-Nth)/Nth
1170 MCP= 90000!/((TMAX*((1-TT)-(TC-1)/THT))*NA)
1180 LPRINT"MDOT*CP(WATTS/DEG K) OF SYSTEM ";MCP
1190 END
```

Appendix C.

```
10 DIM M[10,10],S[10],U[1024]
20 DIM TM[10,10],TS[10],TU[1024]
30 REM DPR IS DEGREES PER RADIAN
40 REM RT IS THE DESIRED RECIEVER OPERATING TEMPERATURE
50 REM TAN(ALPHA) IS THE TAN OF THE SUN HALF ANGLE AT 1 AU
60 REM ETA B IS THE BLOCKAGE EFFECIENCY DUE TO THE RECIEVER
70 REM ETA R IS THE REFLECTIVE COATING EFFECIENCY
80 REM SIGMA IS THE STEPHAN-BOLTZMANN CONSTANT IN WATTS/M^2/K^4
90 REM RRAD IS THE RECIEVER RADIUS
100 REM KS IS THE SOLAR CONSTANT AT 1 AU IN WATTS/M^2
110 DPR = 57.29578
120 INPUT"MIRROR RADIUS IN METERS";MRAD
130 INPUT"PERFECT MIRROR";PER
140 INPUT"MIRROR SURFACE ERROR QUALITY (1 SIGMA)";SQUAL
150 INPUT"DESIRED MISALIGNMENT";BETA
160 RT = 1750
170 TALFA = 4.65424E-03
180 NB = .9870001
190 NR = .9
200 SIG = 5.67E-08
210 RRAD = 1
220 INPUT "DESIRED PERCENTAGE CONVERGENCE(.01=1%)";CON
230 EPSILON = CON*3.141593*.15^2/2
240 TEPS = CON*3.141593*MRAD^2/2
250 FOR DTHB = 45 TO 65 STEP 10
260 THB = DTHB/DPR
270 KS = 1390
280 REM COMPUTE FOCAL LENGTH
290 FLNGTH = MRAD*(1+COS(THB))/(2*SIN(THB))
300 REM COMPUTE APERTURE SHIFT IF MISALIGNMENT EXISTS
310 DIS = FLNGTH*TAN(BETA)
```

```
320 REM THETA A IS THE MIRROR HUB ANGLE (ZERO IF NOT FOR RECIEVER BLOCKAGE)
330 THA = ATN(RRAD/FLNGTH)
340 LPRINT"MIRROR RADIUS (M) ",MRAD
350 LPRINT"MIRROR FOCAL LENGTH",FLNGTH
360 LPRINT"MIRROR RIM ANGLE (DEG)",DTHB
370 LPRINT"MIRROR SPEED (FL/DIA)",FLNGTH/(2*MRAD)
380 IE = 1390*3.141593*MRAD^2
390 LPRINT"INTERCEPTED ENERGY (WATTS)",IE
400 LPRINT"COATING EFFICIENCY",NR
410 LPRINT"BLOCKAGE EFFICIENCY",NB
420 LPRINT"CAVITY TEMPERATURE (K) ",RT
430 LPRINT "PERCENT CONVERGENCE",CON
440 IF PER = 1 THEN GOTO 500
450 FOR ERST = 1 TO 27 STEP 2
460 MER = ERST
470 IF ERST = 25 THEN MER = 26
480 IF ERST = 27 THEN MER = 31
490 MER = SQUAL*MER/10000
500 FOR RCOUNT = 2 TO 18 STEP 4
510 RAPP= RCOUNT*MRAD/1000
520 AAPP = 3.14159*RAPP^2
530 GOTO 1640
540 REM THIS ROMBERG ROUTINE INTEGRATES
550 REM            XITOT R dR
560 REM FROM 0 TO THE APERTURE RADIUS PLUS MISALIGNMENT SHIFT(IF PRESENT)
570 LI1 =(RAPP+DIS)/4
580 LI2 =(RAPP+DIS)/2
590 REM INITIALIZE THE INTEGRATOR
600 K=0
610 R= LI2
620 GOSUB 880
630 S[0]= RVAL
```

```
640 REM INTEGRATING LOOP STARTS HERE
650 IF K=0 THEN GOTO 770
660 SUM= 0
670 FOR I=0 TO 2^K-1
680 DELTAU= 2^(1-K)
690 IF I=0 THEN U[0]=-1+2^(-K)
700 IF I>0 THEN U[I]=U[I-1]+DELTAU
710 R=LI1*U[I]*(3-U[I]^2)+LI2
720 GOSUB 880
730 FX= RVAL
740 SUM=SUM+FX*(1-U[I]^2)
750 NEXT I
760 S[K]= SUM +S[K-1]
770 M[K,0]= 3*LI1*2^(-K)*S[K]
780 IF K=0 THEN GOTO 840
790 FOR J=1 TO K
800 M[K,J]= M[K,J-1]+(M[K,J-1]-M[K-1,J-1])/(4^J-1)
810 NEXT J
820 PRINT"T LOOP";TK;TM(TK,TK),"R LOOP";K;M(K,K)
830 IF ABS(M[K,K]-M[K-1,K-1])<EPSILON GOTO  860
840 K=K+1
850 GOTO  640
860 IG = M(K,K)
870 RETURN
880 REM THIS IS THE INTERIOR INTEGRAL THAT FINDS THE FRACTION
890 REM OF THE CIRCULAR ELEMENT THAT LIES WITHIN THE ELLIPSE
900 REM CHECK FOR CASE 1A
910 IF R<(TWEEK-A) THEN XITOT = 0: GOTO 1490
920 REM CHECK FOR CASE 4
930 IF R>(TWEEK+A) THEN XITOT = 0: GOTO 1490
940 REM CHECK FOR WHEN CASE 1 NOT APPLICABLE
950 IF R>B THEN GOTO 1270
960 REM ANOTHER TEST FOR NOT CASE 1
970 IF (TWEEK-A)>(-R) THEN GOTO 1270
```

```
980 REM COMPUTE THE LARGEST R THAT WILL FIT INSIDE TH ELLIPSE
990 REM FIRST FIND WHERE DRDT IS ZERO USING THE SECANT METHOD
1000 REM FIRST GUESS IS 135 DEGREES
1010 HALT = 0
1020 TP = 2.356194
1030 T = TP
1040 GOSUB 2190
1050 FTP = DRDT
1060 TN = .9899999*TP
1070 T = TN
1080 GOSUB 2190
1090 FTN = DRDT
1100 DTN = TN - TP
1110 GOTO 1180
1120 DTN = DTP*FTP/(FTL-FTP)
1130 TN = TP + DTN
1140 IF ABS(TN-TP)<.017452 THEN HALT = 1
1150 T = TN
1160 GOSUB 2190
1170 FTN= DRDT
1180 FTL = FTP
1190 TL = TP
1200 FTP = FTN
1210 TP = TN
1220 DTP = DTN
1230 IF HALT = 0 THEN GOTO 1120
1240 REM SOLUTION CONVERGED, RMIN COMPUTED
1250 REM CHECK FOR CASE 1
1260 IF R<RMIN THEN XITOT = 6.283185: GOTO 1490
1270 REM TWO POSSIBILITIES LEFT, CASES 2 AND 3
```

```
1280 REM COMPUTE TERMS INSIDE OF SQRT IN C18
1290 CHO = TWEEK*TWEEK*B*B*B*B
1300 CH1 = A*A*B*B*TWEEK*TWEEK
1310 CH2 = -A*A*A*A*B*B
1320 CH3 = A*A*A*A*R*R
1330 CH4 = -B*B*B*B*TWEEK*TWEEK
1340 CH5 = B*B*B*B*A*A
1350 CH6 = -A*A*B*B*R*R
1360 CH = CHO+CH1+CH2+CH3+CH4+CH5+CH6
1370 REM COMPUTE XI1 (COMMON TO BOTH CASES 2 AND 3)
1380 EX1 = (-TWEEK*B*B + SQR(CH))/(A*A-B*B)
1390 OP1 = SQR(R*R-EX1*EX1)
1400 XI1 = ATN(OP1/EX1)
1410 IF XI1<O THEN XI1 = 3.141593+XI1
1420 REM TEST FOR CASE 3
1430 IF (R>ABS(TWEEK-A)) AND (R<(TWEEK+A)) THEN XI2 = 0: GOTO 1480
1440 REM COMPUTE XI2 FOR CASE 2
1450 EX2 = (-TWEEK*B*B-SQR(CH))/(A*A-B*B)
1460 OP2 = SQR(R*R-EX2*EX2)
1470 XI2 = ABS(ATN(OP2/EX2))
1480 XITOT = 2*(XI1+XI2)
1490 RVAL = R*XITOT
1500 REM TEST FOR EXISTENCE OF MISALIGNMENT
1510 IF BETA = 0 THEN RETURN
1520 REM IS RING 'DR' OUTSIDE APERTURE PERIPHERY
1530 IF (-DIS+RAPP)<(-R)THEN FRAC = 0:GOTO 1620
1540 REM IS RING 'DR' INSIDE APERTURE PERIPHERY
1550 IF R<(RAPP-DIS) THEN RETURN
1560 REM COMPUTE INTERSECTION OF RING 'DR' AND APERTURE PERIPHERY
1570 EX3 = (RAPP^2-R^2)/(2*DIS)-DIS/2
1580 OP3 = SQR(R^2-EX3^2)
1590 IF EX3<O THEN PHI = ABS(ATN(OP3/EX3))
1600 IF EX3>O THEN PHI = 3.141593-ATN(OP3/EX3)
1610 FRAC = PHI/3.14159
1620 RVAL = RVAL*FRAC
1630 RETURN
```

```
1640 REM THIS INTEGRATES
1650 REM         RVAL RHO^2 SIN(THETA) dTHETA / ( A B )
1660 REM FROM THETA A (CLOSE TO 0 ) TO THETA B (MIRROR RIM ANGLE)
1670 TLI1 =(THB-THA)/4
1680 TLI2 = (THB+THA)/2
1690 REM INITIALIZE THE INTEGRATOR
1700 TK=0
1710 THETA= TLI2
1720 GOSUB 1970
1730 TS[0]=THVAL
1740 REM INTEGRATING LOOP STARTS HERE
1750 IF TK=0 THEN GOTO 1870
1760 TSUM= 0
1770 FOR TI=0 TO 2^TK-1
1780 TDELTU= 2^(1-TK)
1790 IF TI=0 THEN TU[0]=-1+2^(-TK)
1800 IF TI>0 THEN TU[TI]=TU[TI-1]+TDELTU
1810 THETA = TLI1*TU[TI]*(3-TU[TI]^2)+TLI2
1820 GOSUB 1970
1830 TFX= THVAL
1840 TSUM=TSUM+TFX*(1-TU[TI]^2)
1850 NEXT TI
1860 TS[TK]= TSUM +TS[TK-1]
1870 TM[TK,0]= 3*TLI1*2^(-TK)*TS[TK]
1880 IF TK=0 THEN GOTO 1930
1890 FOR TJ=1 TO TK
1900 TM[TK,TJ]= TM[TK,TJ-1]+(TM[TK,TJ-1]-TM[TK-1,TJ-1])/(4^TJ-1)
1910 NEXT TJ
1920 IF ABS(TM[TK,TK]-TM[TK-1,TK-1])<TEPS GOTO 1950
1930 TK=TK+1
1940 GOTO  1740
1950 TIG = TM(TK,TK)
1960 GOTO 2050
```

```
1970 REM THIS IS THE FUNCTION THAT ARE TRYING TO INTEGRATE
1980 RHO = 2*FLNGTH/(1+COS(THETA))
1990 TWEEK = RHO*TAN(2*MER)/COS(THETA)
2000 B = RHO*TALFA
2010 A= B/COS(THETA)
2020 GOSUB 540
2030 THVAL= IG*RHO*RHO*SIN(THETA)/(A*B)
2040 RETURN
2050  NE = 2*TIG/(3.14159*(MRAD^2))
2060  NC = NB*NR*NE-((SIG*AAPP*RT^4)/(KS*3.14159*MRAD^2))
2070 LPRINT
2080 LPRINT"MISALIGNMENT (MRAD)",BETA
2090 LPRINT"ERROR BAND (MRAD)",MER
2100 LPRINT"RECIEVER APERTURE RADIUS",RAPP
2110 LPRINT"ENERGY EFFICIENCY",NE
2120 LPRINT"COLLECTION EFFICIENCY",NC
2130 LPRINT"POWER IN APERTURE (W)",IE*NC
2140 NEXT RCOUNT
2150 IF PER = 1 THEN GOTO 2300
2160 NEXT ERST
2170 NEXT DTHB
2180 GOTO 2300
2190 REM THIS SUBROUTINE COMPUTES DR/D(THETA) AND R
2200 ES = A*A/(B*B)
2210 TEE = ES - TWEEK*TWEEK/(B*B)
2220 D1 = ES+(1-ES)*COS(T)^2
2230 D2 = SQR(TEE+COS(T)^2*(1-TEE))
2240 D3 = (A*COS(T)*(1-TEE)/D2+TWEEK)*D1
2250 D4 = 2*COS(T)*(1-ES)*(TWEEK*COS(T)+A*D2)
2260 DRDT = (-SIN(T)/D1^2)*(D3-D4)
2270 IF HALT = 0 THEN RETURN
2280 RMIN = (TWEEK*COS(T)+A*D2)/D1
2290 RETURN
2300 END
```

Appendix D.

```
10 DIM M[10,10],S[64],U[128]
15 CALL BAS87
20 TS= 270
30 INPUT"DESIRED DISSIPATED POWER (PER WING)";TDPWR
40 INPUT"CPMDOT(PER WING)";CPM
50 INPUT"INLET TEMPERATURE";TIN
60 INPUT"OUTLET TEMPERATURE";TOUT
70 INPUT"NUMBER OF RADIATOR ASSEMBLIES";RASS
75 INPUT"DESIRED REYNOLDS NUMBER INSIDE RADIATOR PIPES";RE
80 INPUT "PRINTED OUTPUT(1=YES,0=NO)";PFLAG
100 LPRINT"DESIRED DISSIPATED POWER",TDPWR
110 LPRINT"NUMBER OF RAD. ASSEMBLIES",RASS
115 LPRINT"REYNOLDS NUMBER INSIDE RADIATOR PIPES";RE
120 LPRINT"CP*MDOT IS",CPM
130 LPRINT"INLET TEMPERATURE IS",TIN
140 LPRINT"OUTLET TEMPERATURE IS",TOUT
150 LPRINT            792
155 MDOT = CPM/(140*RASS)
160 DDPWR = TDPWR/RASS
170 MU= TOUT/TIN
180 W = 8
190 WLAST = W
200 THCK= .02
210 TBTH= .25
220 PW = 460480!*MDOT/RE       1,652,890
230 LAMBDA=1.35
240 HF= .0054831*RE^.8/PW      .005022
245 LPRINT"FILM COEFFICIENT IS";HF
246 LPRINT
250 EM= .95
260 SIGMA= 5.67E-12
```

```
270 REM COMPUTE FIRST GUESS OF RAD AREA PER ASS'Y
280 FGRA = (CPM/(SIGMA*EM*6))*(1/TOUT^3-1/TIN^3)
290 LLAST = FGRA/(W*.9)
300 GOSUB 1460
310 LLAST = L
320 IF PFLAG = 0 THEN GOTO 360
360 MAX=QTV
370 TEST = QTV
375 AMP = 1
380 W=W+AMP*W/100
390 GOSUB 1460
410 IF QTV<= MAX THEN W=W-AMP*(W/100):GOTO 435
420 MAX = QTV
425 AMP = AMP+1
430 GOTO 380
435 AMP = 1
440 THCK=THCK+AMP*THCK/100
442 GOSUB 1460
450 IF QTV<= MAX THEN THCK=THCK-AMP*THCK/100:GOTO 535
460 MAX = QTV
465 AMP = AMP+1
470 GOTO 440
535 AMP = 1
540 W=W-AMP*W/100
550 GOSUB 1460
580 IF QTV<=MAX THEN W=W+AMP*W/100:GOTO 675
590 MAX = QTV
595 AMP = AMP+1
600 GOTO 540
675 AMP = 1
680 THCK = THCK-AMP*THCK/100
690 GOSUB 1460
720 IF QTV<=MAX THEN THCK=THCK+AMP*THCK/100:GOTO 750
730 MAX = QTV
735 AMP = AMP+1
740 GOTO 680
```

```
750 IF (TEST-MAX)/TEST>.008 THEN TEST=MAX:GOTO 375
760 PFLAG = 1
770 GOSUB 1250
800 STOP
810 REM THE FOLLOWING SECTION IS A ROMBERG INTEGRATOR FOR THE DIFFERENTIAL
820 REM EQUATION GOVERNING THE RADIATOR PHYSICS.
830 EPSILON = .0001
840 LI1 = 1/4
850 LI2 = 1/2
860 REM INITIALIZE THE INTEGRATOR
870 K=0
880 X= LI2
890 IF IFLAG = 1 THEN GOSUB 2620
930 S[0]= VALUE
940 REM INTEGRATING LOOP STARTS HERE
950 IF K=0 THEN GOTO 1100
960 SUM= 0
970 FOR I=0 TO 2^K-1
980 DELTAU= 2^(1-K)
990 IF I=0 THEN U[0]=-1+2^(-K)
1000 IF I>0 THEN U[I]=U[I-1]+DELTAU
1010 X=LI1*U[I]*(3-U[I]^2)+LI2
1020 IF IFLAG = 1 THEN GOSUB 2620
1060 FX= VALUE
1070 SUM=SUM+FX*(1-U[I]^2)
1080 NEXT I
1090 S[K]= SUM +S[K-1]
1100 M[K,0]= 3*LI1*2^(-K)*S[K]
1110 IF K=0 THEN GOTO 1160
1120 FOR J=1 TO K
1130 M[K,J]= M[K,J-1]+(M[K,J-1]-M[K-1,J-1])/(4^J-1)
1140 NEXT J
1150 IF ABS(M[K,K]-M[K-1,K-1])<EPSILON GOTO  1180
1160 K=K+1
1170 GOTO  940
```

```
1180 IG=MIK,K]
1190 IF IFLAG <> 1 THEN GOTO 1230
1200 QDISS=(23/10)*(LAMBDA*THCK*L/W)*IG
1210 GOSUB 2980
1220 QTV = RASS*QDISS/TRV
1230 RETURN
1240 REM
1250 REM THIS SUBROUTINE OUTPUTS VITAL DATA.
1260 REM
1270 IF PFLAG = 0 THEN GOTO 1360
1280 LPRINT"LENGTH IS";L
1290 LPRINT"WIDTH IS";W
1300 LPRINT"PERIMETER IS";PW
1310 LPRINT"THICKNESS IS";THCK
1320 LPRINT"TOTAL POWER PER VOLUME RATIO IS",QTV
1330 LPRINT"POWER DISSIPATED PER ASS'Y IS",QDISS
1340 LPRINT"MASS/POWER ELEC. IS ";TDPWR*.0102/(QTV*90);" KG/KWe"
1341 VEE = RE*1.09956E-04/PW
1342 DP = 3.036*(L/100)*(PW/314.1593)^(-1.25)*VEE^1.75
1344 KPC = DP*CPM*6.00856E-06
1346 LPRINT"WATTS TO PUMP COOLANT (PER WING) ";KPC
1350 LPRINT
1360 PRINT"LENGTH IS";L
1370 PRINT"WIDTH IS";W
1380 PRINT"PERIMETER IS";PW
1390 PRINT"THICKNESS IS";THCK
1400 PRINT"TOTAL POWER PER VOLUME RATIO IS",QTV
1410 PRINT"POWER DISSIPATED PER ASS'Y IS";QDISS
1420 PRINT"MASS/POWER ELEC. IS ";TDPWR*.0027/(QTV*90);" KG/KWe"
1424 PRINT"KILOWATTS TO PUMP COOLANT";KPC
1430 PRINT
1440 RETURN
```

```
1450 REM
1460 REM THIS SUBROUTINE ITERATES ON LENGTH TO SATISFY THE CONSTRAINT EQN
1470 REM
1480 HALT1= 0
1490 IFLAG = 1
1500 XP= LLAST
1510 L= XP
1520 GOSUB 2790
1530 GOSUB 810
1540 FXP= QDISS-DDPWR
1550 XN=.9899999*LLAST
1560 L= XN
1570 GOSUB 2790
1580 GOSUB 810
1590 FXN= QDISS-DDPWR
1600 DXN= XN-XP
1610 GOTO 1690
1620 DXN= DXP*FXP/(FXL-FXP)
1630 XN= XP+DXN
1640 IF ABS(XN-XP)<1 THEN HALT1=1
1650 L= XN
1660 GOSUB 2790
1670 GOSUB 810
1680 FXN= QDISS-DDPWR
1690 FXL=FXP
1700 XL= XP
1710 FXP= FXN
1720 XP= XN
1730 DXP= DXN
1740 IF HALT1= 0 THEN GOTO 1620
1750 GOSUB 1250
1760 RETURN
1770 REM
```

```
2610 REM
2620 REM THIS IS THE CONSTRAINT EQUATION THAT NEEDS INTEGRATING
2630 REM
2640 TB=(1+BR*LOG(MU)/LOG(10))*TIN*MU^(X)
2650 VALUE= GAMMA*(TB^4-TS^4)/(1+(8/5)*GAMMA*TB^3)
2660 RETURN
2670 REM
2780 REM
2790 REM THESE ARE THE CONSTANTS FOR THE CONSTRAINT EQN.
2800 REM
2810 GAMMA= (EM*SIGMA*W^2)/(LAMBDA*THCK)
2820 BR= CPM/(HF*PW*L)
2830 RETURN
2840 REM
2980 REM COMPUTE TOTAL RADIATOR VOLUME
2990 REM
3000 TR1 = 2*RASS*L*W*THCK+RASS*TBTH*L*(PW+3.141593*TBTH)
3010 SUM = 0
3020 LS = 2*W+PW/3.141593+2*THCK
3030 FOR ENES = 1 TO RASS
3040 IF ENES = 1 THEN LS=LS-W
3050 SUM = SUM+TBTH*(SQR(ENES)*PW+3.141593*TBTH)*LS
3060 IF ENES = 1 THEN LS = LS+W
3070 NEXT ENES
3080 TRV = TR1+2*SUM
3090 RETURN
3100 REM
3110 REM
3540 END
```

REFERENCES

1. Namkoong, D., Preliminary Test Results of Heat Transfer / Thermal Storage Tube Design Under Simulated Orbital Conditions, NASA TMX-67904, Aug. 1971.

2. Brick, R.,Pense, A.,Gordon,R., Structure and Properties of Engineering Materials, 4th. ed., McGraw-Hill Book Company, New York, N.Y., 1977.

3. Mansteller,J., Tepper,F., Rodgers,S., Alkali Metals Handling and Systems Operating Techniques, Gordon and Breech Science Publishers, Inc., New York, N.Y., 1967.

4. Brayton Cycle Cavity Receiver Design Study, TRW Power Systems, Nov. 1965.

5. Space Station Systems Analysis Study, Part 3, Documentation, Volume 7, SCB Alternate Evolution, Task 10, MDAC. , Sept. 1977.

6. Lurio, C. An Evaluation of Solar Power Mercury Rankine Space Power, MIT Space Systems Lab #3-83, Jan. 1983.

7. Closed Cycle Gas Turbine Optimization - Procedures and Examples, Garrett, 1977.

8. Burns, R. Preliminary Thermal Performance Analysis of the Solar Brayton Heat Receiver, NASA TN D-6268, Mar. 1971.

9. Furukawa, M. Design and Off-Design Performance Calculations of Space Radiators, J. Spacecraft, AIAA 1980.

10. White, F. Fluid Mechanics, McGraw Hill, N.Y., N.Y. 1979.

11. Cosby, Lyle, The Meteoroid Environment and Its Effects on Materials and Equipment, NASA SP-78.

12. Danis, L., Cruzen, S., Schimmel, W., Carbon/ Carbon Components for Advanced Turbine Engines, ASME, Mar. 1981.

13. Kaykaty, G. Analysis of the Maximum Performance of a Paraboloidal Solar Collection System for Space Power NASA TN D-4415, Mar. 1968.

14. Kaykaty, G. Analysis of Performance of Double Reflector System for Collecting Solar Energy, NASA TN D-3534, 1966.

15. Chapman, A. Heat Transfer, 3rd ed., Macmillan Publishing Company, Inc., New York, N.Y., 1967.

16. Taussig, R., et al., Design Investigation of Solar Powered Lasers for Space Applications, Final Report, NASA CR 159554, May 1979.

17. English, R., "Alternative Power Generation Sources" in Future Orbital Power Systems Technology Requirements, a symposium held at LRC, Cleveland, Ohio, May 31 - June 2, 1978, NASA CP-2058, 1978.